MECHANISTIC PROBING OF COMPOUNDS OF BIOLOGICAL AND PHARMACEUTICAL INTEREST BY AMBIENT IONIZATION MASS SPECTROMETRY

by

Tsdale Friesh Mehari

A Dissertation

Submitted to the Faculty of Purdue University

In Partial Fulfillment of the Requirements for the degree of

Doctor of Philosophy

Department of Chemistry

West Lafayette, Indiana

August 2020

THE PURDUE UNIVERSITY GRADUATE SCHOOL
STATEMENT OF COMMITTEE APPROVAL

Dr. R. Graham Cooks, Chair
Department of Chemistry

Dr. Scott McLuckey
Department of Chemistry

Dr. Hilkka I. Kenttämaa
Department of Chemistry

Dr. Kavita Shah
Department of Chemistry

Approved by:
Dr. Christine A. Hrycyna

To Makeda A. Mehari

ACKNOWLEDGMENTS

Firstly, I would like to acknowledge God's grace which has allowed me to reach places that I never thought possible. For giving me to parents, Tarekegne Mehari and Frieshgenet Dabei, who provided unwavering psychological support of all my academic endeavors, and an unyielding standard for greatness. As a descendant of immigrants, I appreciate the sacrifice my parents made by leaving their homeland to provide the freedom and unlimited resources of the education system in this country. The importance they placed on respect, education, character, work ethic, perseverance, and setting near-impossible goals has shaped my life path and lead me directly to the road of chemistry. Through many difficult times, their simple words of encouragement have provided the fuel necessary to complete this academic journey. The birth of my only sibling, Makeda, has renewed my purpose in life and represents all things good in this world. Dr. Tonya G. Goins, my academic mother, even when I was not your student you recognized misguided potential and placed me under your advisement. The confidence you placed on my future capabilities came at a vital time in my life, and I thank you for your continued mentorship and care for my success.

The academic foundation that was built at NC A&T State University is responsible for my arrival to Purdue University. Professors Dr. Margaret Kanipes and Dr. Zerihun Assefa, thank you for being part of the essential support team that lead to my first conference presentations and full financial support for a master's degree under the Rise fellowship (NIH). A special thanks to Dr. Sayo O. Fakayode, my academic father, for the introduction to analytical methods and instrumentation. Dr. Fakayode is a life mentor, and his enthusiastic drive for perfection, self-motivating personality, and humorous scolding has provided a substantial contribution to own personal development. I am grateful to Mr. James King for all the meaningful discussions over instrument troubleshooting and your complete openness to the assistance of students.

Most importantly, I would like to thank my research advisor, Dr. R. Graham Cooks, for allowing me the opportunity of working in Aston Labs beginning from my zero year. Professor Cooks has not only taught me the world of mass spectrometry not previously seen before my arrival, but also the required love of organic chemistry. I am most appreciative of the patience and kindness you have shown me during your mentorship, and the amount of humility displayed from such an accomplished scientist. I am grateful for the many invitations to your home, to meet your family

and the gracious encouragement in my volunteer efforts for the department, though they took me away from the lab. It has been a great privilege to be your student and I am forever grateful for the numerous opportunities for growth and preparation for my career.

I appreciate the guidance from my former lab members, Drs. Valentino Pirro, Christopher Pulliam, Caitlin Falcone, Clint Alfaro, Alan Jarmush, Karen Yannell, Dalton Snyder, Stephen Ayton, Ryan Bain, Patrick Fedick, Kiran Iyer, Ryan Bain, and Adam Hollerbach. I will always have great memories of the robust roundtable talks with Robert Schraeder, Sangeeta Pandey, and Lucas Szalwinski after work that ranged from instrumentation to social issues. I have learned so much culture and language from my international colleagues, Dr. Zhenwei Wei, Dr. Fan Pu, Xingshuo Chen, Lillian Chen, Lingqi Qui, Yanyang Hu and Kai-Hung Huang, I am thankful for the many gifts from your country and for tolerating my mandarin accent. A special recognition is required for the most compatible lab partner I have ever met, Yangjie Li, for the respect and consideration of all my ideas, no matter how farfetched they may have been, and most importantly for her genuine friendship that stretched beyond the laboratory. The overwhelming influence of Dr. Christopher Pulliam is demonstrated throughout this dissertation and will last for many years afterwards, though it does not encompass the continued mentoring and guidance provided even after his tenure in the lab.

To the beautiful friendships made during graduate school, Anthony Pitts-McCoy, Dr. Elissia Franklin, Dr. Reena Blade, Dr. Colby Adolph, Kwame Brown and Kiera Estes, I appreciate all our conversations about science and beyond, the time spent studying for cumes and final exams, the conference and recruitment trips, the mentoring and mentorship, and the overall emotional support that plays an integral role in everyday life. To my friends who have dedicated their time to the recruiting, mentoring and advancement of URM students in the department, Jocelyn Nardo, Athena Jenkins, Abdirahman Abdillahi, De'Shavon Shenault, Nicole Escorcia, I wish you continued strength in your efforts and I am truly proud of your accomplishments that will greatly improve the learning environment, now and in the future.

TABLE OF CONTENTS

LIST OF FIGURES 9
LIST OF SCHEMES 13
ABSTRACT 14
INTRODUCTION 16
1.1 Overview 16
1.1.1 Ambient Ionization 16
1.1.2 Electrospray Ionization 17
1.2 References 19
CHAPTER 2. REACTION MONITORING OF HETEROGENEOUS CHEMICAL REACTIONS BY LAB-DESIGNED SAMPLING PROBE 22
2.1 Abstract 22
2.2 Introduction 23
2.3 Experimental 24
2.3.1 Reagents 24
2.3.2 Sampling Probe 24
2.3.3 Batch synthesis of N-methylnicotinic acid 25
2.3.4 Batch synthesis of octyl 1-methyl-1-pyridine-3-carboxylate 25
2.3.5 Batch synthesis of N-(4-(dimethylamino)phenyl)benzamide 25
2.3.6 Batch synthesis of *tert*-butyl phenylcarbamate 25
2.3.7 nESI-MS Analysis 26
2.4 Results and Discussion 26
2.4.1 Esterification reaction progress 26
2.4.2 Acylation reaction progress 30
2.4.3 Protection reaction progress 31
2.5 Conclusions 32
2.6 References 32
CHAPTER 3. REACTION ACCELERATION AT AIR-SOLUTION INTERFACES: ANISOTROPIC RATE CONSTANTS FOR KATRITZKY TRANSAMINATION 34
3.1 Abstract 34

3.2 Introduction 34
3.3 Experimental 35
3.3.1 Reagents 35
3.3.2 Batch experiments 36
3.3.3 nESI-MS experiments 36
3.4 Results and discussion 37
3.4.1 The Katritzky Transamination reaction 37
3.4.2 Claisen-Schmidt condensation 46
3.4.3 Imine Formation 48
3.5 Conclusion 49
3.6 References 50
CHAPTER 4. REACTION ACCELERATION AT SOLID-SOLUTION INTERFACES: KATRITZKY TRANSAMINATION BY GLASS NANOPARTICLES 53
4.1 Abstract 53
4.2 Introduction 53
4.3 Experimental 55
4.3.1 Reagents 55
4.3.2 Glass wool experiments 56
4.4 Results and Discussion 56
4.4.1 Katritzky Transamination reaction 56
4.4.2 Claisen-Schmidt 68
4.4.3 Imine Formation 69
4.5 Conclusions 70
4.6 References 71
CHAPTER 5. ACCELERATED OXIDATION OF ALKANES IN THIN FILMS AND MICRODROPLETS USING FENTON'S CATALYST USING REACTIVE PAPER SPRAY IONIZATION MASS SPECTROMETRY 72
5.1 Abstract 72
5.2 Introduction 72
5.3 Experimental 74
5.3.1 Reagents 74

5.3.2 Paper spray experiments 74
5.4 Results and Discussion 74
5.4.1 Long chain alkane experiments 74
5.4.2 short chain alkane experiments 76
5.4.3 Branched alkane experiments 77
5.5 Conclusion 79
5.6 References 79
CHAPTER 6. ELECTROCYCLIZATION AND DIMERIZATION OF ETHYNYL ANILINES IN MICRODROPLETS 82
6.1 Abstract 82
6.2 Introduction 82
6.3 Experimental 83
6.3.1 Reagents 83
6.3.2 Spray-based reactions 83
6.3.3 Bulk-phase reactions 84
6.3.4 Organic synthesis 84
6.3.5 Theoretical chemistry 94
6.4 Results and Discussion 95
6.4.1 4-Ethynyl-N,N-dimethylaniline dimerization 95
6.4.2 4-Ethynylaniline dimerization 106
6.4.3 4-Ethynyl-N,N-diethylaniline dimerization 108
6.5 Conclusions 113
6.6 References 114
VITA 118

LIST OF FIGURES

Figure 2.1 Nano electrospray ionization mass spectrum of reaction starting material, side products and final reaction product. 28

Figure 2.2 Representative MS of reaction progress of the esterification reaction 28

Figure 2.3 Nano electrospray ionization mass spectra of: A) full scan of the synthesized methylated DMAP. B) full scan of the synthesized methylated nicotinic acid. C) MS/MS spectra of reaction product from A. D) MS/MS spectra of reaction product from B. 29

Figure 3.1 (a) Measured relative ion signals from mixed solutions of isolated product pyridinium and pyrylium reactant to calculate yield and rate constant. (b) Three replicates are shown in the calibration curve. (c) The linearity of a single replicate is good even at low concentration ratio. 38

Figure 3.2 (a) Zero yields seen in full MS of freshly mixed reactant solution validated the non-accelerating nESI-MS analysis across the concentration range. (b) Test by MS shows no residue on the well plate after performing the Katritzky reaction in droplets (130 μL; 1000 μM) for 5 min 39

Figure 3.3 Tandem MS of reactants, intermediate and product for the model Katritzky reaction (isolation width used is not larger than 2 Th. CID refers to collision energy and NL to signal intensity). 41

Figure 3.4 Bulk (0.3-mL and 1.2-mL) kinetics of the Katritzky reaction (Scheme 1a) at 50 μM. 42

Figure 3.5 Bulk kinetics of Katritzky reaction (1b) using TTP as the reactant at 50 μM for two different volumes (0.3 mL and 1.2 mL) 43

Figure 3.6 Bulk kinetics of Katritzky reaction (1c) using TMP as the reactant at 50 μM in two different volumes (0.3 mL and 1.2 mL) 43

Figure 3.7 (a) Three MS spectra of each pyrylium salt (TMP/TPP/TTP) in acetonitrile at 50 μM (b)MS of equimolar (50 μM) pyrylium salts (TMP, TPP, TTP) mixture in acetonitrile. The numbers indicate relative MS peak areas. Note that (a) and (b) are normalized separately. 44

Figure 3.8 Rate constant enhancements of bulk reactions using their own reference rate constants at the high concentrations in large volumes (reference for unstirred bulk solutions at room temperature: k0bulk = k500 μM, 1.2 mL = 0.00058 M-1s-1). The numbers indicate that volume effects in bulk solutions were enhanced by a larger surface-to-volume (S/V) ratio difference (4-fold enhancement in S/V ratio from 1.2-mL solutions to 0.3-mL solutions. 46

Figure 3.9 Bulk kinetics of the Claisen-Schmidt reaction at 5 mM in plastic vials of different volumes tested by ESI-MS with automatic sampling with a) 2 eq of KOH; b) 20 eq of KOH. 47

Figure 3.10 Bulk kinetics of the Imine formation reaction at 5 mM in plastic vials of different volumes tested by ESI-MS with automatic sampling. 49

Figure 4.1 Bulk kinetics of the Katritzky reaction at 50 μM: a) glass vials at 300 μL; b) glass vials at 1200 μL; c) silanized glass vials at 300 μL; b) silanized glass vials at 1200 μL. 58

Figure 4.2 Bulk kinetics of the Katritzky reaction (Scheme 1a) at 50 μM in different vials. 59

Figure 4.3 Bulk kinetics of the Katritzky reaction (Scheme 1a) at 5 μM in different vials tested by ESI-MS with automatic sampling. 60

Figure 4.4 Bulk kinetics of the Katritzky reaction (Scheme 4.1a) at 50 μM in different vials tested by ESI-MS with automatic sampling. 61

Figure 4.5 Bulk kinetics of the Katritzky reaction (Scheme 4.1a) at 500 μM in different vials tested by ESI-MS with automatic sampling. 61

Figure 4.6 MS of Katritzky reaction (Scheme 1a) at 50 μM in plastic vials without particles vs. with glass or silanized glass particles added. 62

Figure 4.7 Bulk kinetics of the Katritzky reaction (Scheme 4.1a) at 50 μM in plastic vials with different types of wool supernatant added or without addition. 63

Figure 4.8 Bulk kinetics of the Katritzky reaction (Scheme 4.1a) at 50 μM in plastic vials with different amounts of the same glass wool supernatant added. The linearity of the plot reflects the enhancement of rate constants. 64

Figure 4.9 Katritzky reaction (Scheme 4.1a) rate constants at 50 μM increase with increasing amounts of glass nanoparticles. (Acceleration factor at 75% glass wool solution: 128 for unstirred bulk at room temperature for 2 h). 65

Figure 4.10 Bulk kinetics of the Katritzky reaction (Scheme 4.1a) at 50 μM in plastic vials with the same glass wool supernatant added but of different total volumes of solutions. There is a 1.8-fold increase in rate constants for volume effect (the same as in Chapter 3 using plastic vials without glass addition). 66

Figure 4.11 Bulk kinetics of the Katritzky reaction (Scheme 4.1a) at 50 μM in plastic vials with glass particles added vs. without glass particles added. 66

Figure 4.12 Bulk kinetics of the Katritzky reaction (Scheme 4.1b) at 50 μM in plastic vials with glass particles added vs. without glass particles added. 67

Figure 4.13 Bulk kinetics of the Katritzky reaction (Scheme 4.1c) at 50 μM in plastic vials with glass particles added vs. without glass particles added. 68

Figure 4.14 Bulk kinetics of the Claisen-Schmidt reaction at 5 mM in glass vials of different volumes tested by ESI-MS with automatic sampling. 69

Figure 4.15 Bulk kinetics of the Imine formation reaction at 5 mM at different volumes tested by ESI-MS with automatic sampling in a) glass vials; b) silanized glass vials. 70

Figure 5.1 Methodology for the Accelerated Oxidation of alkanes using Paper Spray Ionization. 73

Figure 5.2 Paper spray ionization mass spectra of n-heptadecane as a model alkane to identify optimum oxidizing agent. 75

Figure 5.3 Representative MS of oxidation products, oxidized dimers and radical degradation of decane where *m/z* 142 represents the ionized alkane. 76

Figure 5.4 Representative MS of oxidation products, oxidized dimer and radical degradation of nonane where *m/z* 127 represents the ionized alkane 77

Figure 5.5 Representative MS of oxidation products, oxidized dimers and radical degradation of heptamethylnonane where *m/z* 225 represents the ionized alkane. 78

Figure 5.6 Representative MS of oxidation products of squalane where *m/z* 421 represents the ionized alkane. 79

Figure 6.1 400 MHz 1H NMR spectrum of compound (**5**) in CDCl3. 86

Figure 6.2 400 MHz 1H NMR spectrum of compound **2** in CDCl3. 91

Figure 6.3 MS and MS^2 spectra: a-b) synthesized covalent bond dimer; c) covalent bond dimer generated in spray experiments. 91

Figure 6.4 400 MHz ^{13}C NMR spectrum of compound 4 in $CDCl_3$. 92

Figure 6.5 400 MHz ^{1}H NMR spectrum of compound 4 in $CDCl_3$. 93

Figure 6.6 400 MHz ^{1}H-^{1}H COSY spectrum of compound 4 in $CDCl_3$. 94

Figure 6.7 Chemical process simulated by computation (eV). 95

Figure 6.8 a) MS analysis of 4-Ethynyl-*N*,*N*-dimethylaniline (**1**, observed at *m/z* 146 as $[M+H]^+$) forms three dimer species **2** ($[2M+H]^+$ observed as at *m/z* 291), **3** ($[2M-H]^+$ observed at *m/z* 289) and **4** ($[2M-3H]^+$ observed at *m/z* 287), b) highlighted region of interest expanded to show the three products observed in electrospray analysis. 96

Figure 6.9 CID spectrum of covalent bond dimer **2** results in a major peak observed at *m/z* 276 due to loss of a methyl radical. 97

Figure 6.10 CID spectrum of covalent bond dimer **2** results in a major peak observed at *m/z* 247 due to loss of a dimethylamino radical. 98

Figure 6.11 CID spectra of covalent bond dimers result in major peaks at the loss of a methyl radical and a dimethylamino radical: a) dimer *m/z* 291 formed from **1**; b) dimer *m/z* 293 formed from **5**; c) dimer *m/z* 299 formed from **6**; b) dimer *m/z* 299 formed from **7**. The corresponding fragments observed in the MS^2 were shown in right hand side. 99

Figure 6.12 Radical initiators **9** and **10** utilized in bulk synthesis. 100

Figure 6.13 Bulk reaction progress of **1** with copper (II) perchlorate hexahydrate radical intiator: a) MS spectrum of after initial mixing; b) MS^2 spectrum of *m/z* 289 shows the loss of a methyl radical and a dimethylamino radical, which mirrors the covalent dimer CID spectrum; Bulk reaction progress of **1** with tris(4-bromophenyl)aminium hexachloroantimonate c) MS spectrum after initial mixing; d) MS spectrum after 1 hr of reaction time. 101

Figure 6.14 CID spectrum of dimer **3** results in a major peak observed at *m/z* 274 due to loss of a methyl radical and *m/z* 245 corresponds to a loss of a dimethylamino radical. 102

Figure 6.15 CID spectrum of dimer **3** results in a major peak observed at *m/z* 287 due to loss of dihydrogen and *m/z* 273 corresponds to a loss of a methane. 103

Figure 6.16 Bulk reaction progress of **1** with benzoyl peroxide radical initiator: a) MS spectrum after initial mixing; b) MS spectrum after 24 h of reaction time; c) MS^2 spectrum of *m/z* 287 where *m/z* 271 corresponds to a methyl radical loss and *m/z* 272 corresponds to a loss of methane; d) MS^3 spectrum for *m/z* 287 and *m/z* 271. 104

Figure 6.17 CID spectrum of dimer **4** results in a major peak observed at *m/z* 272 due to loss of a methyl radical and *m/z* 271 corresponds to a loss of a methane. 105

Figure 6.18 a) MS analysis of 4-ethynylaniline (**25**, observed at *m/z* 118 as $[M+H]^+$) forms one dimer species **26** ($[2M+H]^+$ observed as at *m/z* 235), b) MS^2 spectra of covalent bond dimer at *m/z* 235 shows a fragment loss of aniline forming *m/z* 142. 107

Figure 6.19 nESI-MS analysis of 4-Ethynyl-*N*,*N*-diethylaniline (**27**) a) MS spectrum with the region of interest highlighted; b) highlighted region is expanded to show the monomer and dimer product observed in the spray; c) expanded region of monomer observed at *m/z* 174 as $[M+H]^+$; expanded region of unexpected dimer $[2M+H]^+$ observed as at *m/z* 348. 109

Figure 6.20 Enhanced scan nESI-MS analysis of 4-Ethynyl-*N*,*N*-diethylaniline. 109

Figure 6.21 CID spectrum of three observed dimers observed at: a) *m/z* 348; b) *m/z* 347; and c) *m/z* 346; with peaks representing fragmentation due to losses of a methyl radical, ethyl radical, methyl and ethyl radicals or a dimethylamino radical, and a diethylamino radical. 110

Figure 6.22 CID spectrum of dimer **28** results in a minor peak observed at *m/z* 332 due to loss of a methyl radical. 111

Figure 6.23 CID spectrum of dimer **28** results in a major peak observed at *m/z* 318 due to loss of an ethyl radical. 111

Figure 6.24 CID spectrum of dimer **28** results in a minor peak observed at *m/z* 303 due to loss of a methyl and ethyl radical. 112

Figure 6.25 CID spectrum of dimer **28** results in a major peak observed at *m/z* 275 due to loss of a dimethylamino radical. 113

LIST OF SCHEMES

Scheme 2.1 Steglich Esterification of a carboxylic acid with a terminal alcohol. 26

Scheme 2.2 DMAP-catalyzed esterification of a nicotinic acid and n-octanol. 27

Scheme 2.3 Amide bond formation between an acyl chloride and an amine. 30

Scheme 2.4 Amine protection between a tert-butoxycarbonyl and a diamine. 31

Scheme 3.1 Katritzky transamination: the reaction between pyrylium salts (TPP, TTP, TMP) and *p*-anisidine to form pyridinium salts. 37

Scheme 3.2 Proposed mechanism of the model Katritzky reaction (note: K1, K2, K3 indicate equilibrium constants and k1 indicates rate constant.) 40

Scheme 3.3 Claisen-schmidt reaction of 6-hydroxy-1-indanone with 2-methoxybenzaldehyde. 47

Scheme 3.4 Imine formation reaction of dibutylpropane-1,3-diamine with 3-hydroxybenzaldehyde. 48

Scheme 4.1 Katritzky transamination reactions of pyrylium salts (TPP, TTP, TMP) and p-anisidine to form pyridinium salts. 57

Scheme 4.2 Claisen-Schmidt reaction of 6-hydroxy-1-indanone with 2-methoxybenzaldehyde.68

Scheme 4.3 Imine formation reaction of dibutylpropane-1,3-diamine with 3-hydroxybenzaldehyde. 70

Scheme 5.1 Generation of hydroxyl radical species vs Fenton's chemistry. 73

Scheme 6.1 Synthetic route to 4-(ethynyl-d)-N,N-dimethylaniline (**5**). 84

Scheme 6.2 Synthetic route of 4-ethynyl-*N*,*N*-dimethylaniline-2,3,5,6-d_4 (**6**). 85

Scheme 6.3 Synthetic route of 4-ethynyl-N,N-bis(methyl-d_2)aniline (**7**). 87

Scheme 6.4 Synthetic route of 8-(4-(dimethylamino)phenyl)-N,N-dimethylnaphthalen-2-amine (**2**). 89

Scheme 6.5 4-ethynyl-*N*,*N*-dimethylaniline (**1**, *m/z* 146) forms three dimer species when electrosprayed, a covalent bond dimer (**2**, *m/z* 291) and two dehydrogenation products, **3** (*m/z* 289), and **4** (*m/z* 287). 96

Scheme 6.6 4-ethynylaniline (**25**, *m/z* 118) forms one dimer when electrosprayed, a covalently bound dimer species **26** ($[2M+H]^+$ observed as at *m/z* 235). 107

Scheme 6.7 4-Ethynyl-*N*,*N*-diethylaniline (**27**, *m/z* 174.1) forms four dimer species when electrosprayed, a dimer with delocalized charge (*m/z* 346), a covalently bound dimer (**28**, *m/z* 347) a doubly bound dimer (m/z 348), and a doubly charged dimer species (**29**, *m/z* 174.8).....110

ABSTRACT

This thesis covers the four topics discussed in each of the following paragraphs. It is unified by the dual ability of ambient ionization mass spectrometry as a useful analytical tool allowing for monitoring of chemical reactions, in addition to its capability to accelerate reaction rates using the same equipment under accelerating or non-accelerating conditions. The ability to manipulate reactions and monitor the subsequent effects to the rate of the reactions can provide vital information for many industrial arenas. Current process analytical technology (PAT) is extremely time-consuming, and typically costly due to dependence on analysis conducted at the end stage of production. Additionally, many chemical reactions found to be useful in pharmaceutical or manufacturing industries are labor intensive and require harsh conditions such as heat or expensive catalysts. Several methods have been developed to overcome these current limitations, while providing vital information on short-lived intermediates, degradation products, and accelerated reaction rates. A sampling device was developed and coupled with nESI allowing for monitoring of heterogeneous chemical reactions by mass spectrometry without the additional requirement of separation (filters, chromatography, etc.) In addition, this technique maintains the high sensitivity, specificity, speed and structural elucidation provided by mass spectrometry analysis. The analysis provided kinetic profiles of all reactants, intermediates, products and coproducts throughout the course of the reaction.

The ability to effectively control chemical reactions and their rates is a priority across several fields of study. Several factors affecting reaction rates, such as heat and catalysts selected, have been well studied. However, there has been recent interest in exploring the capabilities for reaction acceleration in charged microdroplets. It is known that reaction rates on the surface of a droplet greatly differ from reactions occurring in the droplet. The Katritzky transamination reaction was used as a model to identify the effects of the air-solution interface on reaction acceleration by varying the air-liquid surface to volume ratio. The significant increase in reaction rate constants was further enhanced by solid–solution interfacial effects observed after addition of glass nanoparticles.

The effective degradation of non-polar hydrocarbons is an environmental concern as they are the main composition of waste generated from petroleum processing. Saturated alkanes are relatively stable molecules which present a challenge for analysis by mass spectrometry without

the use of extreme experimental conditions. A rapid analysis method by paper spray ionization was developed that allows for the oxidation products of saturated alkanes to be monitored by MS in under two minutes. This method relies on the generation of a hydroxyl radical by reacting iron (III) chloride with aqueous hydrogen peroxide on the principle of Fenton's chemistry. The presence of this radical in direct contact with an alkane produces several oxidation products which can be easily monitored by MS. The reagents are added to a paper triangle sequentially, creating a thin film which allows reaction acceleration in relatively small volumes analyzed directly from paper at atmospheric pressure.

The dimerization of 4-ethynylaniline derivatives in acetonitrile was monitored by nano electrospray ionization mass spectrometry. Dimer products formed by electrocyclization and radical processes were observed that are not detected as a corresponding bulk reaction. This gas-phase reaction has been interrogated in a solution phase analog with radical initiators and characterized by ^{1}H NMR. This work demonstrates that compounds can be synthesized by the electrospray process. Future studies may reveal how this observation affects the interpretation of the MS results involving electrospray.

INTRODUCTION

1.1 Overview

Mass spectrometry (MS) is a robust analytical technique used to analyze one or more ioniable species present in a sample. The process involves generation of ions in order to measure their mass-to-charge ratios (*m/z*), and results are typically represented as a mass spectrum (ion intensity vs. mass/charge).[1-3] These measurements can reveal identities of unknown compounds, quantification of known compounds, and determination of chemical and structural properties of these charged species. Mass spectrometers are sophisticated instruments providing high sensitivity and specificity of detection. The development of ambient ionization mass spectrometry has created an alternative workflow eliminating or minimizing sample preparation and allowing for direct analysis of a broad range of samples.[2] This ionization technique can follow reaction progress in bulk solutions and enhance rate effects in microdroplets and high surface-to-volume systems. The various ionization sources available for the chemical analysis of small and large molecules by ambient ionization mass spectrometry has led to wide spread use in numerous applications.[2-6]

1.1.1 Ambient Ionization

The development of ambient ionization sources has provided the ability to perform mass spectrometric analysis methods with minimal to no sample preparation. There are a basic set of characteristics that must be met with any ambient MS technique with starting with the generation of ions in open air. This allows for the direct surface analysis of samples with unconventional shapes and sizes, including solid materials ranging from drugs to fabrics.[7-10] The versatility of ambient MS ion sources is demonstrated in its interchangeable capabilities between most mass spectrometers containing atmospheric pressure interfaces. Generally, this eliminates the need for any modification requirements to the ion transfer optics or the vacuum interface when utilizing various ambient ion sources on the same MS instrument. A key advantage of the use of ambient MS methods is the introduction of surface analysis based on well-established ionization mechanisms.[3, 15] The majority of these sources rely on the fundamentals of electrospray ionization (ESI) which ionizes samples without causing significant fragmentation.

1.1.2 Electrospray Ionization

Electrospray ionization is a soft ionization technique developed at Yale University in 1981 by John B. Fenn and colleagues.[16] These scientists demonstrated the ability to ionize large biomolecules with relatively little to no fragmentation, and extension of the mass range of analyte analysis by producing multiple charged ions.[16, 17] Much of the success of this technique is attributed to the compatibility of the ESI-MS interface with gas chromatography (GC) and liquid chromatography (LC), in addition to the introduction of ESI as a viable alternative to the traditionally used (EI).

Traditionally, ESI is an atmospheric ionization technique whereby ions are produced by application of DC potentials to an analyte solution contained in a narrow, sharp emitter causing an accumulation of charge at the tip of the emitter. As the voltage is applied in an electric field, the resultant high potential causes the shape of the liquid droplet surface to become converted into a conical shape whose apex emits a thin stream of charged droplets. These charged microdroplets formed from the Taylor cone undergo Coulombic fission producing smaller, secondary droplets. Rapid solvent evaporation yields bare ions which are ejected towards the inlet of the mass spectrometer.[18-21] This occurs once the magnitude of the electrostatic forces of the applied field become similar in magnitude to the forces of the surface tension of the solution.

There are two main theories to explain the mechanism of ion formation as a result of droplet desolvation: 1) the ion evaporation model (IEM) or 2) the charge residue model (CRM). The first model or IEM states that initial droplets formed from the spray emitter undergo Coulombic fission to generate smaller, secondary droplets and lightly solvated ions.[19] This occurs as a result of a rapid decrease in droplet size caused by solvent evaporation until the charge on the surface of the droplet exceeds the Rayleigh limit and is a generally accepted model for small molecules. The second model, or CRM explains the formation of ions from larger molecules such as proteins and nucleic acids.[20-22] This theory states that as a droplet undergoes evaporation and reaches the Rayleigh limit, it declusters producing smaller charged droplets and leaving charges behind which are then transferred to the analyte to form an ion.[22] It must be noted that both of these models are centered around the basis of droplet evaporation and provides well documented evidence in the literature. Recently, a third model has been proposed, the chain elongation model (CEM), which explains that part of a chain escapes the droplet surface and moves into the gas phase while maintaining some of the original charge. This model is widely accepted; however, its application

is restricted to significantly larger molecules such as unordered polymers. Over the past few decades, several other mechanisms of electrospray ionization have been proposed to describe this phenomenon.[20-23] Many of these fundamental principles of electrospray ionization are generally accepted, though not fully understood. A further understanding of the mechanism could help to develop methods to increase ionization efficiency of this technique and provide insight into the reactivity of this method.

The ability to form gas phase ions from charged microdroplets is called ionization efficiency (IE) and greatly depends on the nature of the solvents used during the analysis. Ionization efficiency is an important factor to consider when using ESI for analysis as it enables the sensitivity required to detect analyte species at relatively low concentrations.[12, 25-27] IE remains relatively poor and directly effects the interpretation of the data generated. It is important that the high voltages used during ionization experiments are able to overcome the high surface tensions of the solvent being used during the experiment. Each chemical species has a different IE determined by the ratio of ions delivered to the inlet of the mass spectrometer to the number of molecules introduced by the ionization source. The charge transfer rate, concentration of analyte molecules, transmission of ions to the mass spectrometer, and the humidity level are a few other aspects that affect ionization efficiency.[25]

Initial designs of ESI emitters involved approximately 200 um wide blades made of 17 stainless steel. Further optimization of these designs was made by Mann et al with the use of glass capillaries of significantly smaller diameters (ca. 1-5 um) as emitters. This technique is widely used today and commonly known as nano-electrospray ionization (nESI). nESI uses much lower sample volumes and has higher ionization efficiencies compared to traditional ESI methods. nESI also eliminates the use of a heated sheath gas to assist desolvation and operates at flow rates of about 20 nL/min.[28] In addition to nESI, there are a variety of ionization sources, some of which are considered ambient ionization techniques, since the ionization occurs at atmospheric pressure and temperature and no sample preparation is required.

Some of the more popular ambient ionization sources include desorption electrospray ionization (DESI) and direct analysis in real time (DART).[28-31] DESI uses a primary ESI spray plume directed at an angle towards a sample surface from which primary droplets desorb the analyte from the surface.[30] Impact on the thin film surface generates secondary droplets containing the desorbed analyte at a complementary angle toward the inlet of the MS for direct analysis. Some

other variants of ambient ionization techniques include paper spray ionization (PS), extractive and electrospray ionization (EESI).[30-32] Paper spray ionization is an ambient ionization technique which the analyte of interest in placed on a paper substrate that is cut to a sharp tip, solvent is added creating a chromatographic step and the solvent wicks through the paper.[33-35] Once a voltage (3-5 kV) is applied, an electrospray plume is formed from the tip of the paper creating various spray methods depending on the amount of solvent applied to the paper (microdroplets vs thin film). Easy ambient sonic spray ionization (EASI) is a simple variant of ESI in which a flow rate sheath gas is used to provide a soft desolvation method in comparison to ESI, and does not require the need for an applied voltage.[36]

Manipulation of Chemical Reactions

The monitoring of chemical reactions by MS has been utilized in numerous applications, and has increasingly become the preferred method for the investigation of many types of reactions.[2,6] This method is characterized as either an online or offline analysis for probing reaction species, kinetic rates, percent yields and reaction completion.[21] Additionally, the ability to monitor reaction intermediates can provide essential information on the mechanistic pathway of the reaction. Typically, reaction monitoring is performed by offline analysis due to its simplicity, and reduced time constraints that can allow for replicate sampling. Online analysis can provide real-time kinetic information and is the mode of choice for relatively fast reactions with short-lived intermediates.[21] Reaction acceleration differs from reaction monitoring by performing the analysis under accelerating conditions, such as adding the effects of heat, distance, evaporation, pH, concentration, volume, etc.

1.2 References

1. L. Gao, Q. Song, G. E. Patterson, R. G. Cooks and Z. Ouyang; Analytical Chemistry, 2006, 78, 5994-6002.
2. L. Li, T.-C. Chen, Y. Ren, P. I. Hendricks, R. G. Cooks and Z. Ouyang; Analytical Chemistry, 2014, 86, 2909-2916.
3. L. Gao, A. Sugiarto, J. D. Harper, R. G. Cooks and Z. Ouyang; Analytical Chemistry, 2008, 80, 7198-7205.

4. Y. Ren, J. Liu, L. Li, M. N. McLuckey and Z. Ouyang; Analytical Methods, 2013, 5, 6686-6692.

5. Zumla A, George A, Sharma V, Herbert N, Baroness Masham of Ilton (2013) Lancet 382(9907):1765–1767.

6. Monkongdee P, et al. (2009) Am J Respir Crit Care Med 180(9):903–908.

7. World Health Organization (2013) (WHO, Geneva).

8. Liu C, Zhao Z, Fan J, Lyon CJ, Wu HJ, Nedelkov D, Zelazny AM, Olivier KN, Cazares LH, Holland SM, et al. Proc Natl Acad Sci U S A. 2017;114(15):3969–74.

9. D.G. Peters, C. Ji. J. Chem. Educ., 83 (2) (2006), p. 290

10. P.E. Young, A. Campbell. J. Chem. Educ., 59 (8) (1982), p. 701

11. S.F. Teunissen, A.M.A.P. Fernandes, M.N. Eberlin, R.M. Alberici. TrAC Trends Anal. Chem., 90 (Suppl. C) (2017), pp. 135-14.

12. Fedick, P. W.; Bain, R. M.; Bain, K.; Mehari, T. F.; Cooks, R. G. Int. J. Mass Spectrom. 2018, 430, 98– 103, DOI: 10.1016/j.ijms.2018.05.009.

13. Raker, J.; Holme, T.; Murphy, K. J. Chem. Educ. 2013, 90 (11), 1443– 1445, DOI: 10.1021/ed400175w.

14. Yan, X.; Bain, R. M.; Cooks, R. G. *Angew. Chem., Int. Ed.*2016, *55* (42), 12960– 12972, DOI: 10.1002/anie.201602270

15. 15 Bain, R. M.; Pulliam, C. J.; Yan, X.; Moore, K. F.; Müller, T.; Cooks, R. G. *J. Chem. Educ.* 2014, *91* (11), 1985– 1989, DOI: 10.1021/ed500288m

16. 16. Bain, R. M.; Pulliam, C. J.; Raab, S. A.; Cooks, R. G*J. Chem. Educ.* 2016, *93*(2), 340– 344, DOI: 10.1021/acs.jchemed.5b00263

17. Schrader, R.; Fedick, P.; Mehari, T.; Cooks, R. Journal of Chemical Education 2019 96 (2), 360-365. DOI: 10.1021/acs.jchemed.8b00658.

18. Jarmusch AK, Pirro V, Baird Z, Hattab EM, Cohen-Gadol AA, Cooks RG. Proc Natl Acad Sci U S A. 2016;113(6):1486–91.

19. Baumann, M.; Baxendale, I. R., J. Org. Chem. 2015, 11, 1194-1219.

20. Malet-Sanz, L.; Susanne, Flavien., J. Med. Chem. 2012, 55 (9), 4062-98.

21. Vikse, K. L.; Ahmadi, Z.; Manning, C. C.; Harrington, D. A.; McIndoe, J. S. Angew. Chem. Int. Ed. 2011, 50 (36), 8304-6.

22. Wu, C.; Qian, K.; Nefliu, M.; Cooks, R. G. J. Am. Soc. Mass Spectrom. 2010, 21, 261-7.

23. Wu, C.; Ifa, D. R.; Manicke, N. E.; Cooks, R. G., Anal Chem. 2009 Sep 15;81(18):7618 doi: 10.1021/ac901003u.

24. M. Girod, E. Moyano, D. I. Campbell and R. G. Cooks, Chem. Sci., 2011, 2, 501–510.

25. S. Narayan, J. Muldoon, M. G. Finn, V. V. Fokin, H. C. Kolb and K. B. Sharpless, Angew. Chem. Int. Ed., 2005, 44, 3275– 3279; Angew. Chem., 2005, 117, 3339–3343.

26. Fenn, J. B.; Mann, M.; Meng, C. K.; Wong, S. K.; Whitehouse, C. M. Science 1989, 246,64.

27. Smith, R. D.; Loo, J. A.; Edmonds, C. G.; Barinaga, C. J.; Udseth, H. R. Anal. Chem. 1990,62, 882.

28. Lee, J. K.; Banerjee, S.; Nam, H. G.; Zare, R.N., Q Rev Biophys. 2015,48, 437-444.

CHAPTER 2. REACTION MONITORING OF HETEROGENEOUS CHEMICAL REACTIONS BY LAB-DESIGNED SAMPLING PROBE

2.1 Abstract

The ability to monitor reactions is vital in many industries (e.g., manufacturing of chemicals, petrochemicals, pharmaceuticals, and polymers) in order to ensure product purity and quality. In addition to improving product quality, effective monitoring of manufacturing processes alleviates the dependence of analytical testing at the end stage of production, which in turn reduces cost and time. Unfortunately, monitoring of batch slurry reactions at the site of production is challenging and usually requires extensive sample preparations before analysis of the heterogeneous reaction mixtures. Reaction monitoring by mass spectrometry (MS) can provide real-time information about reaction progress; however, previous efforts have been limited to homogeneous solutions. Heterogeneous reactions pose challenges with uniform sampling and clogged plumbing which limit the utility of previous devices.

We demonstrate the simplest setup to achieve heterogeneous reaction monitoring through the use of a lab-built sample probe which is capable of acquiring reproducible kinetic information of pharmaceutically important, slurry-like mixtures. Proof of concept experiments were conducted by monitoring three heterogeneous reactions: (i) esterification of nicotinic acid, (ii) amide bond formation from an amine, and (iii) iodine catalyzed boc protection of a diamine. These highly concentrated solutions can be tracked over time without fear of clogging spray emitters or saturation of ion detection, by using common laboratory supplies. Dissolution solvent (DS) serves a dual purpose by assisting in stable spray quality and washing of probe between each sample measurement. Furthermore, with the addition of internal standards to the dissolution solvent it is expected that quantitative analysis may be achieved. Addition setup including peek tubing, with an attached split valve for waste, attached to a nESI ionization source would allow for a fully automated sampling approach.

2.2 Introduction

Heterogeneous reactions are used in the synthesis of drugs, reagents, polymers, and a number of other chemical-based products. The potential for the efficient, detailed analysis of these types of reactions continues to draw interest from a broad range of disciplines in academia and industry.[1-5] Reaction progress measurements of the changes in starting materials, reaction intermediates, and major and minor reaction products can be monitored over the course of a chemical reaction, providing important mechanistic details of a chemical reaction.[3 ,4, 6-10] Most analytical methods are developed for the analysis of homogeneous solutions due to the instrumentation available, and the necessity for sample preparation.

Mass spectrometry has proven to be a useful tool in reaction monitoring as it allows scientists to monitor the reaction kinetics of a wide range of reactions, as well as identify final reaction products.[11-13] Additionally, it is these details that allow scientists to optimize current reactions or to create new chemical processes. However, this valuable information can become lost due to the lack of current analytical technology capable of observing chemical transformations under particular synthetic conditions.[4, 14, 15] This is particularly true for reactions involving heterogeneous reagents, especially solid/liquid slurries. A number of techniques allow for monitoring in real time, including FT-IR, UV-vis and EPR spectroscopy.[16-18] However, these techniques only monitor soluble components of a reaction, and require additional equipment such as compressed reactors or multi-configuration valve systems.

Herein, we describe a prototype sampling probe capable of sampling heterogeneous slurry (solid and solution) reactions. A lab-designed, sampling probe containing two fused-silica capillaries is placed directly in line with a continuously stirring heterogeneous reaction mixture in the open position to allow reaction solution to flow through the probe into a compartment held at a fixed volume, without interrupting the flow of the slurry. When the probe is set to the closed position, and the dissolution solvent is directly delivered to the trapped reaction sample through one of the connecting capillary lines. The addition of a syringe pump would further allow for flexibility of flow rates and dilution factors, although this has been tested for feasibility, it has not been implemented for the generation of the kinetic data represented in this chapter. The homogeneous sample is then extracted through the second capillary and analyte ions are directly analyzed by mass spectrometry using nano-electrospray ionization (nESI). This ionization method uses non-accelerating conditions that are ideal for the monitoring of bulk-phase reactions.[14, 19, 20]

The rate of conversion can be calculated as a ratio of the product signal intensity vs. the reactant signal intensity of the chemical reaction as a function of time. Kinetic data is represented as a time profile displaying the reaction progress of three proof-of-concept, heterogeneous chemical reactions: (i) esterification of nicotinic acid with n-octanol, (ii) amide bond formation of a diamine with benzoyl chloride (iii) a molecular iodine catalyzed, N-BOC protection of 2-aminopyridine. The absolute signal intensity of all starting materials, intermediates, products and by products *m/z* peaks are summed together to act as a normalization tool. The individual peak intensities are divided by the summed quantity and the average of three replicates is represented by a data point at each corresponding time point. This is an approximation as it assumes there is negligible difference in the ionization efficiency between the starting material and the product formed.

2.3 Experimental

2.3.1 Reagents

All chemical reagents were purchased from Sigma-Aldrich (St. Louis, MO) and used as received without further purification.

2.3.2 Sampling Probe

The lab-designed sampling probe was composed of a stainless steel sample compartment attached to a copper pipe containing two fused-silica capillaries, each attached to a syringe. The probe was set to the open position and directly introduced into a heterogeneous reaction mixture to allow undisturbed flow of the reaction solution, while capturing the reaction on the compartment walls as it flows through the probe. As the probe is removed from the reaction slurry, it is kept in the open position allowing for the majority of the mixture to return to the slurry solution and only a small aliquot of the heterogeneous sample remains in the sampling chamber. The sampling probe is then set to the closed position, and the dissolution solvent (1:1 ACN/DCM), is directly delivered to the sample compartment through one capillary, ie. the introduction capillary. The sampling compartment can hold a maximum volume of 400 µL without causing overflow into the copper tubing. Applied positive pressure as a result of the syringe introducing the DS into the first capillary allows for simultaneous desolvation and dissolution in the same process. The newly

homogeneous sample is extracted through the secondary capillary, ie. withdrawal capillary, by the negative pressure applied by the second syringe. Sample aliquots (<10 µL) of the diluted reaction mixture were directly analyzed via nESI-MS. Dissolution solvent was then washed through capillary lines twice to eliminate any cross contamination, and confirmed as the MS spectra of the second wash being nearly identical to that of blank solution.

2.3.3 Batch synthesis of N-methylnicotinic acid

A solution mixture containing 3.08g (25 mmol) of nicotinic acid and 6.25 mL (100 mmol) methyl iodide in 75 mL of ethanol was refluxed for 4 hours, then cooled in an ice-bath for 20 minutes. The suspension was filtered, and yellow crystalline solid was recrystallized in ethanol. MS (ESI+): m/z (%) 138 (100, $[M]^+$). 1H NMR (400 Hz/55 MM).

2.3.4 Batch synthesis of octyl 1-methyl-1-pyridine-3-carboxylate

Reaction solution containing 1.23 g (10 mmol) of nicotinic acid and 623 µL (10 mmol) of methyl iodide is added to 10 mL of dichloromethane (DCM). 61 mg (5 mol %) of dimethylaminopyridine (DMAP) and 3.14 mL (20 mmol) of 1-octanol was stirred at room temperature. Reaction mixture is cooled over ice. 2.26 g of dicyclohexylcarboiimide (DCC) is added to cooled solution mixture and stirred over ice for 5 minutes.

2.3.5 Batch synthesis of N-(4-(dimethylamino)phenyl)benzamide

The acetonitrile solution (10 mL) of benzoyl chloride (0.309 g, 2.2 mmol) was added dropwise to an acetonitrile solution (20 mL) of N, N-dimethyl-p-phenylenediamine (0.272 g, 2 mmol) and allowed to stir at room temperature.

2.3.6 Batch synthesis of *tert*-butyl phenylcarbamate

To a magnetically stirred mixture composed of aniline (1 mmol) and $(Boc)_2O$ (1 mmol), a catalytic amount of iodine (10 mol %) in methanol (5 mL) was introduced at room temperature.

2.3.7 nESI-MS Analysis

Experiments were performed by spraying diluted, 10-uL aliquots directly into an LTQ ion trap mass spectrometer (Thermo Fisher Scientific, San Jose, CA) using nano-ESI (nESI) emitters with ca. 5 µm diameter tip made from pulled borosilicate glass using a Flaming/Brown micropipette puller (P-97 by Sutter Instruments).

2.4 Results and Discussion

2.4.1 Esterification reaction progress

Initially, the method was performed according to literature as a one-pot synthesis of nicotinic acid with n-octanol in the presence of dichloromethane (DCM), dicyclohexylcarboiimide (DCC) as the coupling agent, and 4-dimethylaminopyridine (DMAP) as the catalytic agent (Scheme 1a). Preliminary results demonstrate the difficulty with monitoring certain molecules by mass spectrometry. In order to calculate kinetic progress of the chemical reaction, a minimum of one starting material and the final product should be visible in the spectra throughout the course of the reaction. The protonated form of nicotinic acid results in the formation of a zwitterion which cannot be observed by mass spectrometry due to the presence of opposing charges present on one molecule. Subsequently, a minor peak at *m/z* 123 was observed for the catalyst.

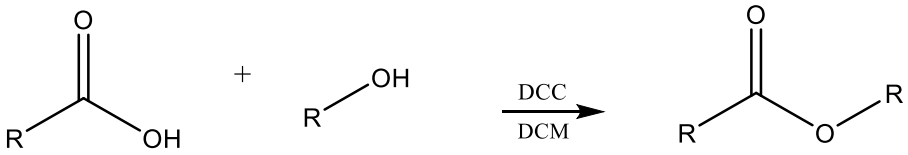

Scheme 2.1 Steglich Esterification of a carboxylic acid with a terminal alcohol.

We deliberately introduced methyl iodide into the previous method, and subsequently observed a new starting material peak at *m/z* 137 which corresponds to 1-methyl, 4-dimethylaminopyridine. Though this results in a loss of its catalytic ability by the addition of a methyl group on the pyridine, catalytic DMAP (*m/z* 123) is still present in the reaction and is consumed before the methylated version. We propose the mechanism for the formation of the ester (Scheme 1b) as a two-step process. Initially, the ester is formed by activation of the carboxylic

acid by DMAP which removes the hydrogen of the hydroxyl group, resulting in a nucleophilic attack by that oxygen onto one of the doubly bound nitrogens in DCC. This generates several rearrangements as DCC and DMAP provide and remove a hydrogen eventually forming an O-acylisourea intermediate. The activated carboxylic acid experiences a nucleophilic attack by the alcohol to form dicyclohexylurea (DCU) and the ester. The ester is more electrophilic than the remaining methylated DMAP and will abstract the methyl group to form the final reaction product.

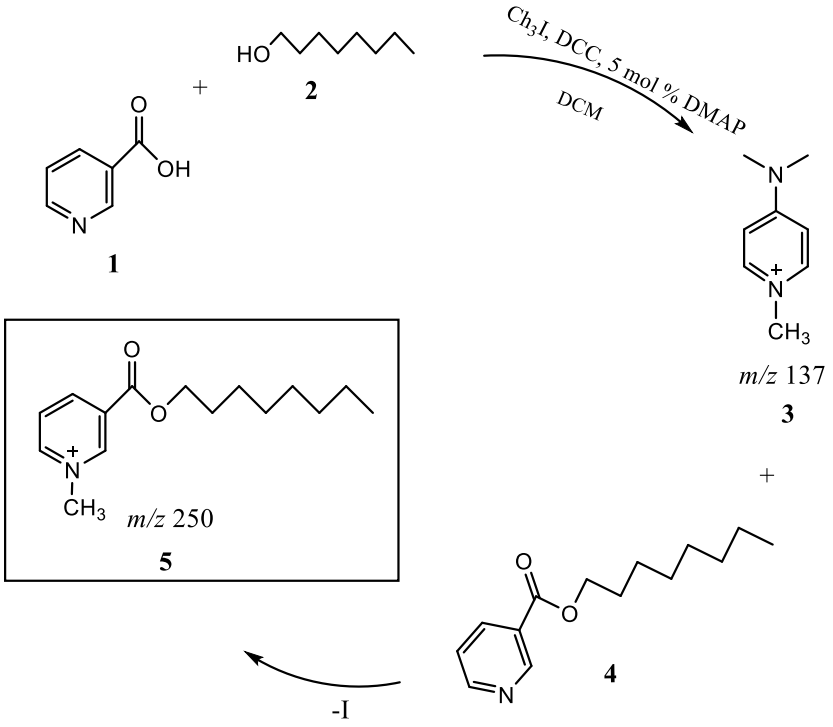

Scheme 2.2 DMAP-catalyzed esterification of a nicotinic acid and n-octanol.

In this reaction, DCC activates the carboxyl group of nicotinic acid and is accelerated by DMAP to eliminate side reactions by acting as an acyl transfer-agent. However, side products were initially observed at *m/z* 306 and *m/z* 337 (Fig 1.), corresponding to DCC derivatives identified by MS/MS data (Figure 2 and Figure 3). The signal intensity of these ions decrease greatly in the first twenty minutes, resulting in a corresponding signal increase in the starting material and product ion peaks (Fig. 4). Altogether, the starting material required forty minutes to reach its highest concentration as the parent peak based on signal intensity. Shortly after this time, the product signal reached its maximum signal intensity after approximately 400 minutes.

To validate the proposed mechanism, we synthesized 1, 4-methyl dimethylpyridine and trigonelline and repeated the experiments without methyl iodide to investigate the reaction mechanism (Fig.3).

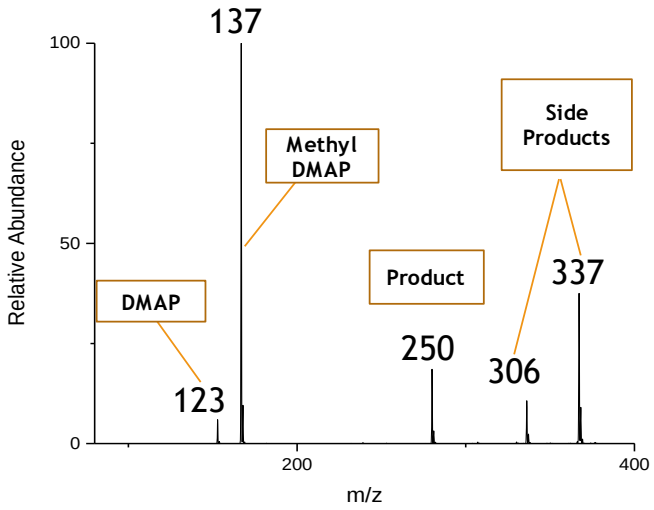

Figure 2.1 Nano electrospray ionization mass spectrum of reaction starting material, side products and final reaction product.

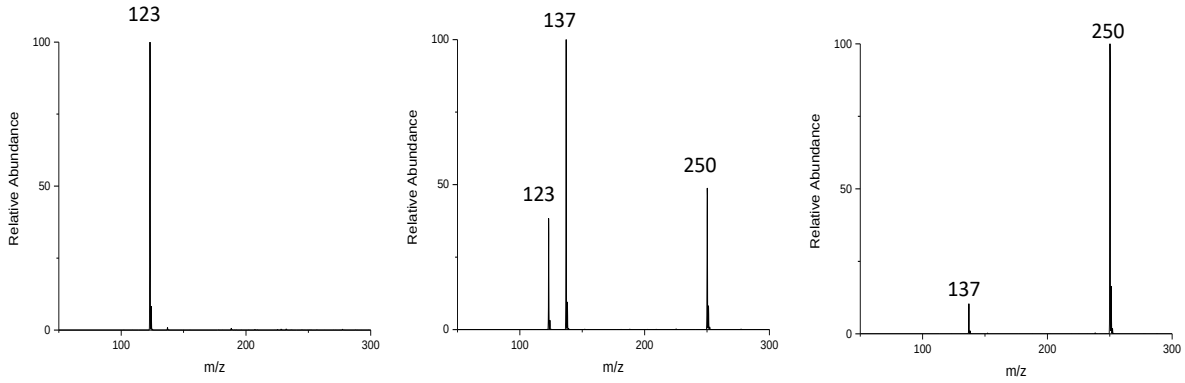

Figure 2.2 Representative MS of reaction progress of the esterification reaction

Here we form the same reaction product as evident in the tandem mass spectrometry data (Fig.3C and 3D), the ion at *m/z* 138 is the loss of the alcohol chain. In the case of N-methyl DMAP (Fig. 3A) there is no product formed, yet in the experiment using N-methyl nicotinic acid (Fig. 3B), there is relatively no signal intensity for any starting material.

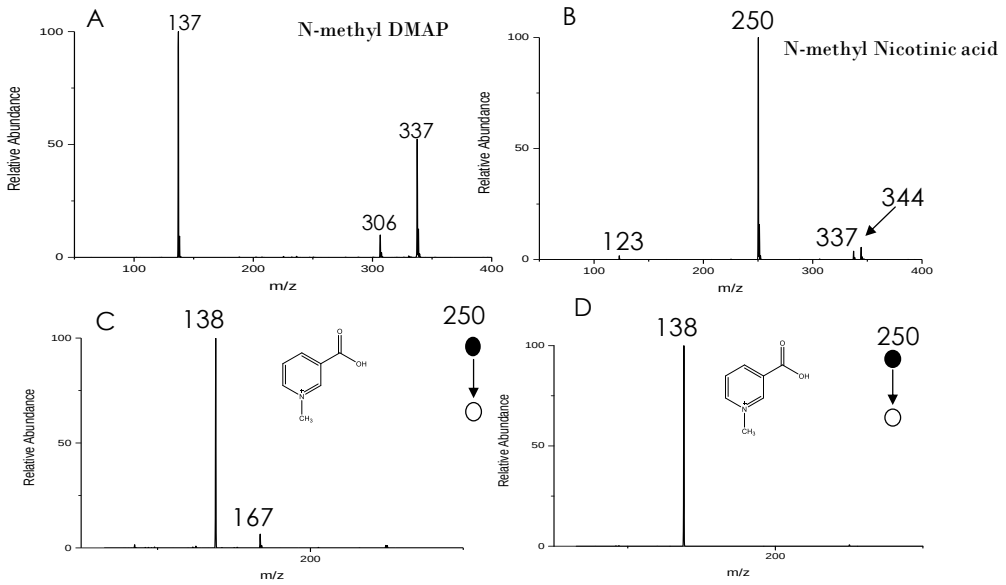

Figure 2.3 Nano electrospray ionization mass spectra of: A) full scan of the synthesized methylated DMAP. B) full scan of the synthesized methylated nicotinic acid. C) MS/MS spectra of reaction product from A. D) MS/MS spectra of reaction product from B.

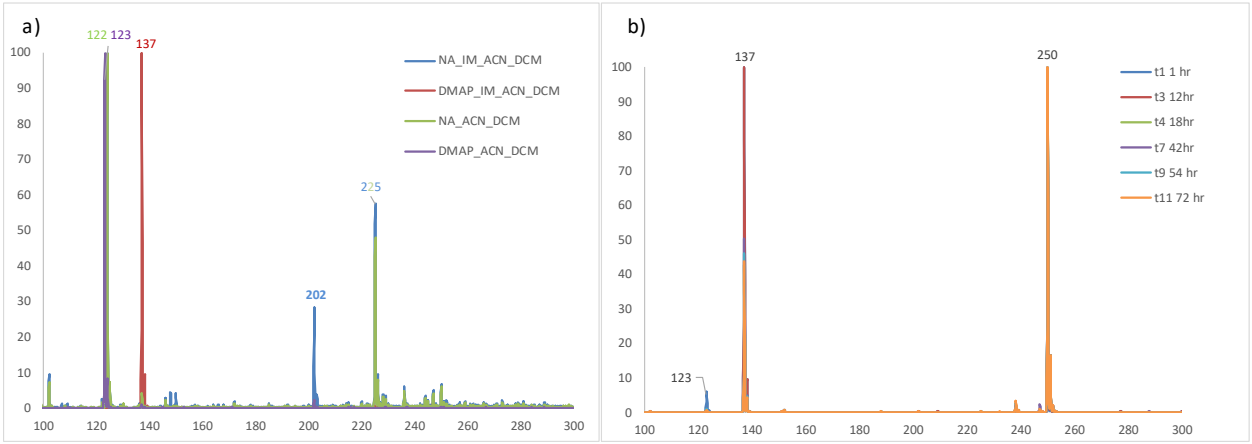

Figure 2.4 ESI-MS analysis of: a) reagents and side products present in reaction mixture, b) overlay of reagent ion intensity at *m/z* 137 and product ion intensity at *m/z* 250.

2.4.2 Acylation reaction progress

Additionally, we further tested the capability of the heterogeneous sampling probe by monitoring the acylation of N, N-dimethyl-p-phenylenediamine (DMPA) by benzyl chloride (Scheme 2). In this reaction, the carbonyl group of the benzyl chloride experiences a nucleophilic attack by the lone pair on the diamine, which is followed by an elimination of the chloride. Here, the formation of the product ion peak occurred relatively quickly in comparison to the previous reaction (Fig. 4).

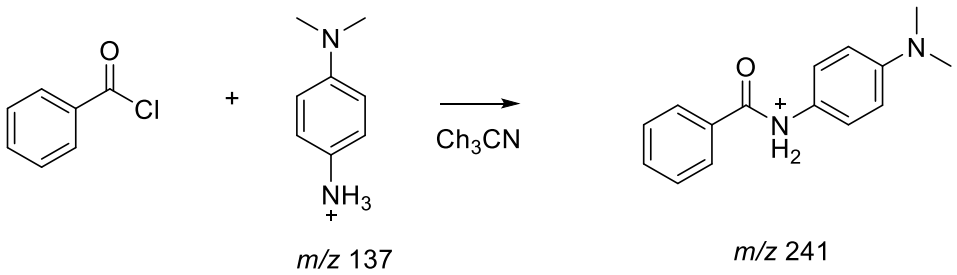

Scheme 2.3 Amide bond formation between an acyl chloride and an amine.

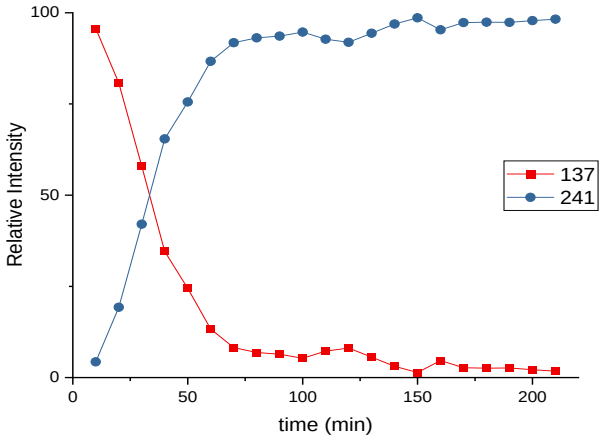

Figure 2.5 Kinetic profile for the acylation reaction progress as an amine (*m/z* 137) is converted into a diamine (*m/z* 241).

Within five minutes, new signals at *m/z* 241 and *m/z* 263 appeared correlating to the product ion and its sodiated adduct, respectively. The product ion signal intensity reached its maximum

after approximately one hour of reaction time. Signal intensity of the sodiated product ion peak was incorporated into the calculation for the conversion ratio.

2.4.3 Protection reaction progress

Multistep organic synthetic reactions frequently utilize functional groups such as tert-butoxycarbonyl (BOC) to aid the protection and deprotection of specific organic compounds. The benefits of the synthetic method for protection and deprotection throughout a multistep synthesis containing specific functional groups that may need to be conserved, allows for chemoselective transformations. A protecting group is often introduced prior to a particular reaction step and later removed, in order to preserve a specific group that otherwise would not survive. There are numerous types of protecting groups, each with individual requirements that must be met to cause their removal once the molecule has progressed to a stage in the reaction scheme that will not cause reactivity at the functional group in the remaining steps. The mild, selective, and efficient protecting group used in this experiment is commonly referred to as "Boc" and is primarily utilized in the protection of amines in multistep syntheses, due to its stability toward catalytic hydrogenation and resistance against basic and nucleophilic reactions. Its most extensive use is found in the areas of peptide synthesis and medicinal chemistry.

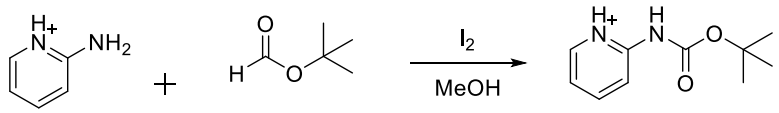

m/z 95 *m/z* 102 *m/z* 195

Scheme 2.4 Amine protection between a tert-butoxycarbonyl and a diamine.

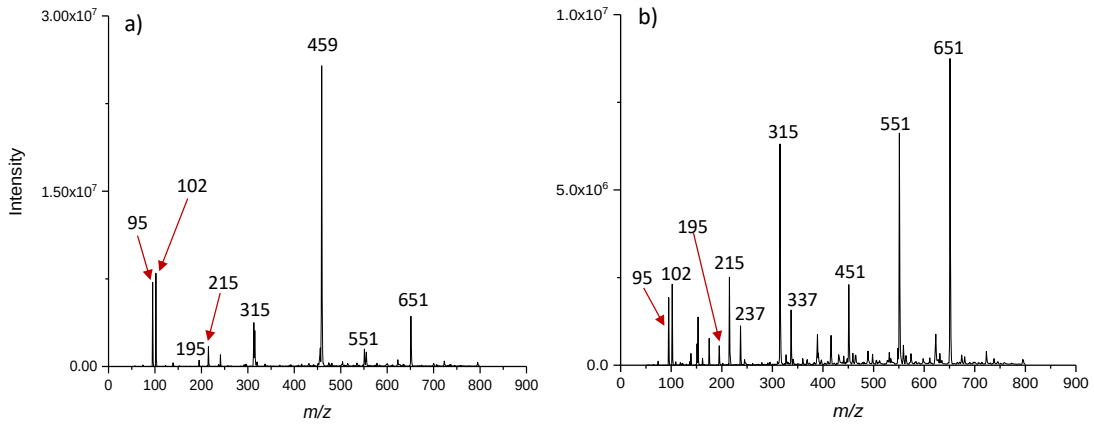

Figure 2.6 MS analysis of the protection reaction progress: a) after initial mixing; b) after 24 hrs.

2.5 Conclusions

These specific reactions were selected based on their fundamental importance in organic synthesis. All three proof-of-concept reactions demonstrate the robustness of the sampling probe for heterogeneous reaction monitoring by mass spectrometry using various organic solvents under different conditions for a range of reaction times.

2.6 References

1. Baumann, M.; Baxendale, I. R., The synthesis of active pharmaceutical ingredients (APIs) using continuous flow chemistry. Beilstein J. Org. Chem. 2015, 11, 1194-1219.

2. Malet-Sanz, L.; Susanne, Flavien., Continuous flow synthesis. A pharma perspective. J. Med. Chem. 2012, 55 (9), 4062-98.

3. Yan, X.; Sokol, E.; Li, X.; Li, G.; Xu, S.; Cooks, R. G., On-line reaction monitoring and mechanistic studies by mass spectrometry: Negishi cross-coupling, hydrogenolysis, and reductive amination. Angew. Chem. Int. Ed. 2014, 53, 5931-5.

4. Rougeot, C.; Situ, H.; Cao, B. H.; Vlachos, V.; Hein, J. E., Automated reaction progress monitoring of heterogeneous reactions: crystallization-induced stereoselectivity in amine-catalyzed aldol reactions. React. Chem. Eng. 2017, 2, 226-31.

5. Leu, M., Heterogeneous reactions of N_2O_5 with H_2O and HCl on ice surfaces: Implications for Antarctic ozone depletion. Geophys Res Lett. 1988, 15 (8), 851-4.

6. Espy, R. D.; Wleklinski, M.; Yan, X.; Cooks, R. G., Beyond the flask: Reactions on the fly in ambient mass spectrometry. Trends Anal. Chem. 2014, 57, 135-146.

7. Yan, X.; Bain, R. M.; Li, Y.; Q, R.; Flick, T.; Cooks, R. G., Online inductive electrospray ionization mass spectrometry as a process analytical technology tool to monitor the synthetic route to Anagliptin. Org. Process Res. Dev. 2016, 20, 940-7.

8. Augusti, R.; Chen, H.; Eberlin, L. S.; Nefliu, M.; Cooks, R. G., Atmospheric pressure Eberlin transacetalization reactions in the heterogeneous liquid/gas phase. Int. J. Mass Spectrom. 2006, 253 (3), 281-7.

9. Banerjee, S.; Zare, R. N., Syntheses of Isoquinoline and Substituted Quinolines in Charged Microdroplets. Agnew. Chem. Int. Ed. 2015, 54 (49), 14795-9.

10. Bain, R. M.; Pulliam, C. J.; Thery, F.; Cooks, R. G., Accelerated Chemical Reactions and Organic Synthesis in Leidenfrost Droplets. Angew. Chem. Int. Ed. 2016, 55 (35), 10478-82.

11. Lee, J. K.; Banerjee, S.; Nam, H. G.; Zare, R. N., Acceleration of reaction in charged microdroplets. Quart. Rev. Biophys. 2015, 48 (4), 437-44.

12. Yan, X.; Bain, R. M.; Cooks, R. G., Organic Reactions in Microdroplets: Reaction Acceleration Revealed by Mass Spectrometry. Angew. Chem. Int. Ed. 2016, 55 (42), 12960-12972.

13. Lee, J. K.; Kim, S.; Nam, H. G.; Zare, R. N., Microdroplet fusion mass spectrometry for fast reaction kinetics. Proc. Natl. Acad. Sci. 2015, 112 (13), 3898-3903.

14. Iyer, K.; Yi, J.; Bogdan, A.; Talaty, N.; Djuric, S. W., R. G., Accelerated multi-reagent copper catalyzed coupling reactions in micro droplets and thin films. React. Chem. Eng. 2018, 3 (2), 206-9.

15. Santos, S. S.; Rosso, G. B.; Pilli, R. A.; Eberlin, M. N., The mechanism of the Stille reaction investigated by electrospray ionization mass spectrometry. J. Org. Chem. 2007, 72 (15), 5809-12.

16. Foley, D. A.; Doecke, C. W.; Buser, J. Y.; Merritt, J. M.; Murphy, L.; Kissane, M.; Collins, S. G.; Maguire, A. R.; Kaerner, A., ReactNMR and ReactIR as reaction monitoring and mechanistic elucidation tools: the NCS mediated cascade reaction of α-thioamides to α-thio-β-chloroacrylamides. J. Org. Chem. 2011, 76 (23), 9630-40.

17. Grabow, K.; Bentrup, U., Homogeneous catalytic processes monitored by combine in situ ATR-IR, UV-Vis and Raman spectroscopy. ACS Catal. 2014, 5 (4), 2153-64.

CHAPTER 3. REACTION ACCELERATION AT AIR-SOLUTION INTERFACES: ANISOTROPIC RATE CONSTANTS FOR KATRITZKY TRANSAMINATION

3.1 Abstract

The acceleration of chemical reactions in confined volumes has been widely demonstrated in many systematic studies and these accelerated rates are attributed to the limited solvation of the reactants at the surface. Interest in the role of the air-solution interface in these reaction rate acceleration studies has increased. This study investigated the factors controlling reaction rates in bulk solutions of constant surface area, yet different volumes over a concentration range covering three orders of magnitude. Rate acceleration factors (relative to bulk) of more than an order of magnitude were observed by mass spectrometry in the reaction rate acceleration of the Katritzky transamination reaction of p-anisidine with three pyrylium salts of varying surface activities. Strikingly, results demonstrate that the significant role of interfacial effects on Katritzky reaction acceleration seen in confined systems of small volumes can be replicated in bulk solutions.

3.2 Introduction

Significant interest in the manipulation of the kinetic rates of chemical reactions is a primary objective in chemical and pharmaceutical industries where time and cost is a major consideration. Many mass spectrometric studies have demonstrated reaction rate acceleration in confined volumes including Leidenfrost levitated droplets[1-11], emulsions[12-17], micelles[18], depositions of thin films[19-21], microfluidic devices[22], charged microdroplets[23-33] from electrospray ionization and other spray methods. Observations of these enhanced rates have been attributed to several contributing factors such as desolvation, droplet size and lifetime, temperature, reagent confinement and interfacial effects unique to the air-solvent interface. These interfacial effects are hypothesized to be due to partial solvation of the reactants at the interface demonstrated by enhanced reactivity in microdroplet reactions. Evidence favors the high surface to volume ratio as an important feature of acceleration by creating a more reactive environment at the surface. Empirical observations of enhanced surface adsorption of reactants and products in numerous

droplet studies indicate the reaction rates increased by several orders of magnitude when compared to the corresponding reaction conducted in the bulk solution.

Traditionally, the bulk solution serves as a corresponding control in accelerated studies and must be conducted under relatively harsh conditions. The use of an acid or base for catalysis provides an alternative reaction pathway at a lower activation energy. Thermal acceleration due to elevated temperatures increases molecular interactions between reactants, while agitation by stirring also allows for faster diffusion and mixing. This is a directly related to the higher activation energy demand for desolvation in the condensed phase required for the reaction to proceed, and resulting in the slower reaction rate. Studies have shown the capability to accelerate bulk reaction mixtures by solvent removal in a rotary evaporator causing an increased rate due to a concentration effect of the reagents[34]. In nearly all cases, a typical bulk reaction is held at a constant volume and allowed to reach completion before any solvent removal[34]. In this study, we report enhanced rate effects observed in bulk solutions of confined volumes, conducted under ambient conditions, and without the need for the addition of a catalyst or laboratory apparatus. By removing several factors known to affect reaction rates; such as pH changes and reagent concentration due to solvent evaporation, results provide evidence that increased surface area-to-volume ratios is a dominate factor responsible for interfacial reactivity in these reactions.

3.3 Experimental

3.3.1 Reagents

2,4,6-Triphenylpyrylium tetrafluoroborate (98%), 2,4,6-tri(*p*-tolyl)pyrylium tetrafluoroborate salt (≥95%), 2,4,6-trimethylpyrylium tetrafluoroborate and *p*-anisidine (≥99%) were purchased from Sigma-Aldrich while acetonitrile (Optima® grade) was purchased from Fisher Scientific. Reagents were used as received and dissolved in pure acetonitrile to prepare stock solutions in plastic Eppendorf tubes. Reaction solutions over a large concentration range were prepared by serial dilution in acetonitrile, then freshly mixed in stoichiometric amounts to the desired reaction mixture concentration just before the analysis.

3.3.2 Batch experiments

Bulk kinetic studies were performed under ambient conditions with total volumes of either 0.3 mL or 1.2 ml of reaction mixtures. Equimolar solutions which were first thoroughly mixed by pipet and subsequently allowed to remain undisturbed in plastic sample vials for a designated amount of time. Periodic sampling was conducted using 10-μL aliquots for analysis by nanoelectrospray with an ion trap mass spectrometer.

3.3.3 nESI-MS experiments

Standard, thick- wall borosilicate glass without filament (B150-86-10) was purchased from Sutter Instruments, cleaned by sonication in an organic solvent mixture (acetone: methanol: 2-propanol = 1: 1: 2; HPLC grade) to remove any organic contaminates, flushed with deionized water to remove solvents and oven dried. The cleaned glass capillaries were allowed to cool to room temperature before being pulled into nESI spray emitters with ca. 2 um tip inner diameter using a Flaming/Brown micropipette puller (P-97 by Sutter Instruments). The newly fabricated tip diameter was then estimated from the measurement of the scale located in the eyepiece of a Konus™ Campus Binocular microscope (#5306) at 100x magnification. The nESI electrodes were created by fitting a Ag wire purchased from Warner Instruments and mounting in an E Series Electrode Holder. Non-accelerating conditions were maintained by clamping the nESI sprayer emitter to a ring stand placed very close (ca. 3 mm) to the instrument inlet. During nESI-MS analysis, the electrode is kept in constant contact with the sample aliquots placed in the glass capillary to determine reaction progress.

To avoid the possibility of signal carryover between analysis of each sample, the Ag electrode wire is wiped using Kimwipes from Kimtech Science® saturated with methanol to eliminate any cross contamination between sampling. No carry-over signal was detected in MS spectra of blank solutions composed of pure acetonitrile collected in between trials. All experiments were performed using an LTQ instrument (ThermoFisher, San Jose, California) for mass analysis. Nanoelectrospray analysis in the positive ion mode was performed with a 1.5 kV potential applied directly to the electrode by a copper alligator clip. Optimized instrumental parameters included a heated inlet capillary temperature of 300 °C. Low-current potentials of 15 V and 65 V were applied to the inlet capillary and tube lens; respectively. All mass spectra were

recorded in a mass range from m/z 50 -700 and represented as an average of 100 scans. Data processing for rate constant calculations correspond to peak height ratios of the ion intensities of interest.

3.4 Results and discussion

3.4.1 The Katritzky Transamination reaction

The model reaction selected for surface interrogation is the Katritzky transamination of a pyrylium heterocycle, shown in **Scheme 1a**; this reaction converts an amine to a pyridinium salt.[36-42] Katritzky transamination reagents of 2,4,6-triphenylpyrylium tetrafluoroborate and *p*-anisidine were dissolved in acetonitrile in stoichiometric amounts without the addition of any external catalyst. This robust reaction allows for efficient reaction monitoring of the conversion of a pre-charged species into formation of a different pre-charged species analyzed by mass spectrometry.

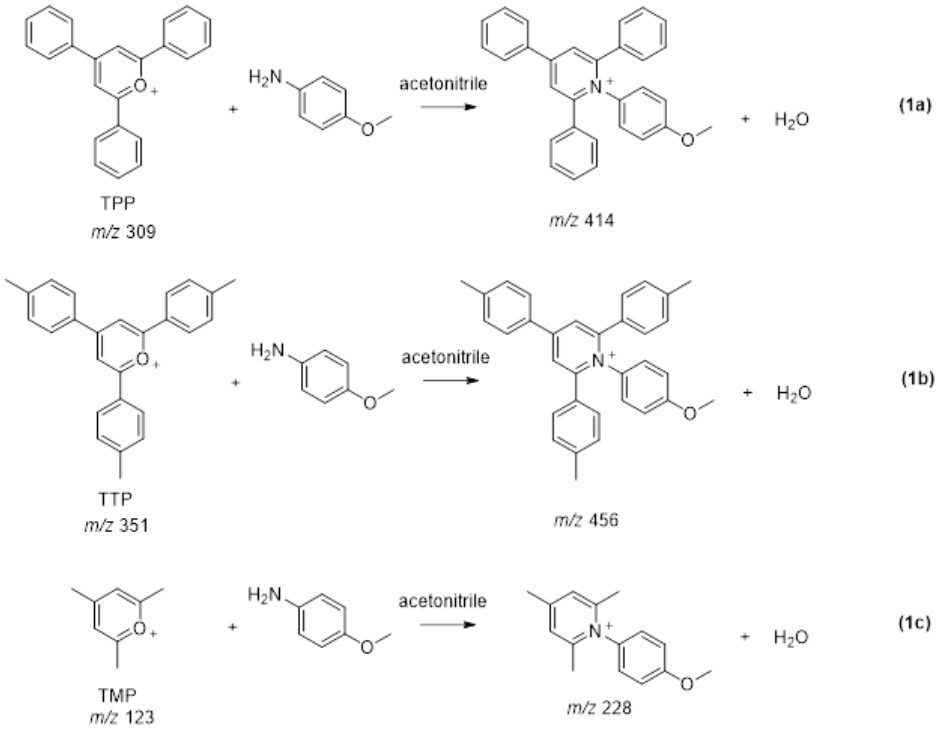

Scheme 3.1 Katritzky transamination: the reaction between pyrylium salts (TPP, TTP, TMP) and *p*-anisidine to form pyridinium salts.

Charged species produce high ionization efficiencies of detection in a linear ion trap allowing for accurate measurements of reaction kinetics. This is evident in the linearity of signal intensity ratios between the two pre-charged compounds and observed concentration ratios as low 1 to 0.0001, as seen in **Figure 1**.

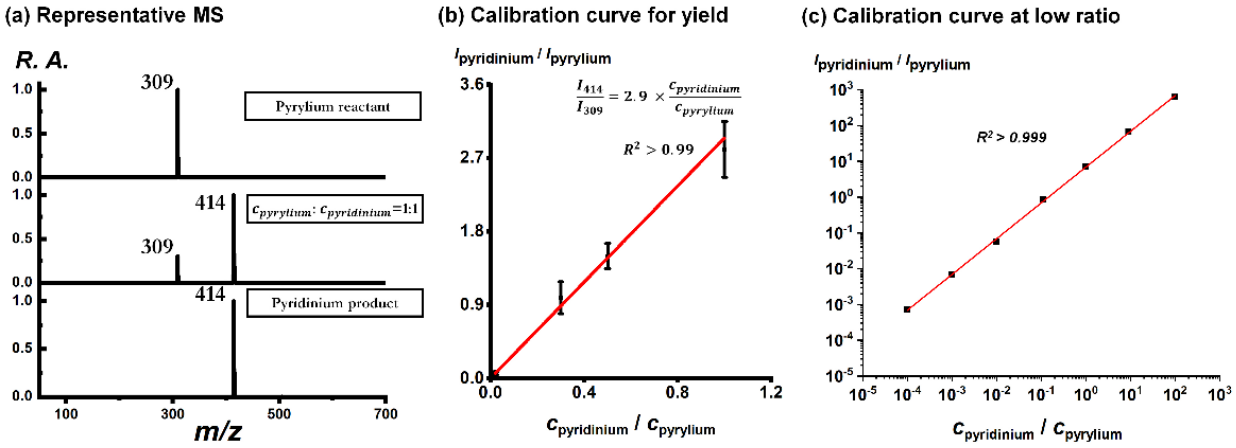

Figure 3.1 (a) Measured relative ion signals from mixed solutions of isolated product pyridinium and pyrylium reactant to calculate yield and rate constant. (b) Three replicates are shown in the calibration curve. (c) The linearity of a single replicate is good even at low concentration ratio.

Reaction acceleration in this study is directly reflective of phenomena occurring in the condensed phase reaction and not reflective of gas-phase chemistry due to MS analysis. Therefore, all nESI-MS measurements of product yield were collected by maintaining a significantly short distance (ca. 3mm) between the nESI sprayer tip and MS inlet to eliminate solvent evaporation which causes undesired reaction acceleration during the analysis step. MS analysis under non-accelerating conditions was confirmed by analyzing freshly mixed reaction solutions, which showed less than 0.1% yield at all concentrations (Figure 2), compared to minimum yield of 10 % of the same reaction under accelerated conditions at respective concentrations.

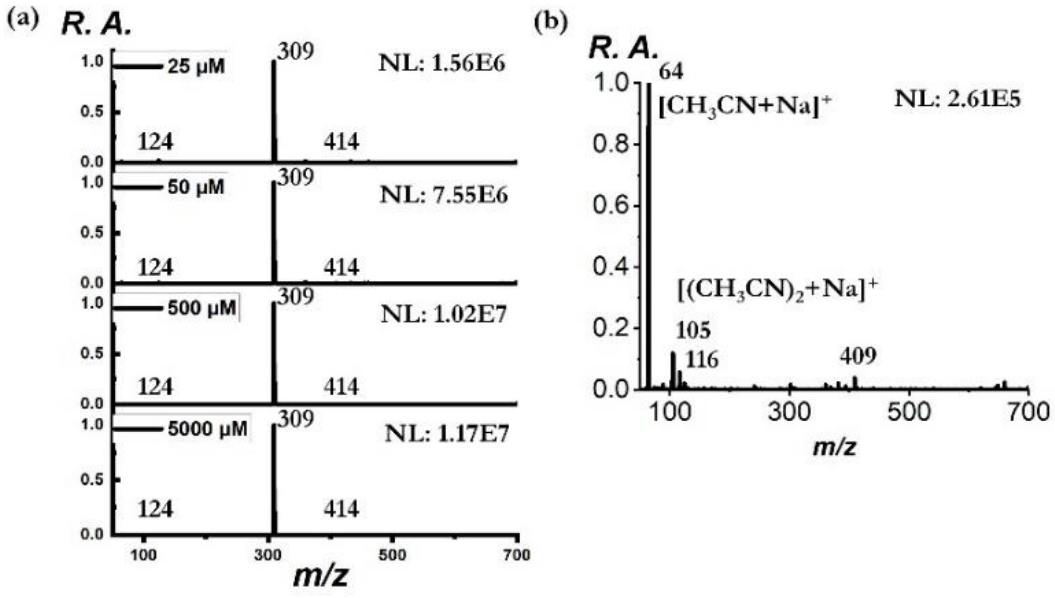

Figure 3.2 (a) Zero yields seen in full MS of freshly mixed reactant solution validated the non-accelerating nESI-MS analysis across the concentration range. (b) Test by MS shows no residue on the well plate after performing the Katritzky reaction in droplets (130 µL; 1000 µM) for 5 min

Ion intensity ratios of the reagent and product are obtained from the nESI analysis method as shown in Eq.1. Equation 2 is derived from Eq.1 to use the MS data to calculate concentrations at certain times in the kinetic studies. The underlying mechanism of the Katritzky reaction is shown in Scheme 2, and has been studied extensively. It is well understood that the reaction occurs by a number of fast steps leading to the ring opened intermediate, which proceeds the final electrocyclic ring closure step being the rate-limiting step. The use of a 2nd order rate equation to calculate the rate constant is validated in using Equation 3.

$$[\mathbf{reactant}] = \mathbf{2.9}\,[\mathbf{product}] \cdot \frac{I_{309}}{I_{414}} \qquad \textbf{Eq.1}$$

$$[\mathbf{reactant}] = \frac{[reactant]}{[product]+[reactant]} \cdot c_0 = \frac{2.9\,I_{309}}{I_{414}+2.9\,I_{309}} \cdot c_0 \qquad \textbf{Eq. 2}$$

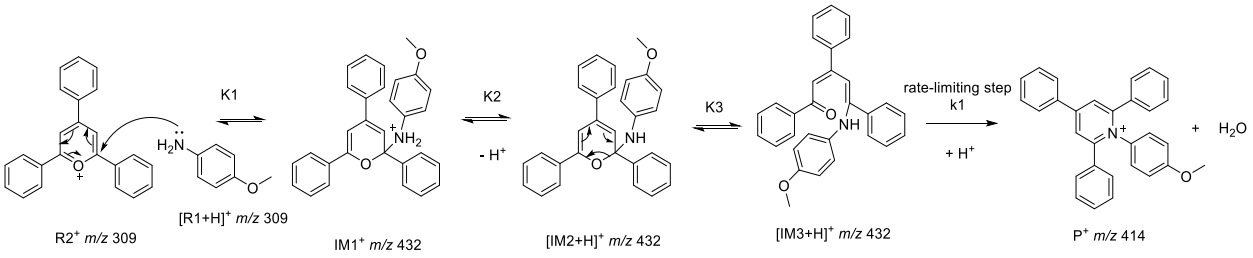

Scheme 3.2 Proposed mechanism of the model Katritzky reaction (note: K1, K2, K3 indicate equilibrium constants and k1 indicates rate constant.)

$$\frac{d[P]}{dt} = k1 \cdot [IM3][H^+] = k1 \cdot K3 \cdot [IM2][H^+] = k1 \cdot K3 \cdot K2 \cdot [IM1] \qquad \textbf{Eq. 3}$$

In the experiments, the two reactants were mixed in stoichiometrically equal amounts: $c(R1) = c(R1) = c_0$. At any time, *t*, assume that $[R1] = [R2] = c$, so $[P] = c_0 - c$, the rate equation can be written as follows:

$$rate = \frac{d[P]}{dt} = -\frac{dc}{dt} = k \cdot c^2$$

The integrated rate law for a 2nd-order reaction can then be expressed as:

$$-\int_{c_0}^{c} \frac{1}{c^2} \cdot dc = k \cdot \int_{0}^{t} dt$$

$$\frac{1}{c} - \frac{1}{c_0} = k \cdot t$$

Based on the integrated rate law for a 2nd-order reaction and Eq. 3, the rate constant *k*, as defined in **Eq. 4**, can be calculated using the MS ion intensity ratio, while taking into consideration the reaction time *t* and initial reactant concentration c_0.

$$k = \frac{[product]}{[reactant] \cdot t \cdot c_0} = \frac{I_{414}}{2.9\, I_{309} \cdot t \cdot c_0} \qquad \textbf{Eq. 4}$$

The MS intensities are corrected for ionization efficiencies after the calibration described in Figure 1. Tandem MS data was collected for each of the expected transamination products, as displayed in Figure 3.3. The spectra obtained for these compounds confirm the identity of the reaction products and are in agreeance with fragmentations found in literature.[13]

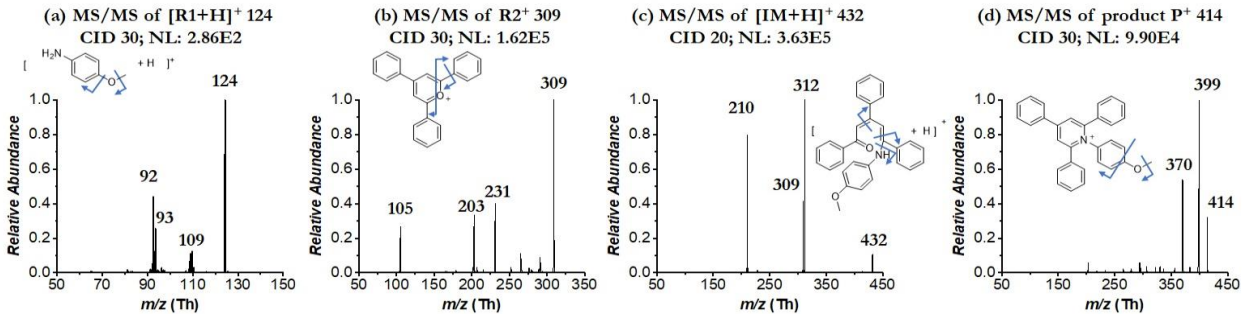

Figure 3.3 Tandem MS of reactants, intermediate and product for the model Katritzky reaction (isolation width used is not larger than 2 Th. CID refers to collision energy and NL to signal intensity).

Experiments were performed in bulk solutions of the Katritzky reagents by measuring the kinetics under different concentrations and reaction volumes. Interestingly, similar interfacial effects are observed in the undisturbed bulk solutions at room temperature, typically seen in confined systems of significantly smaller volumes. Concentrated reaction mixtures displayed no measureable difference in bulk kinetics between the 0.3-mL bulk and the 1.2-mL bulk reaction mixtures contained in cylindrical plastic vials of the same dimensions. However, at the lower concentration of 50 μM, the 0.3-mL bulk rate constant was 1.8-times greater than that observed in 1.2-mL bulk, as shown in (Figure 3.4).

The scope of the kinetic study was expanded to determine the extent of acceleration by providing a comparison between three different pyrylium salts, 2,4,6-triphenylpyrylium tetrafluoroborate (TPP), 2,4,6-tri(*p*-tolyl)pyrylium tetrafluoroborate (TTP), and 2,4,6-trimethylpyrylium tetrafluoroborate (TMP) as shown in **Scheme 1**.

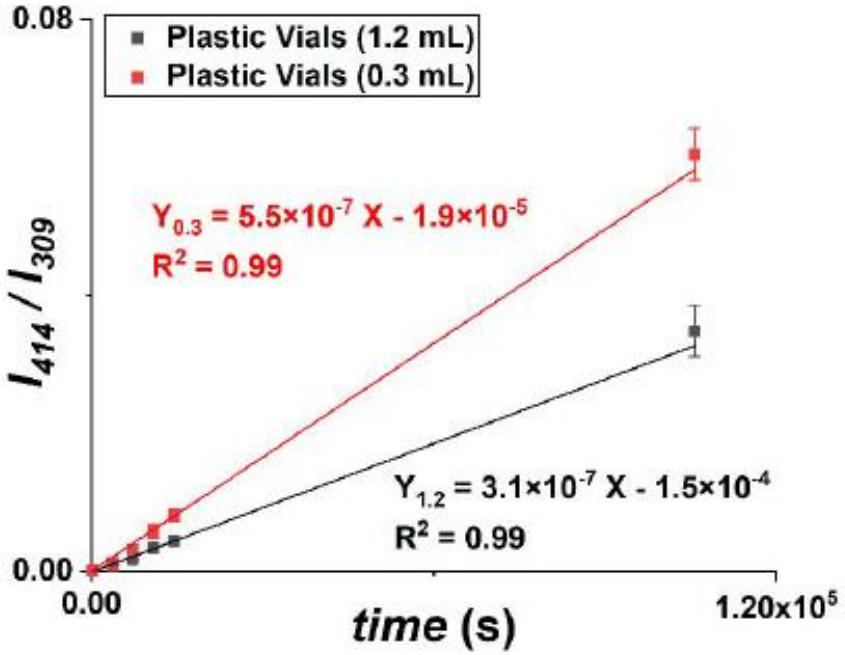

Figure 3.4 Bulk (0.3-mL and 1.2-mL) kinetics of the Katritzky reaction (Scheme 1a) at 50 μM.

Reaction monitoring by MS analysis was performed by recording signal intensity changes of the reactant and product cations over time to follow reaction progress. In these experiments, all three reactions were tested at 50 μM for two volumes representing two different surface-to-volume ratio systems. Reactions with TTP elicited the highest rate constant enhancement (1.9-fold, shown in Figure 3.5) which was slightly lower than that with TPP (1.8-fold), while reactions with TMP elicited the lowest rate constant enhancement (1.5-fold, shown in Figure 3.6) of the three pre-charged salts examined. Interestingly, the observed increase in surface affinity seems to directly correlate to the increase in electron density of the particular substituents bound to the pyrylium ring (-Ch_3> -Ph > -$PhCh_3$).

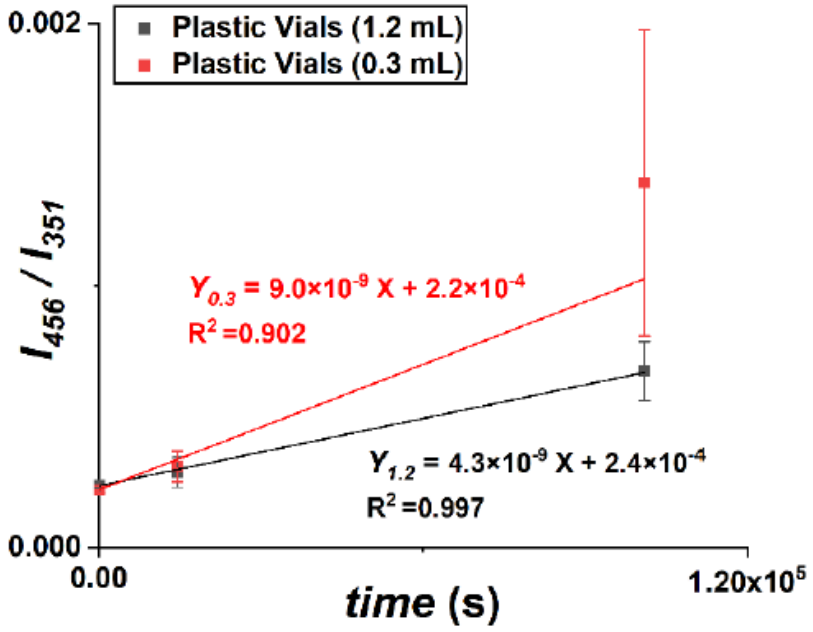

Figure 3.5 Bulk kinetics of Katritzky reaction (1b) using TTP as the reactant at 50 µM for two different volumes (0.3 mL and 1.2 mL)

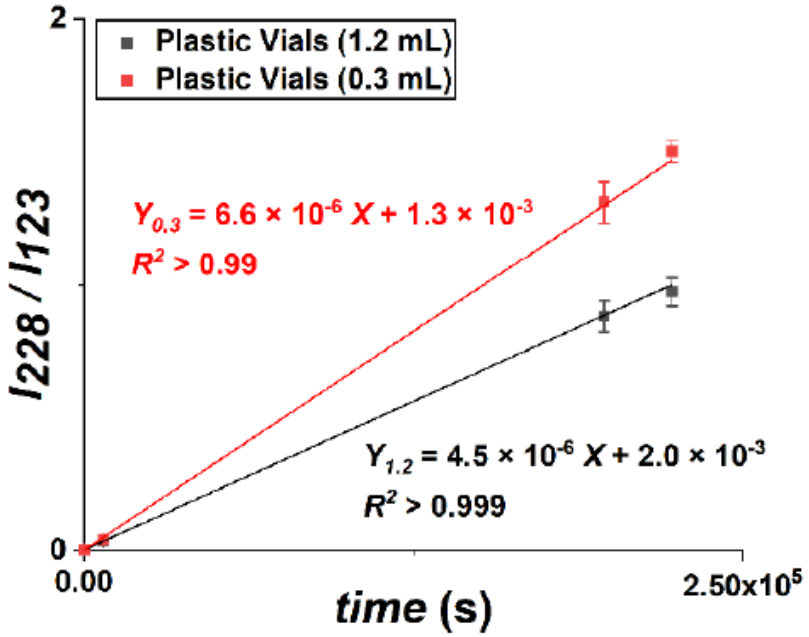

Figure 3.6 Bulk kinetics of Katritzky reaction (1c) using TMP as the reactant at 50 µM in two different volumes (0.3 mL and 1.2 mL)

Encouraged by the demonstrated surface effects on the acceleration of the reaction in bulk solutions, we infer that the observed small differences in acceleration among the three precharged salts is due to their surface activity. To investigate the tendency of molecules to adsorb to the surface of the reaction vessel, we first measured the ionization efficiencies of each pure compound as a reference, displayed in Figure 3.7. Individual mass spectra (Figure 3.7a**)** were recorded for 50 μM solutions of each pyrylium salt dissolved in acetonitrile and injecting ions for only 0.3 ms, with AGC (automatic gain control) turned off.

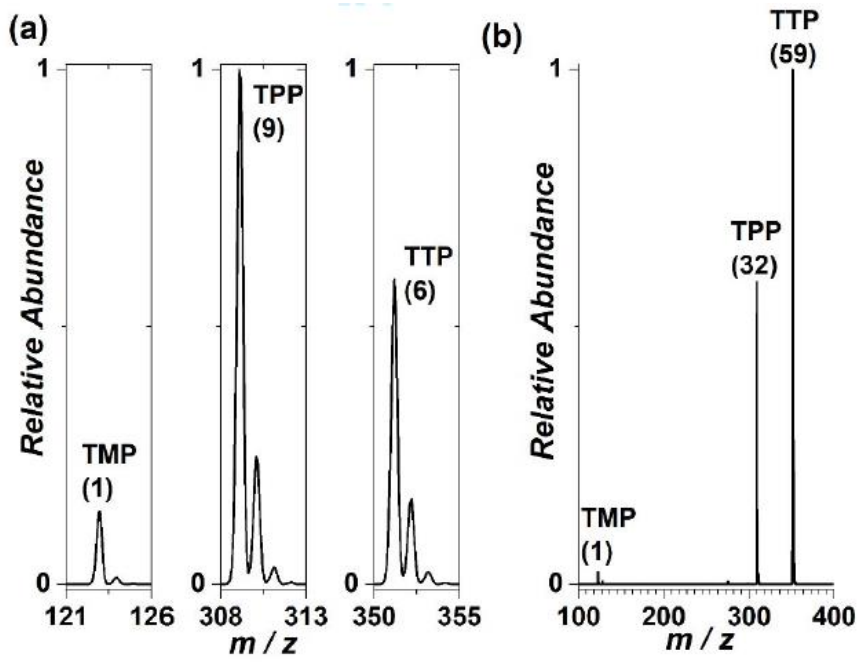

Figure 3.7 (a) Three MS spectra of each pyrylium salt (TMP/TPP/TTP) in acetonitrile at 50 μM (b)MS of equimolar (50 μM) pyrylium salts (TMP, TPP, TTP) mixture in acetonitrile. The numbers indicate relative MS peak areas. Note that (a) and (b) are normalized separately.

The detected ion currents of TPP and TTP were found to be 9-times and 6-times more intense than that of TMP. Mass spectra from a mixture containing each salt was then recorded and the relative ion currents used to characterize their surface activity. Figure 3.7b shows the nESI-MS from an equimolar mixture of the three salts in acetonitrile at a concentration of 50 μM each. It is shown that ion current intensities of TMP are up to 32-times and 59-times less intense than ion currents of TPP and TTP, respectively. Surface activity trends were constructed after correction by the ionization efficiency ratios measured from Figure 3.7a. TMP displayed the least surface

affinity followed by TPP and then TTP with a measured surface preference to be 1:3:10 (TMP:TPP:TTP). Surface reactivity has been previously reported for this reaction in the literature.[45]

The data in Figures 3.4-3.6 require that the reaction occur at a minimum of two different rates which we suggest correlates to reactions proceeding at the surface of the bulk (300 µL) and reactions occurring in the interior of the solution (1200 µL). The bulk volume and surface effects (2-fold enhancement in rate constants) can be considered in terms of a shell-core model used to explain reaction acceleration in smaller systems of high surface-to-volume ratios. It is proposed that there are at least three contributing factors: a) accelerated reactions near the surface due to increased rate constants, yet with a negligible effect of increased concentration at the surface; b) non-accelerated reactions at the interior of the bulk solution c) minor mass transfer between the surface and the interior of the bulk solution in the absence of heat.

The rate constants calculated for the bulk is dependent on the fraction of reactants adsorbed to the surface of the solution in order to participate in the surface reaction may be dominated by two effects: a) a minor contribution due to mass transfer from the interior of the solution to the surface; b) the reaction capacity of the surface. The high surface-volume system provides a shorter distance of travel of the reactants and products from the interior to the surface allowing for mass transfer and a higher turnover number at the surface.

The kinetic rates monitored at low volumes are higher than those at high volumes for bulk reaction solutions. The surface-to-volume ratio (air-solution interface) of the 1.2-mL solution is calculated to be 0.065 mm^{-1} and that of the 0.3-mL solution to be 0.26 mm^{-1}. As the volume of a reaction mixture decreases, the surface/volume ratio increases and thus the fraction of reactants that can access the surface per unit time increases. As the concentration of reagents in a reaction mixture decreases, this capacity does not change yet a larger portion of the reagents can reach the surface region per unit time to give a higher overall rate constant by effective mass transfer. Although mass transfer is limited in the unstirred bulk reactions, the 4-fold enhancement in surface-to-volume ratio dictates volume as a dominate factor over concentration, as shown in **Figure 3.8**. At low concentrations, the increased surface/volume ratio leads to the observed increase in reaction rate.

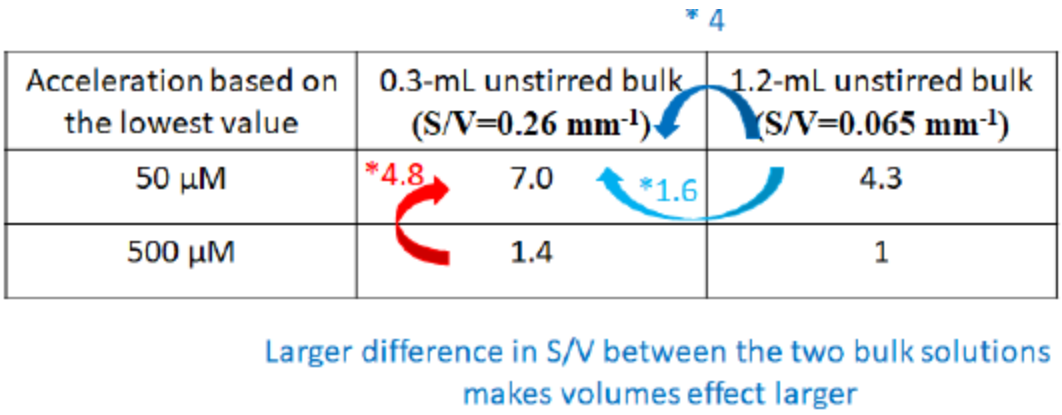

Figure 3.8 Rate constant enhancements of bulk reactions using their own reference rate constants at the high concentrations in large volumes (reference for unstirred bulk solutions at room temperature: $k_{0bulk} = k_{500\ \mu M,\ 1.2\ mL} = 0.00058\ M^{-1}s^{-1}$). The numbers indicate that volume effects in bulk solutions were enhanced by a larger surface-to-volume (S/V) ratio difference (4-fold enhancement in S/V ratio from 1.2-mL solutions to 0.3-mL solutions.

These arguments account for the observed increase in overall rate in bulk solutions as the surface area is held constant and the volume is decreased. By using more surface-active reactants (e.g. TTP instead of TMP), such effects are enhanced as expected and this observation further supports the role of surface effects in reaction acceleration. The results provide evidence for the previously suggested mechanism: partial solvation of reagents at the air-solution interface provide a unique, polar environment resulting in a reduced activation barrier and increased reaction rate evident by an increased rate constant. Additionally, the data demonstrates the high throughput ability of the low concentration, low volume system conducted in commonly used LC-MS autosampler vials. The increase in reaction rate caused mainly due to a volume effect observed in reaction solutions of the same concentration may have a future influence in factors governing regarding method development. Given these interesting findings, a significant question is whether these capabilities can be extended to other reactions of use in chemical synthesis.

3.4.2 Claisen-Schmidt condensation

Aldol condensation reactions are extensively used in organic synthesis by providing a facile method for carbon-carbon bond formation. These condensation reactions typically involve an enol or enolate ion reacting with a carbonyl compound to form a beta-hydroxyaldehyde or beta-

hydroxyketone, followed by dehydration to give a conjugated enone.[24,46] Condensation reactions between an aliphatic aldehyde or ketone with an aromatic carbonyl compound lacking an alpha-hydrogen to form an alpha, beta-unsaturated aldehyde or ketone are known as Claisen-Schmidt condensation.[49] Previous studies have demonstrated high chemoselectivity when conducted in the presence of an acid or a base, and occur much faster in confined volumes than in the bulk solutions.[13-14,28,35] Here, we studied the interfacial effects of the Claisen-Schmidt reaction of 6-hydroxy-1-indanone with 2-methoxybenzaldehyde in bulk solutions, Scheme 3.7.

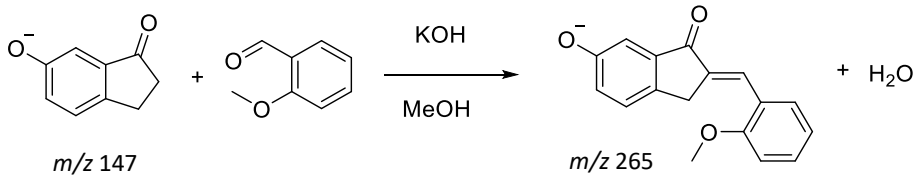

Scheme 3.3 Claisen-schmidt reaction of 6-hydroxy-1-indanone with 2-methoxybenzaldehyde.

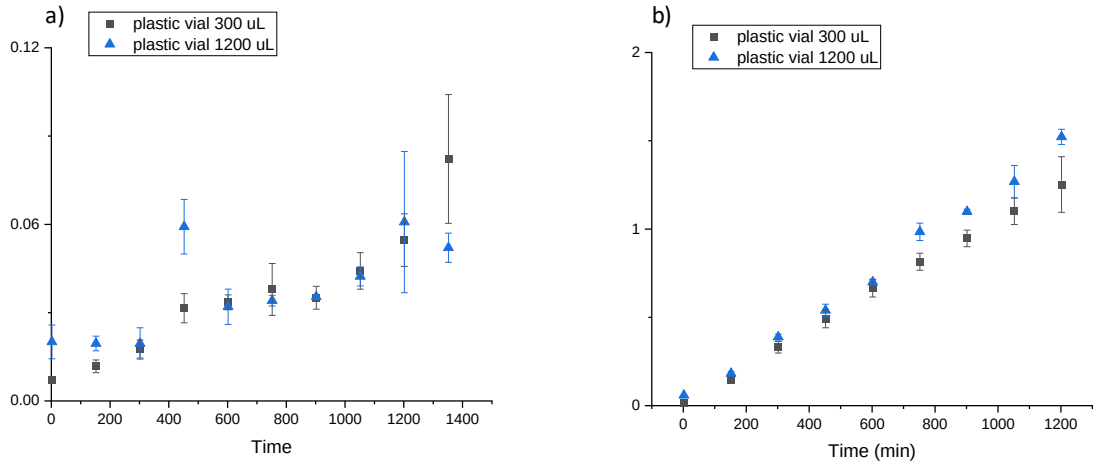

Figure 3.9 Bulk kinetics of the Claisen-Schmidt reaction at 5 mM in plastic vials of different volumes tested by ESI-MS with automatic sampling with a) 2 eq of KOH; b) 20 eq of KOH.

Bulk kinetics of the base-catalyzed Claisen-Schmidt reaction is shown in Figure 3.9 and did not demonstrate any acceleration due to the high surface, low volume system. The reaction with 2 eq of potassium hydroxide (Figure 3.9a) produced results with more variance between the measurements. This is due to the relatively minor amounts of product yielded, producing ion intensity signals near the baseline of the measurement. The lack of volume effect for this reaction

is confirmed by the data collected with 20 eq of base (Figure 3.9b). No significant difference is observed during the first 12 hrs of analysis. After this time period, minor rate acceleration is evident in the larger volume (1200 µL).

The Katritzky and Claisen-Schmidt reactions are both base-catalyzed, producing water as one of the products. However, the Katritzky reaction will proceed without the addition of catalyst, where as in the case of Claisen-Schmidt the base is a necessary to initiate the reaction. These differences may account for the positive effect of volume observed in Katritzky, that is not observed for Claisen-Schmidt.

3.4.3 Imine Formation

Reactions of amines are of significant consideration in many fields as they are the building blocks of molecules found in nature and medicine. Imines are compounds formed from the condensation reaction of ammonia or an amine with a carbonyl compound.[29,47] Structures contain a carbon-nitrogen double bond, and those formed by amines are relatively more stable than those formed by ammonia. This study considered the interfacial effects of the of the imine formation by reaction of dibutylpropane-1,3-diamine with 3-hydroxybenzaldehyde, illustrated in Scheme 3.7.

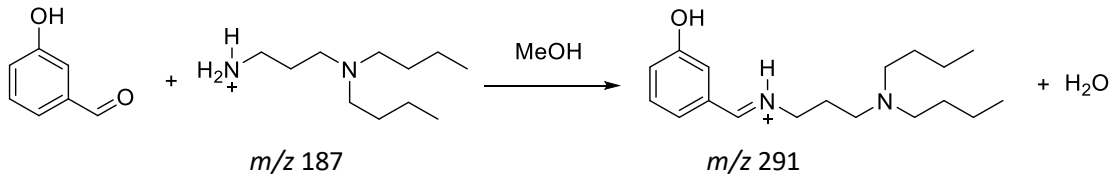

Scheme 3.4 Imine formation reaction of dibutylpropane-1,3-diamine with 3-hydroxybenzaldehyde.

MS results display the relatively slow reaction requiring long reaction times in the absence of a catalyst, as shown in Figure 3.10. Initially, the reaction appeared to be accelerated by a volume effect as the 300 µL proceed at a slightly faster rate. Due to the increased variability in the measurements of the 1200 µL solution, it was determined that no significant difference in the reactions at the two volumes can be determined.

It should be noted that both reactions displaying negative effects were analyzed in methanol, whereas positive results were detected in acetonitrile. Solvent choice is known to greatly affect the

ability for a reaction to proceed forward, especially as the accelerated rate is based on partial solvation theory. In the case of Katritzky, the reaction proceeded significantly faster in methanol than in acetonitrile, however the stability of the spray method greatly suffered producing more error in between replicate sampling. This may explain the results described for the condensation reactions.

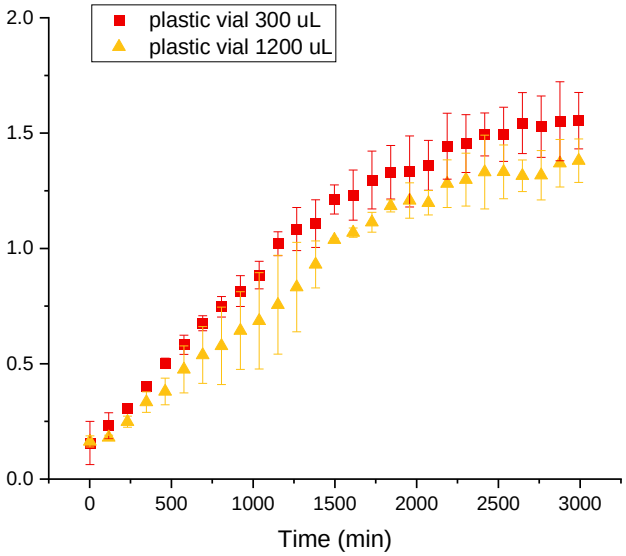

Figure 3.10 Bulk kinetics of the Imine formation reaction at 5 mM in plastic vials of different volumes tested by ESI-MS with automatic sampling.

3.5 Conclusion

In summary, the reported study provides convincing evidence that the Katritzky transamination reaction can be accelerated at the air-solution interface of bulk solutions of high surface-to-volume ratios. By varying the volume while holding the surface area constant, the kinetic effect of surface-to-volume ratios was observed. The reaction rate observed at the bulk air-solution interface is 1.8 times faster in reactions of smaller volumes, compared to larger volumes with equal surface area, indicating that the surface of the reaction vessel is involved in enhancing the rate of reaction. For the Katritzky reaction studied, the rate can be further enhanced with reagents having greater surface affinities resulting in greater surface adsorption and hence reaction

acceleration. It is concluded that reactions with surface-active reactants can be accelerated at lower concentrations in systems of higher surface-to-volume ratios. These results reinforce the suggestion that limited solvation of reagents heavily contribute to the increased rate constants observed in reactions occurring at the air-solvent interface.

The Claisen-Schmidt and imine formation reactions did not appear to be effected by the high-surface, low-volume systems. All three reactions proceed by different mechanisms, and only share an elimination of water which does not seem to contribute to the results. It may be of interest to reexamine these reactions in other organic solvents, such as acetonitrile, and even in water to evaluate the possibility of reactions occurring at the air-water interface of this established system.

3.6 References

1. M. Girod, E. Moyano, D. I. Campbell and R. G. Cooks, *Chem. Sci.*, 2011, **2**, 501–510.
2. T. Müller, A. Badu-Tawiah and R. G. Cooks, *Angew. Chem. Int. Ed.*, 2012, **51**, 11832–11835; *Angew. Chem.*, 2012, **124**, 12002–12005.
3. K. Badu-Tawiah, D. I. Campbell and R. G. Cooks, *J. Am. Soc. Mass Spectrom*, 2012, **23**, 1077–1084.
4. S. Banerjee and R. N. Zare, *Angew. Chem. Int. Ed.*, 2015, **54**, 14795–14799; *Angew. Chem.*, 2015, **127**, 15008–15012
5. J. Kyoo Lee, S. Kim, H. Gil Nam, R. N. Zare and O. Korea, *Proc. Natl. Acad. Sci.*, 2015, **112**, 3898–3903.
6. Y. Li, X. Yan and R. G. Cooks, *Angew. Chem. Int. Ed.*, 2016, **55**, 3433–3437; *Angew. Chem.*, 2016, **128**, 3494–3498
7. S. Banerjee, E. Gnanamani, X. Yan and R. N. Zare, *Analyst*, 2017, **142**, 1399–1402.
8. W. Zhang, H. Cheng and J. Liu, *ACS Sustain. Chem. Eng.*, 2018, **6**, 8125–8129.
9. P. W. Fedick, R. M. Bain, K. Bain, T. F. Mehari and R. G. Cooks, *Int. J. Mass Spectrom.*, 2018, **430**, 98–103.
10. W. Zhang, S. Yang, Q. Lin, H. Cheng and J. Liu, *J. Org. Chem.*, 2019, **84**, 851–859.
11. X.-P. Liu, H.-Y. Wang and Y.-L. Guo, *Int. J. Mass Spectrom.*, 2019, **435**, 1–6.
12. N. Sahota, D. I. AbuSalim, M. L. Wang, C. J. Brown, Z. Zhang, T. J. El-Baba, S. P. Cook and D. E. Clemmer, *Chem. Sci.*, 2019, **10**, 4822–4827.

13. K. Badu-Tawiah, D. I. Campbell and R. G. Cooks, *J. Am. Soc. Mass Spectrom.*, 2012, **23**, 1461–1468.

14. X. Yan, R. Augusti, X. Li and R. G. Cooks, *Chempluschem*, 2013, **78**, 1142 – 1148.

15. Z. Wei, M. Wleklinski, C. Ferreira and R. G. Cooks, *Angew. Chem. Int. Ed.*, 2017, **56**, 9386–9390; *Angew. Chem.*, 2017, **129**, 9514–9518.

16. Z. Wei, X. Zhang, J. Wang, S. Zhang, X. Zhang and R. G. Cooks, *Chem. Sci.*, 2018, **9**, 7779–7786.

17. S. Narayan, J. Muldoon, M. G. Finn, V. V. Fokin, H. C. Kolb and K. B. Sharpless, *Angew. Chem. Int. Ed.*, 2005, **44**, 3275–3279; *Angew. Chem.*, 2005, **117**, 3339–3343.

18. D. T. Chiu and R. M. Lorenz, *Acc. Chem. Res.*, 2009, **42**, 649–658.

19. E. C. Griffith and V. Vaida, *Proc. Natl. Acad. Sci.*, 2012, **109**, 15697–15701.

20. Kato, M. Yanagisawa, Y. T. Sato, K. Fujiwara and K. Yoshikawa, *Sci. Rep.*, 2012, **2**, 1–5.

21. Fallah-Araghi, K. Meguellati, J.-C. Baret, A. El Harrak, T. Mangeat, M. Karplus, S. Ladame, C. M. Marques and A. D. Griffiths, *Phys. Rev. Lett.*, 2014, **112**, 028301.

22. M. Zhang, R. Ettelaie, T. Yan, S. Zhang, F. Cheng, B. P. Binks and H. Yang, *J. Am. Chem. Soc.*, 2017, **139**, 17387–17396.

23. Saha-Shah, J. A. Karty and L. A. Bake, *Analyst*, 2017, **142**, 1512–1518.

24. D. N. Mortensen and E. R. Williams, *Chem. Commun.*, 2016, **52**, 12218-12221.

25. R. M. Bain, C. J. Pulliam, F. Thery and R. G. Cooks, *Angew. Chem. Int. Ed.*, 2016, **55**, 10478–10482; *Angew. Chem.*, 2016, **128**, 10634–10638.

26. E. A. Crawford, C. Esen and D. A. Volmer, *Anal. Chem.*, 2016, **88**, 8396–8403.

27. M. I. Jacobs, J. F. Davies, L. Lee, R. D. Davis, F. Houle and K. R. Wilson, *Anal. Chem.*, 2017, **89**, 12511–12519.

28. Y. Li, Y. Liu, H. Gao, R. Helmy, W. P. Wuelfing, C. J. Welch and R. G. Cooks, *Chem. - Eur. J.*, 2018, **24**, 7349–7353.

29. X. Yan, R. M. Bain and R. G. Cooks, *Angew. Chem. Int. Ed.*, 2016, **55**, 12960–12972; *Angew. Chem.*, 2016, **128**, 13152–13166.

30. R. M. Bain, C. J. Pulliam and R. G. Cooks, *Chem. Sci.*, 2015, **6**, 397–401.

31. R. M. Bain, C. J. Pulliam, S. T. Ayrton, K. Bain and R. G. Cooks, *Rapid Commun. Mass Spectrom.*, 2016, **30**, 1875–1878.

32. Z. Zhou, X. Yan, Y.-H. Lai and R. N. Zare, *J. Phys. Chem. Lett.*, 2018, **9**, 2928–2932.

33. H. Arnaud, *C&EN*, **2017**, *95(46)*, 16-18.

34. V. Vaida, *Proc. Natl. Acad. Sci.*, 2017, **114**, 12359–12361.

35. W. Stroberg and S. Schnell, *Biophys. J.*, 2018, **115**, 3–8.

36. U. Gruntz, A. R. Katritzky, D. H. Kenny, M. C. Rezende and H. Sheikh, *J. Chem. Soc., Chem. Commun.*, 1977, 701.

37. R. Katritzky, R. H. Manzo, J. M. Lloyd and R. C. Patel, *Angew. Chem. Int. Ed.*, 1980, **19**, 306; *Angew. Chem.*, 1980, **92**, 315.

38. R. Katritzky, R. T. C. Brownlee and G. Musumarra, *Tetrahedron*, 1980, **36**, 1643–1647.

39. R. Katritzky and R. H. Manzo, *J. Chem. Soc., Perkin Trans. 2*, 1981, 571–575.

40. R. Katritzky, J. M. Lloyd and R. C. Patel, *J. Chem. Soc., Perkin Trans. 1*, 1982, 117–123.

41. R. Katritzky and C. M. Marson, *Angew. Chem. Int. Ed.*, 1984, **23**, 420-429; *Angew. Chem.*, 1984, **96**, 403−413.

42. R. Katritzky and D. E. Leahy, *J. Chem. Soc., Perkin Trans. 2*, 1985, 171–174.

43. X. Ma, J. C. Burton. J. *Fluid Mech*. 2018, **846**, 263-291.

44. A. Bouillant, T. Mouterde, P. Bourrianne, A. Lagarde, C. Clanet, D. Quere. *Nat Phys*. 2018, **14**, 1188-1192.

45. T. Sahraeian, D. S. Kulyk, A. K. Badu-Tawiah. *Langmuir*, 2019, **35**, 14451-14457.

46. H. Nie, Z. Wei, L. Qiu, X. Chen, D. Holden, R.G. Cooks. *Chem Sci*, 2020, **11**, 2356.

47. S. Moldoveanu. *Appl Health Enviro Issues*, 2019, **2**, 327-347.

CHAPTER 4. REACTION ACCELERATION AT SOLID-SOLUTION INTERFACES: KATRITZKY TRANSAMINATION BY GLASS NANOPARTICLES

4.1 Abstract

Chemical interactions with glass substrates and their effect on reaction rates have been interrogated utilizing the Katritzky transamination as a model reaction. Preliminary results reveal an increase in reaction rate in the presence of glass wool in comparison to that of a control. Additionally, three sample vial types for bulk solutions showed significant differences in reactivity, with the greatest acceleration found in an untreated glass vial. Reaction rates in glass substrates were greatly increased at the solid-solution interface of high surface-to-volume systems of bulk solutions. Interestingly, these results display the combined effect of partial solvation of reagents at the interface and catalysis by glass substrates can greatly alter rate constants of chemical reactions.

4.2 Introduction

The use of glass substrates has enlarged the number of applications in chemical and biological sciences due to its numerous unique properties. Typically, glass has been used as solid support in heterogeneous catalysis in a variety of chemical reactions.[1-6] In catalysis, the support can either be in a passive manner that solely restricts the movement of the active catalyst through chemical bonding or fixation.[5-7] The method of activation is usually based on doping the inert glass surface by implantation with metal ions.[4,6] Recently, studies have demonstrated the use of glass wool as a readily available, relatively inexpensive catalyst support for synthesis of important organic reactions by deposition of metal and metal oxide nanoparticles.[4-8] Other studies have observed increase reaction rates by using glass wool as a collection surface, in the absence of any catalysts.[7] This differs from cases in which the intrinsic properties of the support material contribute to the performance of the catalyst, such as conductivity, absorption and scattering properties.[10-12]

Glass is commonly used as a filter, packing material, and for the storage and transport of drugs, environmental samples, and reagents in the biomedical and pharmaceutical industries.

Several occurrences of drug degradation, changes in efficacy and dosage, and product losses have generated interest in identifying the underlying mechanism due to direct glass interactions with the reaction solution.[13-15] A few studies have been reported over the years detailing observations of reaction acceleration in the presence of glass due to mechanisms based on ion exchange, reagent reactivity on glass surface and additional mechanisms based on the manufacturing process of the glass used.[3] The latter effects the composition, physical, and chemical properties of the glass surface. Metal oxides, such as Fe_3O_3, TiO_3 or MnO, can be added to produce amber borosilicate glasses for the protection against UV light, whereas Al_2O_3 is added to improve chemical durability of the glass to resist leaching.[4,7] Reaction acceleration by various glass materials broadly rely on mechanism of glass delamination or flaking from the surface, metal ion interactions between the solvent, reactants, and glass surface, and the adsorption of reactants or products onto the glass surface, with the surface of the glass material as the dominating factor.[2,5]

The use of glass for catalysis was observed to produce a 4-time increase in rate of polymerization of methyl methacrylate in water. By addition of colorless soda lime or amber glass particles in the presence of a sodium bisulfite initiator in comparison to a control.[16] The decrease in the particle size of soda lime glass selected (from 200 to 50 mesh) resulted in a 3.8 times higher conversion from monomer to polymer, as well as a 5.5 times increased rate of polymerization when the initiator concentration was reduced to 0.01 mole/L. The authors attributed the catalytic effect to the dissociation of ions from the initiator-glass complex forming radicals responsible for the polymerization process.[16]

In order to ensure inertness of the glass material, it may be treated by silylation in order to block active functional groups from participating in the reaction. The effect of treating the glass surface and its role in reaction acceleration has been reported for the analysis of an intramolecular Diels-Alder reaction in an untreated or pretreated-glass flasks.[17] The reaction did not occur in the silylated flask, leading the authors to conclude that the epimerization of the starting material was catalyzed by the glass surface. The increased degradation of a commercial fungicide has been shown to be heavily dependent on the container used, where plastic containers inhibited loss of product and soda lime glass containers exhibited a slower rate compared to samples stored in borosilicate glass. These effects were attributed to adsorption or reaction of the product with the surface of the glass container.

Glass surface catalyzed reactions typically involve a nonpolar medium with a polar surface, therefore appropriate selection of solvent has been shown to greatly alter catalysis. Glass-catalyzed ketonization in acetonitrile has been shown to catalyze interconversion due to the weakly basic glass surface of the reaction vessel[17]. The fluorodesilylation reaction by xenon difluoride occurred in a glass flask in comparison to a Teflon tube[18]. However, the reaction in the glass flask was inhibited when conducted in acetonitrile possibly due to loss of acidic protons on the glass surface involved in catalyzing this reaction.

Polar solvents reduce the catalysis of Diels-Alder reactions by silica or glass, whereas neutral and acidic solutions are known to undergo ion exchange between sodium ions in the glass being replaced by hydronium ions of the solution.[16-18] One study concluded that the alkaline species and hydroxyl groups present in the reaction solution can attack the glass surface causing breaking of Si-O bonds.[17] Evidence for this is also suggested in the study of the accelerated conversion of boronic esters in the presence of borosilicate glass, where no reaction occurred with soda-lime glass or silica.[19] It must be stated that the glass surface in that study was first cleaned in a base bath to create etching of the surface, as the authors stated the reaction did not occur in a new, smooth glass flask. This phenomenon has also demonstrated in the glass catalyzed double bond isomerization of an alkyl halide which did not occur in quartz, yet was accelerated by a factor of 2 in the presence of Pyrex glass wool.[20] Pyrex glass contains a considerable amount of boric oxide which may aid in the electrophilic solvation of the halide ion.

In this work, we report significant reaction acceleration of the Katritzky transamination reaction catalyzed by glass nanoparticles in comparison to the control. Silanized glass nanoparticles also caused reaction acceleration, though to a lesser degree. These results are consistent with those obtained by conducting the transamination reaction in untreated glass and silanized glass containers, utilizing results obtained in plastic containers as the control.

4.3 Experimental

4.3.1 Reagents

Non-treated glass wool (GW, Aldrich catalog #: 20384) and silanized glass wool (SGW, Aldrich catalog #: 20411) were purchased from Sigma Aldrich (St. Louis, MO). Plastic vials (PV),

glass vials (GV) and silanized glass vials (SGV) were purchased from Microsolv (Leland, NC). All other chemicals have been previously mentioned in detail in Chapter 3.

4.3.2 Glass wool experiments

All glass wool experiments involved weighing 10 mg of untreated or silanized treated glass wool and diluted in 1 mL of acetonitrile. Solution is allowed to sit undisturbed for 1 min and immediately vortexed for 2-5 seconds. After this time, supernatant of the mixture is poured into a new sample tube and solid glass wool will remain in initial tube. Supernatant is used as glass nanoparticle solutions.

4.4 Results and Discussion

4.4.1 Katritzky Transamination reaction

The model reaction for the interrogation of glass catalyzed acceleration is the Katritzky transamination reaction of various pyrylium salts with p-anisidine to form a pyridinium product, shown in Scheme 4.1. As reported in Chapter 3 of this work, this reaction can be accelerated in high surface-to-volume systems at relatively low concentrations, and used to calculate overall reaction rate constants using nano electrospray ionization mass spectrometry (nESI-MS) as the analytical tool for measurement. In this work, significantly different results were observed by keeping the same experimental workflow, but simply changing the container used as the reaction vessel from plastic vials to glass vials.

Under this new experimental method, the reaction kinetics in bulk was studied in detail by dissolving the two reagents in acetonitrile in stoichiometrically equal amounts at different concentrations without the addition of acid or base. The effect of selecting reactants of greater surface affinity has enhanced the kinetic rate of this reaction significantly in comparison to the control. Bulk kinetic studies were performed by analyzing equimolar solutions of the reaction mixture with addition of glass nanoparticle solution or acetonitrile in the case of the control.

Preliminary analysis involved determining the catalytic effect of the reaction container on the kinetic rate of the Katritzky reaction between 2,4,6-triphenylpyrylium tetrafluoroborate (TPP) and p-anisidine in acetonitrile. To investigate the tendency of glass contaminants to adsorb to the walls of the container, we first prewashed the glass vials (CGV) or the prewashed silianized glass

vials (CSGV) in triplicate with acetonitrile as an additional comparison to the untreated glass vials (UGV) and untreated silanized glass vials (USGV) and used as received, and plastic vials (PV) used as the control, displayed in Figure 4.1. Studies have shown that glass flakes can delaminate from the vial walls into the reaction solution and can cause reaction acceleration or cause a reaction not to occur.

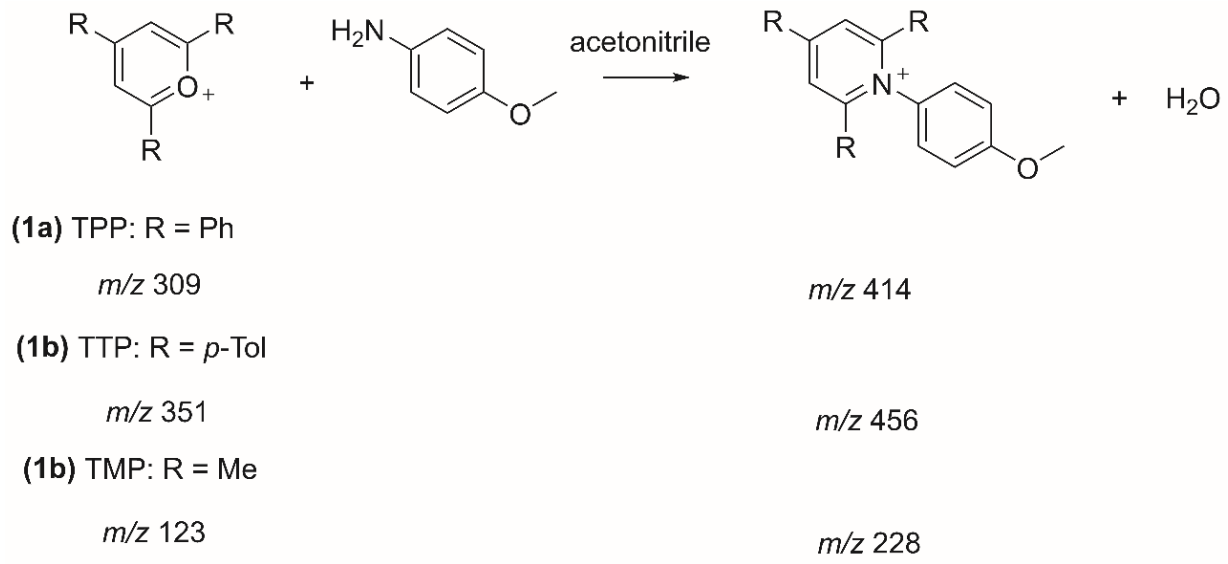

Scheme 4.1 Katritzky transamination reactions of pyrylium salts (TPP, TTP, TMP) and p-anisidine to form pyridinium salts.

In these experiments, 50 µM reaction solutions were tested at 300 µL and 1200 µL volumes in three cylindrical reaction containers of the same inner dimensions. The bulk rate constant of the reaction in the CGV for 300 µL is approximately 2 times greater than that observed in the PV, and a 4 times increase in the UGV in comparison to the PV, as shown in Figure 4.1a. Interestingly, the reaction occurring at 1200 µL displays the same trend, though to a much lesser degree, seen in Figure 4.1b. The uncleaned glass vial used as purchased (UGV) demonstrated a 2-time increase to that of the CSGV, and almost 3 times greater acceleration than that observed in the control (PV). The effect of prewashing the glass vials with solvent acts as a normalization between the effect of the glass compared to no effect obtain in the plastic vials. This trend holds true in the case of the pretreated glass vial containers. The hydroxyl groups of the glass containers may form hydrogen bonding with the reactants involved, resulting in a lower transition energy barrier or alternate pathway, causing the glass to act as a catalyst.

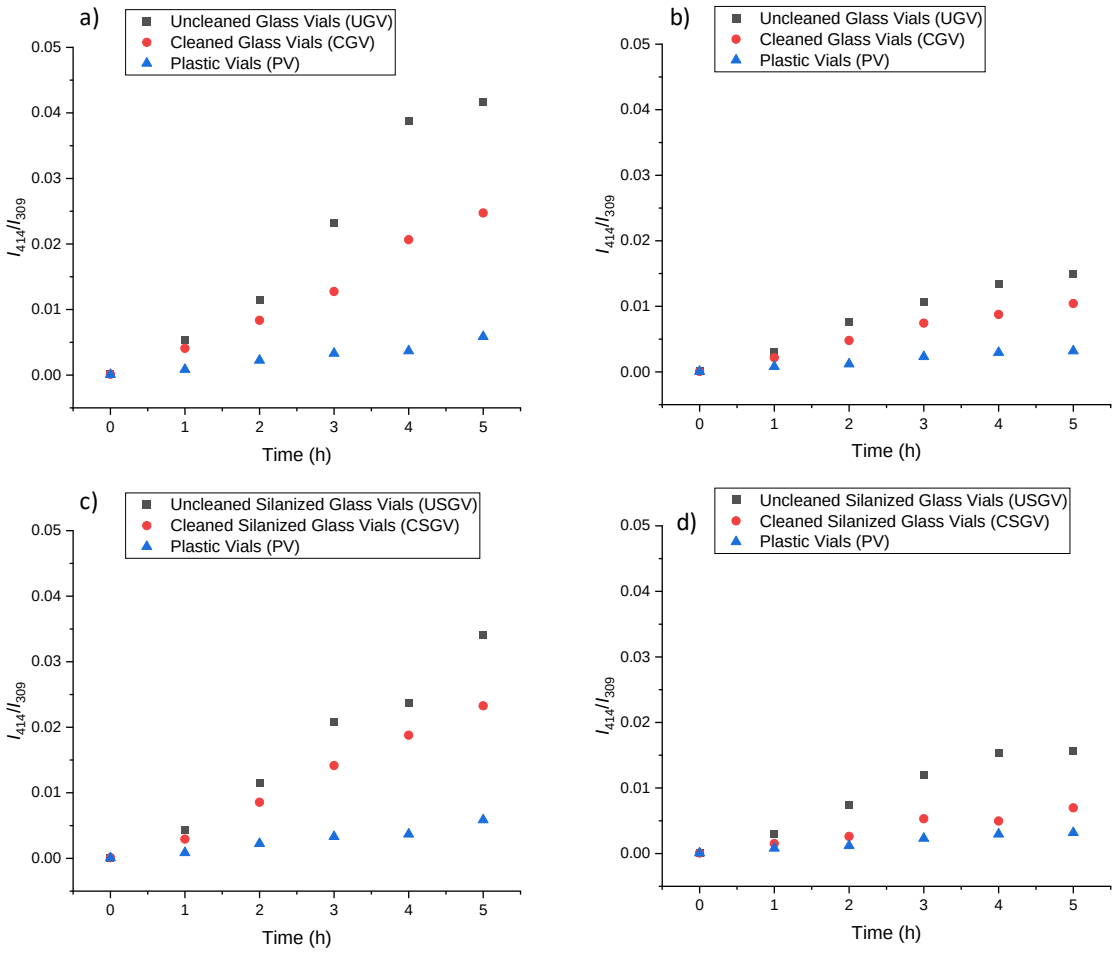

Figure 4.1 Bulk kinetics of the Katritzky reaction at 50 µM: a) glass vials at 300 µL; b) glass vials at 1200 µL; c) silanized glass vials at 300 µL; b) silanized glass vials at 1200 µL.

The effect of the silanized, pretreated vials is seen in Figure 4.1c for the 300 µL reaction and Figure 4.1d 1200 µL reaction solutions. The catalysis due to glass is evident even in the treated glass containers, however the effect of washing the silanized vial seems to have more of an effect at the 1200 µL solutions resembling the control. In the high surface to volume system at 300 uL solutions the effect of washing the container is not as significant. Encouraged by these findings, an optimized bulk kinetic study was conducted to test the reproducibility of the accelerated trends observed for the 50 µM reaction solutions at the 300 µL volume and the effect of prewashing sample vials before analysis. Results displayed in Figure 4.2 provide a validation to the previous observations of the catalytic effect of the presence of glass in the Katritzky transamination reaction. The effect of cleaned glass is 4-times greater than that of using the plastic vials, and 6 times greater when conducted in the unwashed glass vials.

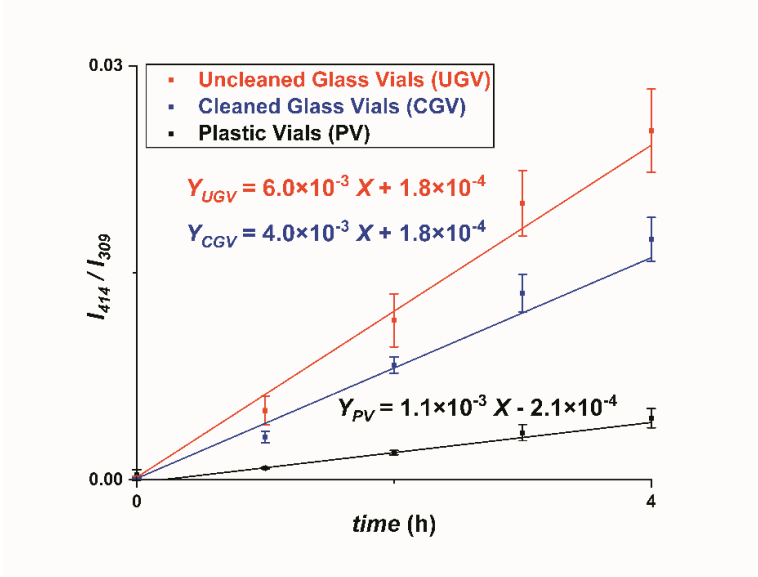

Figure 4.2 Bulk kinetics of the Katritzky reaction (Scheme 1a) at 50 µM in different vials.

The scope of the kinetic study was expanded to determine the extent of acceleration due to effect of reactant concentration. Previously, we demonstrated the increase in accelerated rates of this reaction as the concentration is reduced, with the greatest acceleration observed at 50 µM. Concentrations of bulk solutions below 50 µM caused the reaction to proceed extremely slowly, with relatively little to no product formation over several days. However, due to the enhanced accelerated effect in the presence of glass, we predicted that the glass catalyzed reaction would occur fast enough to monitor changes due to concentration effects. Reaction solutions were tested at 5 µM in untreated glass vial containers and analyzed in triplicates. The reproducibility of the analysis method was also investigated through the use of an automatic sampler system with ESI-MS and monitored over a 24 h period. Acceleration due to reactions conducted in glass vials demonstrate a significant enhancement in comparison to the control reacted in plastic vials, seen in Figure 4.3.

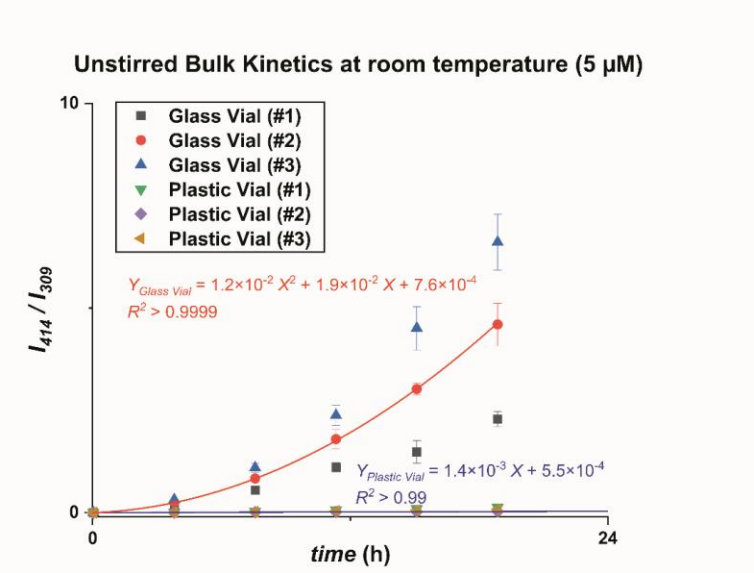

Figure 4.3 Bulk kinetics of the Katritzky reaction (Scheme 1a) at 5 µM in different vials tested by ESI-MS with automatic sampling.

The lower concentration produced more variability between replicates, however it is clearly evident by the nonlinear response seen in Figure 4.3 that there is significant acceleration due to the glass container. The kinetic profile of the 5 µM reaction increases exponentially, which varies from the linear response at the 50 µM reaction solutions (Figure 4.4), and also the 500 µM (Figure 4.5). Figure 4.4 demonstrates the reproducibility of the analysis method which is evident in the linearity and R^2 value close to unity when automatic sampling in used. Acceleration factors were determined for the 50 µM reaction solutions. Reactions occurring in glass vials at 1200 µL were found to be accelerated by a factor of 7 compared to reaction conducted at the same concentration and volume in plastic vial containers. The accelerated rate is increased to a factor of 12 for reactions at the 300 µL reaction solutions.

This also encourages the hypothesis that the variability observed at the lower concentration may be representative to the limit of detection of the linear ion trap used for analysis.

Encouraged by the demonstrated glass surface effects on the acceleration of the reaction rate in bulk solutions conducted in glass containers, we investigated the robustness of the study by determining the extent of acceleration by including a comparison with glass nanoparticles. The manufacturing and treatment processes vary from the glass containers to glass wool, and interest in the cause of the acceleration due to glass may be understood by replacing the glass substrate used for catalysis in these reactions.

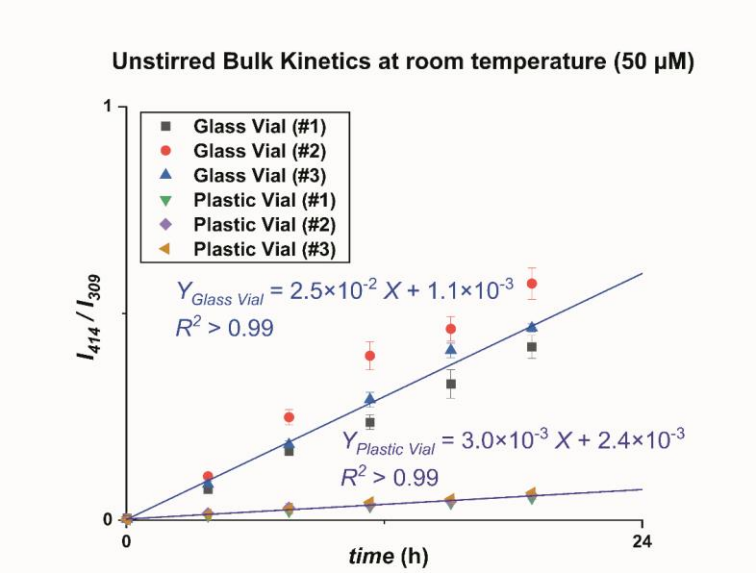

Figure 4.4 Bulk kinetics of the Katritzky reaction (Scheme 4.1a) at 50 µM in different vials tested by ESI-MS with automatic sampling.

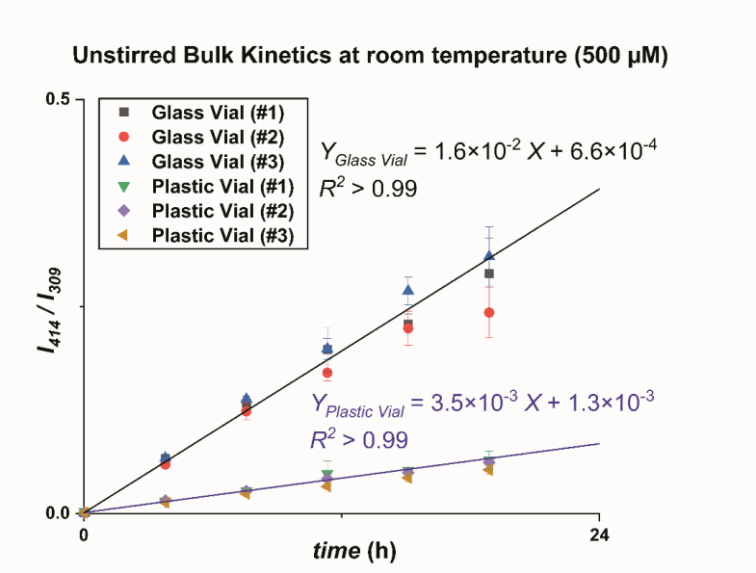

Figure 4.5 Bulk kinetics of the Katritzky reaction (Scheme 4.1a) at 500 µM in different vials tested by ESI-MS with automatic sampling.

For example, the glass containers are made from borosilicate glass material which can contain trace metals such as large amounts of boron involved in the fabrication process. Iron oxides are used to darken the glass container to reduce photo-oxidation damage to the contained samples

change the glass from translucent to amber in color. Figure 4.6 shows the nESI-MS from 50 μM solutions containing an addition of acetonitrile as the control, an addition of glass nanoparticles (GP) in acetonitrile, or an addition of silanized glass nanoparticles (SGP) in acetonitrile. After reaction monitoring for four hours, no product is detected in the control solutions or in that of the SGP solutions. Interestingly, mass spectra of the GP solutions yield a product peak at about 10% relative abundance compared to that of the starting material.

The reaction progress was monitored for over a week resulting in the control reaction producing the same amount of product synthesized in the GP solutions in the previous 4 h time period. Results of the reaction progress due to addition of Gp solutions after a week yielded near complete conversion. Most interestingly is the data obtained by the SGP solutions, which seems to decelerate the reaction rate as evident in comparison to the control data. It may be due to steric hindrance of the bulky silyl groups introduced on the glass particle during silanization treatment process. The reactants and products are in constant movement until equilibrium is reached. As the reactant adsorbs to the surface, the formed product diffuses from the surface back to the center of the solution, and this process may be impeded in the case of the SGP solutions.

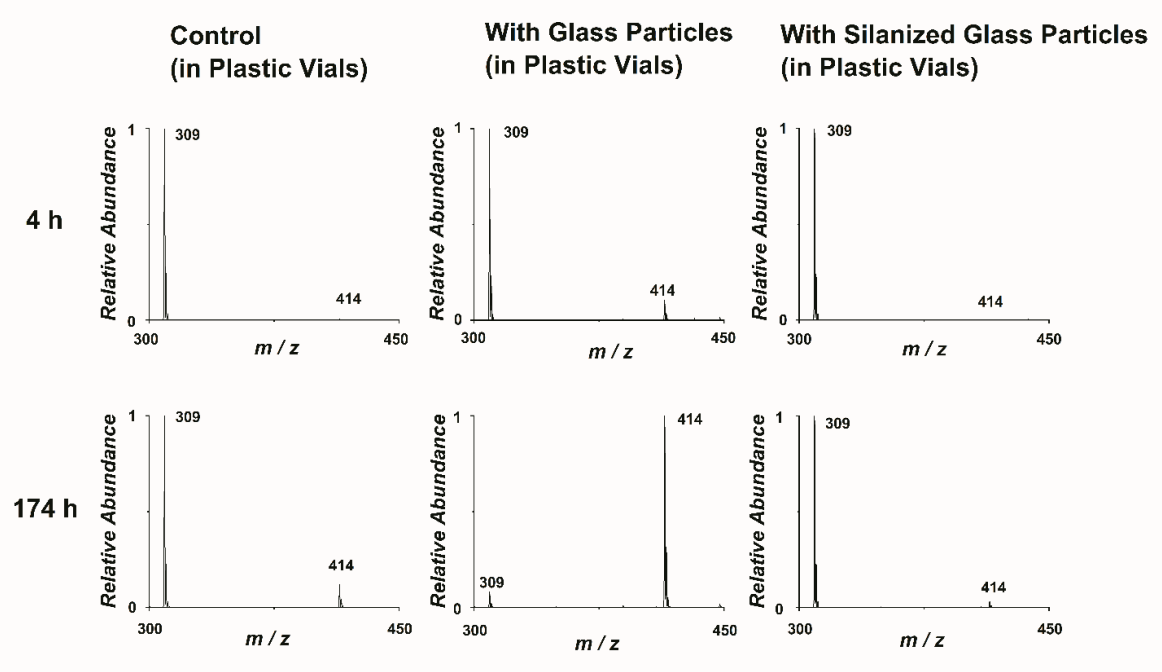

Figure 4.6 MS of Katritzky reaction (Scheme 1a) at 50 μM in plastic vials without particles vs. with glass or silanized glass particles added.

These results led to interest in the qualitative effect of the size and number of glass particles present in the addition solutions. The data suggests that the smaller glass particle sizes (> 200 μM) are the main contributor of the increased acceleration rate observed in Figure 4.7. The effect of filtering the GP solution physically reduces the total number of particles present in the solution, yet there is no significant reduction in acceleration when compared to the unfiltered GP solution. The effect of pretreating the glass nanoparticles with silyl groups significantly reduces the rate of reaction than filtration of the untreated glass particles. The silyl groups added to the nanoparticles during the silanization treatment are relatively bulky functional groups attached to the surface of the glass particles. As previously mentioned, the reaction is not a static process and involves the movement of reactants and products throughout the course of the reaction progress.

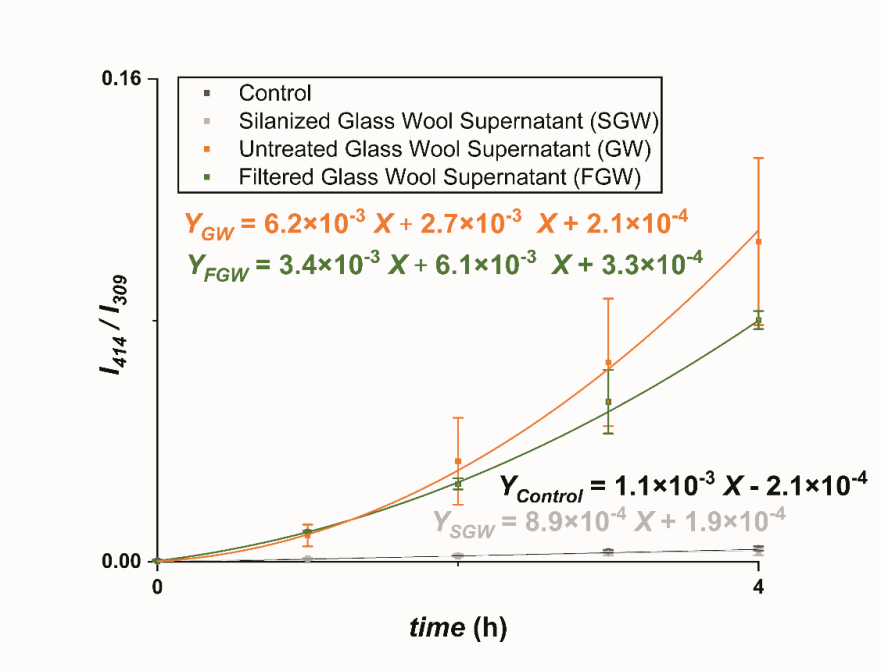

Figure 4.7 Bulk kinetics of the Katritzky reaction (Scheme 4.1a) at 50 μM in plastic vials with different types of wool supernatant added or without addition.

Therefore, sterics may play a role in the reduced acceleration effect observed in the reaction with treated glass particles. Additionally, the methoxy functional group of the aniline in this reaction can interact with the silyl groups and may become trapped by the glass particles, restricting less reactants to reach the surface of the solution where the acceleration occurs.

Treatment with silyl groups is traditionally used to make the glass surface inert, however it is dependent on the efficiency of the process. Silanized container vials from two different batch processes from the same retailer demonstrated different levels of acceleration between batches, yet consistent results from replicates analyzed in containers from the same batch. The study was then expanded to evaluate if the acceleration due to the catalyzed effect of the glass nanoparticles is linearly related to the amount of particles added to the solution, displayed in Figure 4.8.

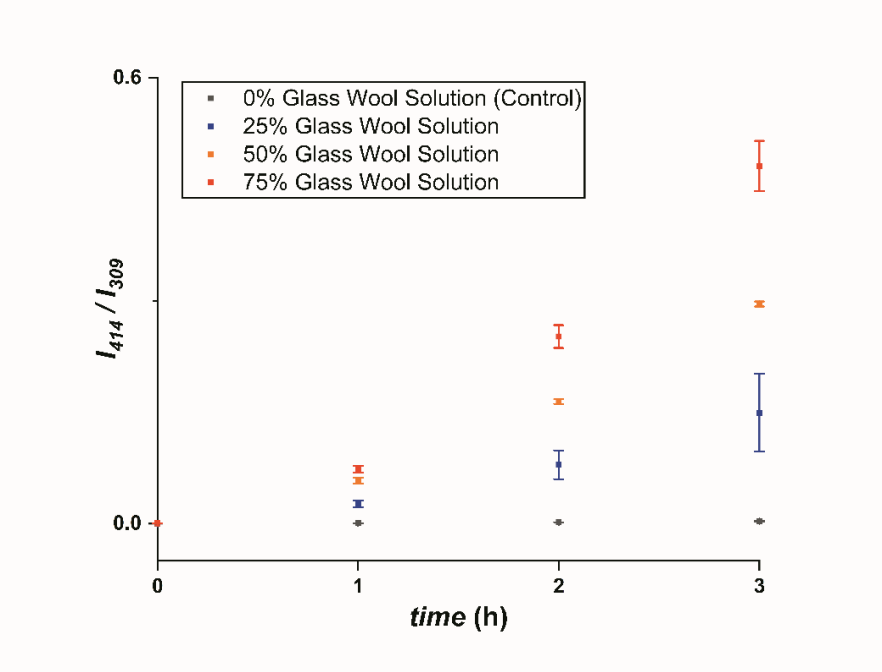

Figure 4.8 Bulk kinetics of the Katritzky reaction (Scheme 4.1a) at 50 µM in plastic vials with different amounts of the same glass wool supernatant added. The linearity of the plot reflects the enhancement of rate constants.

The data obtained at the 2-h time point was selected as it displays the greatest degree of separation with the least amount of variance in the results for 50 µM solutions at 300 µL volume. The ion intensity ratios were then plotted as a function of the amount of glass nanoparticles present in the solution to generate a calibration curve, as seen in Figure 4.9, which can be further used to calculate yield if scale up is of interest. Most importantly, these results provide evidence of the catalytic effect of glass nanoparticles on the reaction rate of the Katritzky transamination reaction. It must be noted that the increase in rate constants from the 0% glass wool solution of the control to the 75 % glass wool solution resulting in an acceleration factor of 128.

Bulk kinetics of the Katritzky reaction (Scheme 1a) at 50 μM in plastic vials was explored again to compare rate acceleration previously observed due to a surface effect with the same volumes of solution, either with the a 50 % addition of glass wool supernatant or with acetonitrile added as the control (Figure 4.10). Interestingly, a 1.8-fold increase in rate constants for volume effect occurs at the same rate as in Chapter 3 using plastic vials without glass addition. Figures 4.11-4.13 shows the comparison of reaction acceleration in high surface to volume ratio system at low concentrations for the three pyrylium salts selected at 50 μM in plastic vials with so percent glass wool addition of solvent added to the reaction mixture to be used as the control.

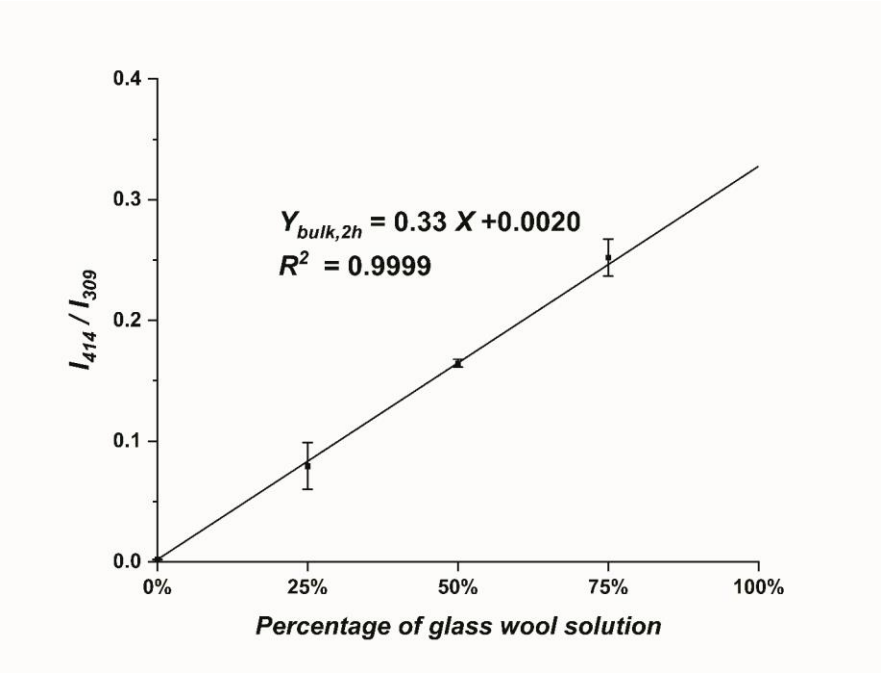

Figure 4.9 Katritzky reaction (Scheme 4.1a) rate constants at 50 μM increase with increasing amounts of glass nanoparticles. (Acceleration factor at 75% glass wool solution: 128 for unstirred bulk at room temperature for 2 h).

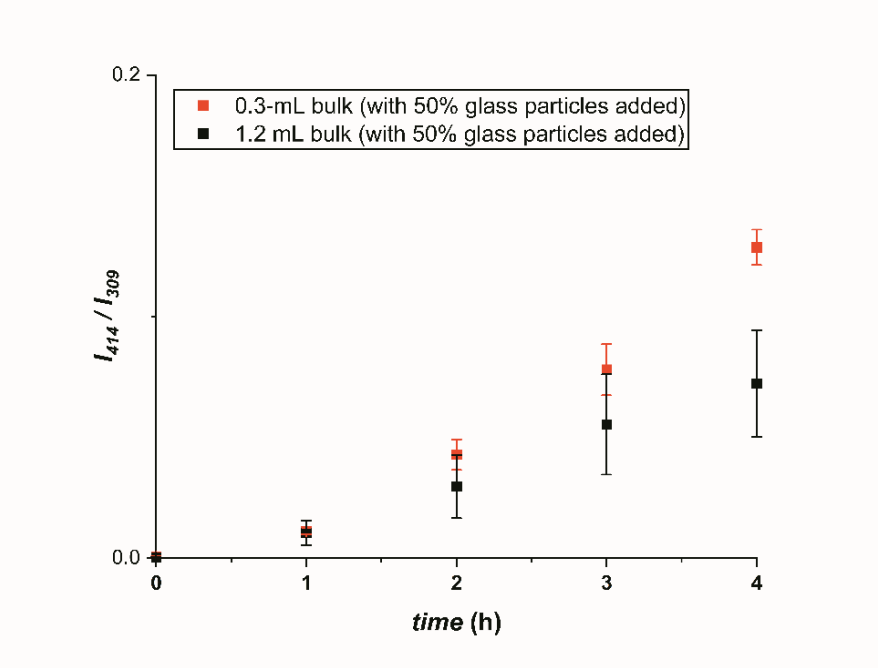

Figure 4.10 Bulk kinetics of the Katritzky reaction (Scheme 4.1a) at 50 μM in plastic vials with the same glass wool supernatant added but of different total volumes of solutions. There is a 1.8-fold increase in rate constants for volume effect (the same as in Chapter 3 using plastic vials without glass addition).

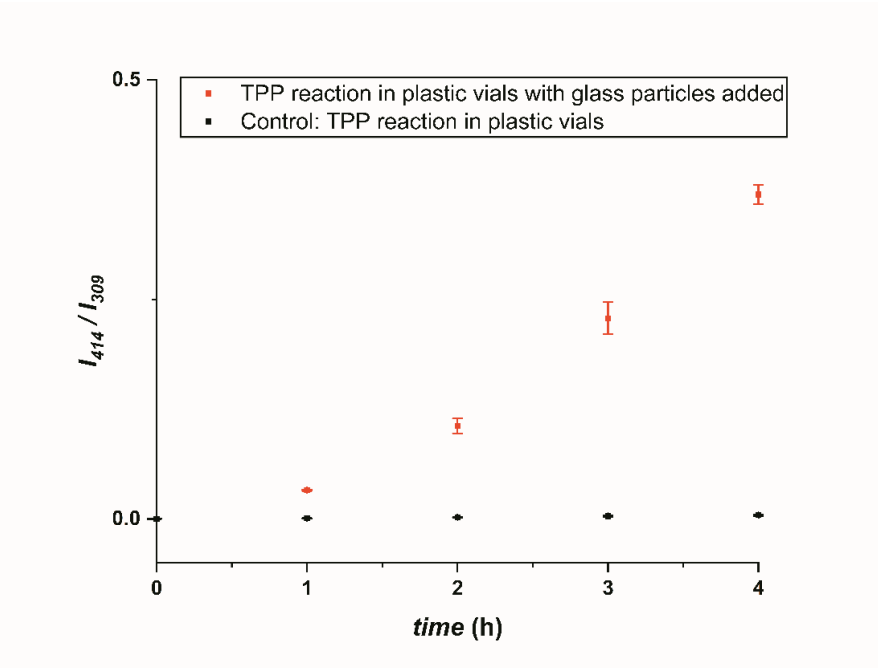

Figure 4.11 Bulk kinetics of the Katritzky reaction (Scheme 4.1a) at 50 μM in plastic vials with glass particles added vs. without glass particles added.

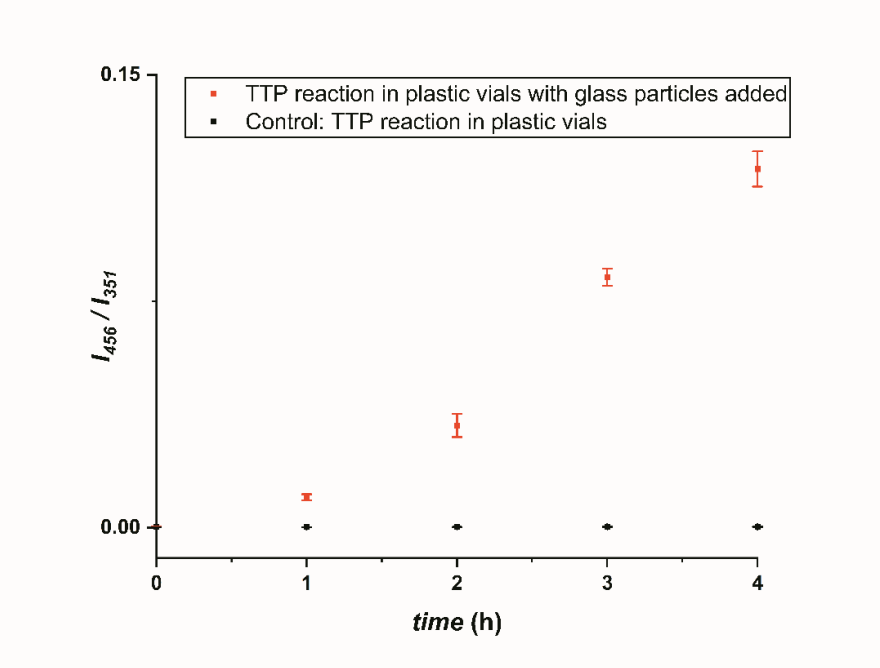

Figure 4.12 Bulk kinetics of the Katritzky reaction (Scheme 4.1b) at 50 μM in plastic vials with glass particles added vs. without glass particles added.

It is has been previously shown that ion current intensities of TMP are up to 32-times and 59-times less intense than ion currents of TPP and TTP, respectively. The ionization efficiency ratios measured from Chapter 3 were used as a normalization tool to construct surface activity trends of the selected pre-charged salts. Interestingly, trends previously observed are still consistent with the glass catalyzed results in thesis work. TTP displayed the greatest surface affinity followed by TPP and then TMP with a measured surface preference to be 10:3:1 (TTP:TPP:TMP). Surface reactivity has been previously reported for this reaction in the literature.[45] However, the enhanced effect due to the presence of glass increased drastically with a measured surface presence 383:82:44 ((TTP:TPP:TMP).

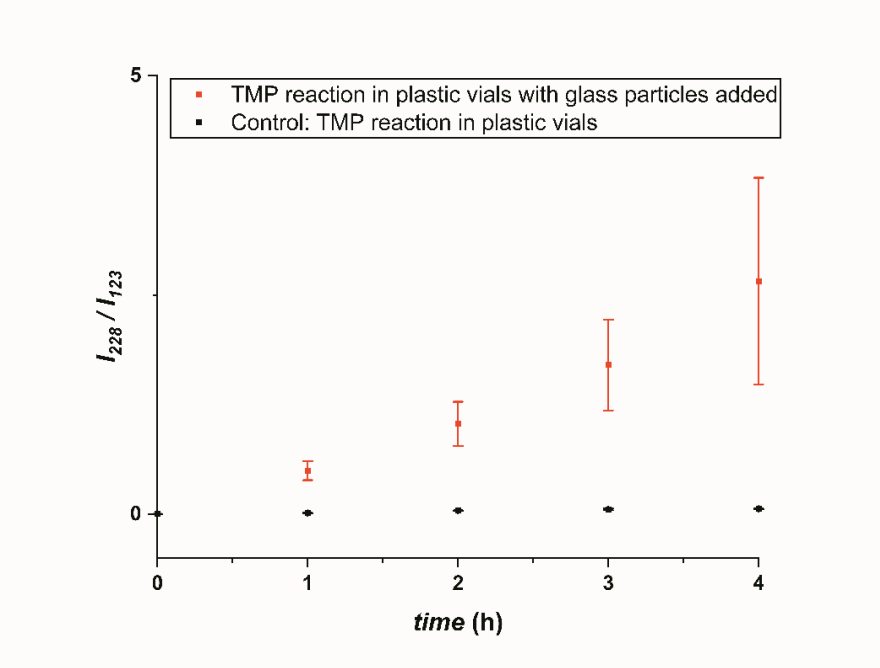

Figure 4.13 Bulk kinetics of the Katritzky reaction (Scheme 4.1c) at 50 μM in plastic vials with glass particles added vs. without glass particles added.

4.4.2 Claisen-Schmidt

Reaction kinetics of the Claisen-Schmidt reaction was evaluated for surface effects due to glass catalysis no previously observed in the absence of glass, shown in Scheme 4.2. Glass vial solutions at 5 mM of two different volumes over the course of three days is shown in Figure 4.14.

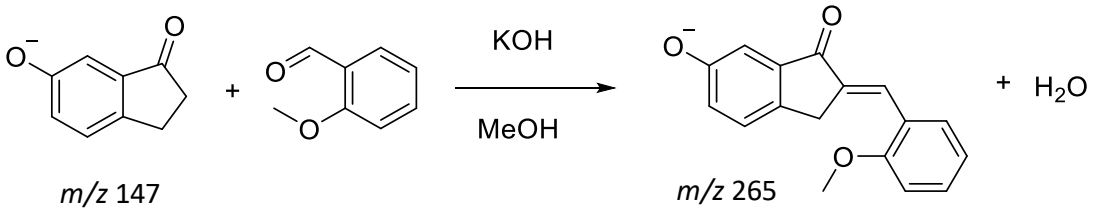

Scheme 4.2 Claisen-Schmidt reaction of 6-hydroxy-1-indanone with 2-methoxybenzaldehyde.

Results confirm previous speculation that this condensation reaction is not affected by high surface to volume constraints, not does it interact with glass when reacted in glass containers. There is no significant difference observed between reactions at 300 μL or 1200 μL for this reaction collected

by electrospray ionization mass spectrometry automatic sampling, indicating this reaction does not accelerate due to a volume effect.

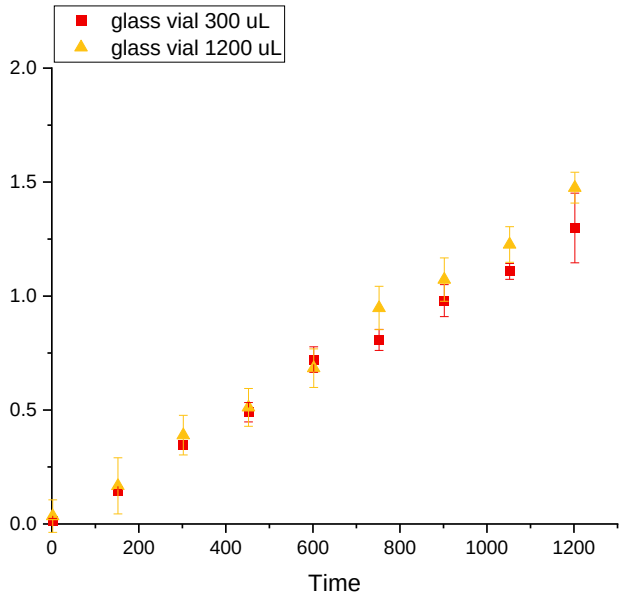

Figure 4.14 Bulk kinetics of the Claisen-Schmidt reaction at 5 mM in glass vials of different volumes tested by ESI-MS with automatic sampling.

4.4.3 Imine Formation

Kinetic analysis of an imine formation reaction (Scheme 4.3) evaluated the effect of the different glass vial containers: untreated and silanized for the 5 mM reaction solution at two different volumes, seen in Figure 4.15. The effect of volume on the reaction at 300 μL and 1200 μL in the glass vials is shown in Figure 4.15a, and initially does not demonstrate any significant difference in the first 24 hours between the two volumes. However, after this time there is minor, yet statistically different rate enhancement at the lower volume reaction. In the case of the silanized glass vials, seen in Figure 4.15b, there appears to follow the same trend of the glass vials, yet no statistical difference is detected at the corresponding time period.

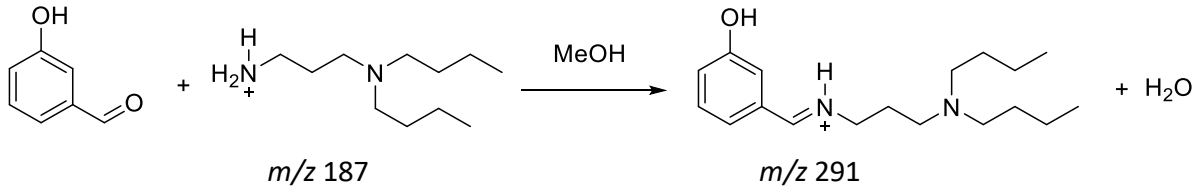

Scheme 4.3 Imine formation reaction of dibutylpropane-1,3-diamine with 3-hydroxybenzaldehyde.

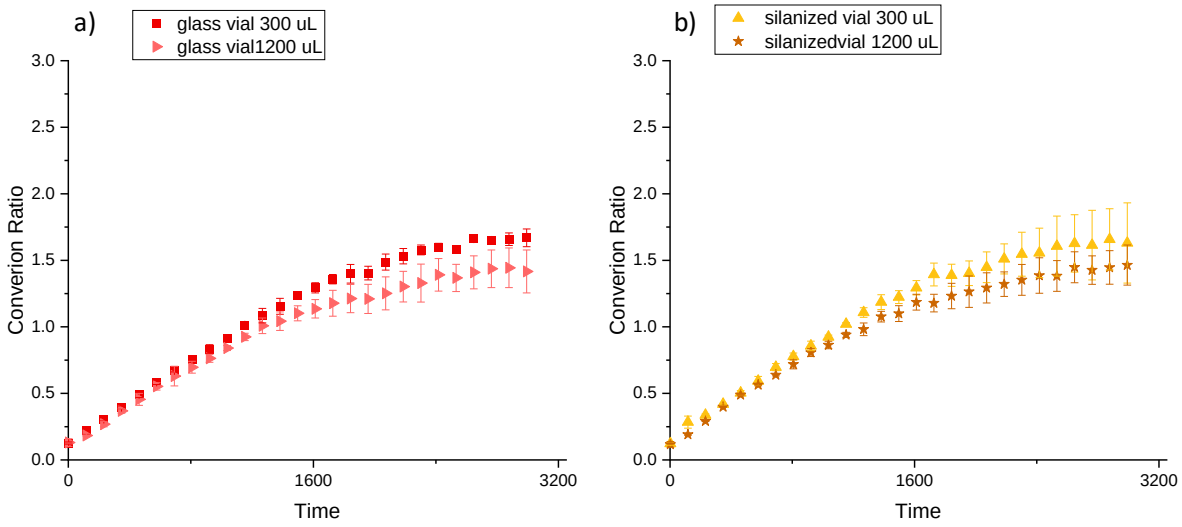

Figure 4.15 Bulk kinetics of the Imine formation reaction at 5 mM at different volumes tested by ESI-MS with automatic sampling in a) glass vials; b) silanized glass vials.

4.5 Conclusions

Here, we have demonstrated the catalysis due to glass in the acceleration of the Katritzky transamination reaction. The reaction rate at the air-solution interface of the glass catalyzed reactions can be accelerated 128-times that of the control for this reaction. The rate enhancement can be further enhanced at high surface-to-volume systems. Reactions with more surface-active reactants displayed drastically larger rate constants at lower concentrations when catalyzed by glass particles. These results further support the mechanism of accelerated reactions observed at air-solution surfaces due to the partial solvation of the reagents at the surface, and solid-solution interfaces due to interaction with glass surfaces. The Claisen-Schmidt and imine formation reactions did not appear to be catalyzed by the presence of glass in high-surface, low-volume

systems. These reactions vary in their mechanistic pathways, yet all undergo dehydration as the final step which does not seem to participate in the catalytic process.

4.6 References

1. W. C. Conner and J. L. Falconer, Chem. Rev., 1995, 95, 759–788.
2. A. Elhage, A. E. Lanterna and J. C. Scaiano, ACS Catal., 2017,7, 250–255.
3. D. Cambie, C. Bottecchia, N. J. W. Straathof, V. Hessel and T. Noel, Chem. Rev., 2016, 116, 10276–10341.
4. A. E. Lanterna, A. Elhage and J. C. Scaiano, Catal. Sci.
5. B. Wang, J. Durantini, J. Nie, A. E. Lanterna and J. C. Scaiano, J. Am. Chem. Soc., 2016, 138, 13127–13130.
6. A. Elhage, B.Wang, M. Marina, M. Luisa Marin, M. Cruz, A. E. Lanterna, J.C. Scaiano, Chem. Sci., 2018, 9, 6844.
7. L. R. Daley and F. Rodriguez, Poly. Eng. and Sci., 1969, 9, 6.
8. J. G. Marsden and S. Sterman, Ind Eng. Chem., 1966, 58, 3.
9. K. A. Andrianov, 1965, Interscience, 109.
10. J. B. Carmicheal, D. J. Gordon, and C. E. Ferguson, J. Gas. Chromatography, 1966 4, 347.
11. D. S. Matteson, W.C. Hiscox, L. Fabry-Asztalos, G. Kim, and W. Siems, 2001, Organometallics, 20, 2920-3.
12. C. A. Ramsden, R. G. Smith, J. Am. Chem. Soc. 1998, 120, 6842-6843.
13. U. Reiser, J. Jauch, E. Herdtweck, Tetra. Assym. 2000, 3345-9.
14. J. J. Devery, J. D. Nguyen, C. Dai and C. R. J. Stephenson, ACS Catal., 2016, 6, 5962–5967.
15. A. B. Moustafa and M. A. Diab, J. App. Poly. Sci., 1975, 19, 1585-91.
16. P. Linder, R. Correa, J. Gino, D. Lemal, J. Am. Chem. Soc., 1996, 118, 2556-63.
17. C. Ramsden and R. Smith, J. Am. Chem. Soc., 1998, 120, 6842-3.
18. S. Pillai, D. Chobisa, D. Urimi, N. Ravindra, J. Pharm. Sci. Res., 2016, 103-11.

CHAPTER 5. ACCELERATED OXIDATION OF ALKANES IN THIN FILMS AND MICRODROPLETS USING FENTON'S CATALYST USING REACTIVE PAPER SPRAY IONIZATION MASS SPECTROMETRY

5.1 Abstract

MS can be utilized for the relative oxidation of non-functionalized, saturated hydrocarbons initiated by oxidation using a modified Fenton's reagent in under ambient conditions using paper spray ionization (PS) mass spectrometry. This was achieved by the combination of thin film and microdroplet formation provided by this ionization method, without the need of pre-analysis filtration or chromatographic separation. This simple analytical method allows for rapid and direct analysis of relatively stable short chain, long chain and highly branched alkanes at atmospheric pressure without sample preparation.

5.2 Introduction

Non-polar hydrocarbons present an additional challenge as they are difficult to analyze by MS under atmospheric conditions.[1-4] The lack of functional groups, aromatic rings and unsaturation in these alkanes in particular can only be analyzed under relatively harsh environmental conditions requiring high voltage input which can lead to unwanted fragmentation.[2-6] As a major constituent of petroleum distillates and industrial waste water, the degradation of alkanes is of great environmental concern.[1, 5-8] The contamination of soils and groundwater by these organic compounds create a widespread issue for remediation efforts.[9-16] Bioremediation by advanced oxidation processes are ideal when time and resources are limited. Fenton's chemistry is an advanced oxidation process involving the catalytic decomposition of hydrogen peroxide by iron (III) chloride to form hydroxyl radicals which can decompose the otherwise stable compounds.[17-19]

We have developed a paper spray ionization method that allows for the oxidation products of saturated alkanes to be monitored by MS in under two minutes. This method relies on the generation of a hydroxyl radical by reacting iron (III) chloride with aqueous hydrogen peroxide on the principle of Fenton's chemistry.

$$Fe^{2+} + H_2O_2 \rightarrow Fe^{3+} + HO\cdot + OH^-$$
$$Fe^{3+} + H_2O_2 \rightarrow Fe^{2+} + HOO\cdot + H^+$$

Scheme 5.1 Generation of hydroxyl radical species vs Fenton's chemistry.

The presence of this radical will come in direct contact with an alkane as it travels through the paper triangle, producing several oxidation products which can be easily monitored by MS. The reagents are added to a paper triangle sequentially, creating a wet, thin film that allows reactions in relatively small volumes to be analyzed directly from paper at atmospheric pressure. Here, the primary goal was the development of a method that would allow for monitoring of relatively stable alkanes through hydroxyl radical oxidation by Fenton's catalyst.

The ability to directly analyze hydrocarbons quickly through forced oxidation and their degradation products under ambient conditions was demonstrated in this study. The use of paper spray ionization removes the need for sample preparation, and the micro-droplets produced from the tip of the paper triangle accelerates the rate of oxidation. The alkane sample is placed in the center of an 8 cm x 8 cm Whatman paper triangle (Fig. 5.1) held in place by a copper alligator clip. A volume of 20 µL of 5 mg/ml iron (III) chloride is dropcast at the rear of the alkane sample spot. When a high voltage (5 kV) is applied to the base of the paper triangle, 50 µL of 30% hydrogen peroxide is slowly added to the rear of the triangle.

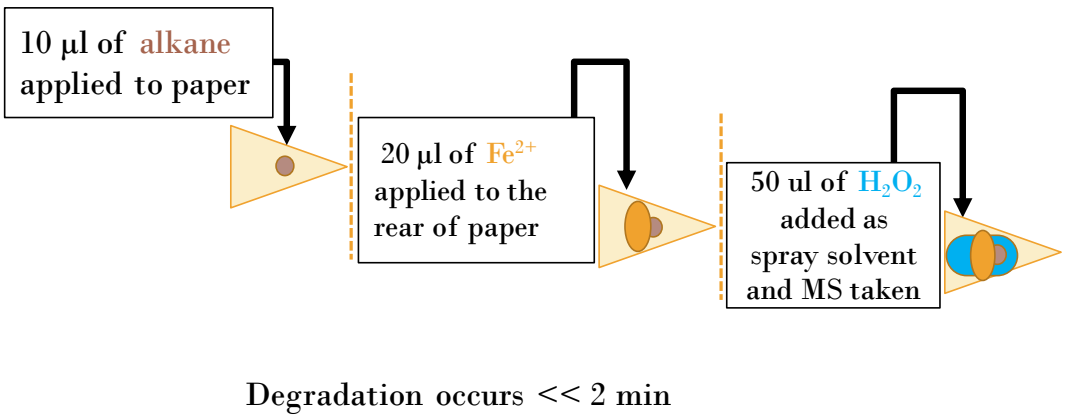

Figure 5.1 Methodology for the Accelerated Oxidation of alkanes using Paper Spray Ionization.

Due to capillary action the peroxide will react with the iron chloride first generating the radical which will subsequently react with the alkane. As the oxidized products travel to the tip of the triangle, micro-droplets are formed and directly enter the mass spectrometer for analysis. Due to the small surface area of the charged droplet and increased analyte concentration as the droplet evaporates, acceleration of the reaction is assumed.

5.3 Experimental

5.3.1 Reagents

All alkanes were purchased from Sigma-Aldrich (St. Louis, MO). HPLC-grade acetonitrile and hydrogen peroxide were purchased from Fisher Scientific (Hampton, NH). Whatman 31 analytical filter paper was purchased from GE Healthcare Bio-Sciences (Pittsburgh, PA).

5.3.2 Paper spray experiments

Whatman 31 filter paper was cut into approximately 8 mm by 10 mm triangles and attached a copper clip (Mueller Electric, Akron, OH) to the base of the triangular-cut paper substrate. This apparatus was placed in front of a Thermo-Fisher LTQ MS (San Jose, CA) and reagents (10 μL of alkane (neat) and 20 μL of 5 mg/ml of iron (III) chloride in acetonitrile) were pipetted sequentially (also known as dropcasting) onto the center of the filter paper and not allowed to dry to maintain a thin film. Elution solvent (40 μL of 30% hydrogen peroxide) was added to the base of the paper, and a 4.5 kV potential was applied for paper spray ionization and MS analysis. Parameters for the MS were spray voltage, 4.5 kV; capillary voltage, 15 V; tube lens, 65 V; capillary temperature, 150 °C; and a mass range of m/z 50–700.

5.4 Results and Discussion

5.4.1 Long chain alkane experiments

We investigated the robustness of the method by analyzing short linear alkanes (nonane and decane), long chain alkanes (heptadecane and heptamethylnonane), and branched alkanes (squalane) in their neat form with no additional sample manipulations. For a target alkane with a

molecular weight M, the mono-oxidized product has a molecular weight of [M+16] and the detected signal at *m/z* $[M+O-H]^+$. In addition to mono-oxidation products, oxidized dimers and trimers, and degradation products were present in the data. Initial studies tested chloroform and peroxide as possible oxidizing agents (Figure 5.2, top and middle).

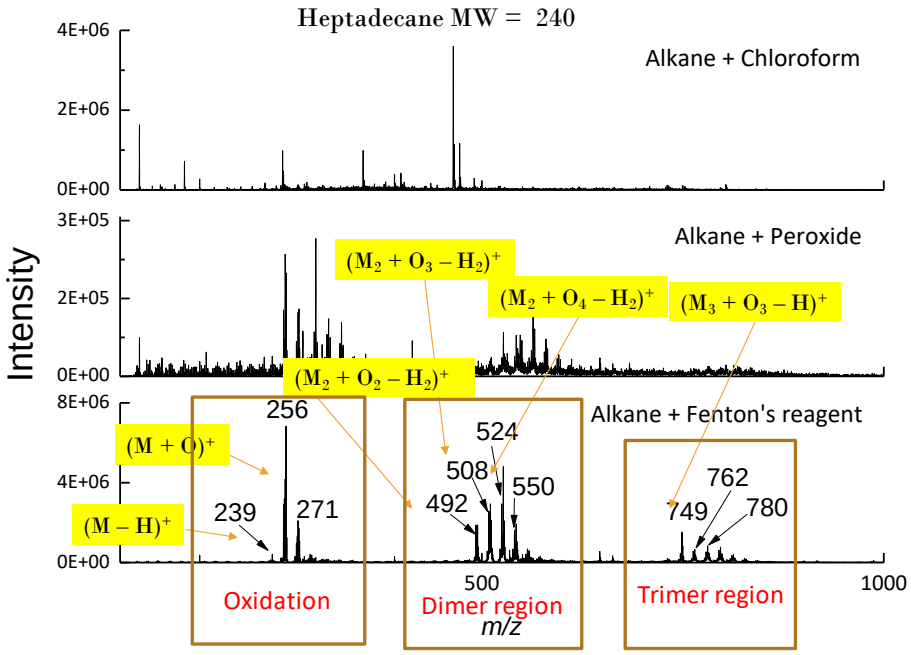

Figure 5.2 Paper spray ionization mass spectra of n-heptadecane as a model alkane to identify optimum oxidizing agent.

Preliminary data utilizing chloroform revealed relatively minimal information with the mono-oxidized product peak at approximately twenty percent of the overall signal intensity. Oxidation was observed with peroxide, yet the signal-to-noise greatly depreciated the data quality. Performing the same method by substituting peroxide for Fenton's catalyst demonstrated the most powerful oxidizing effect while maintaining data integrity (Figure 5.2, bottom). Heptadecane is a long chain, unbranched alkane with a chemical formula of $C_{17}H_{36}$ and is found in several plant species. For the oxidation of heptadecane, we observe the mono-oxidation product ion at *m/z* 256 as the base peak in the spectrum. Several oxidized dimers and trimer were observed in the 400-600 and 700-800 mass range, respectively.

5.4.2 short chain alkane experiments

Decane was selected to identify if the oxidation method is limited to alkanes with longer carbon chains such as in n-heptadecane. Decane is a short, linear alkane with a chemical formula $C_{10}H_{22}$. It is often used for industrial purposes as a type of hydrocarbon solvent commonly used in fuels, such as gasoline. There is clear separation in the mass ranges corresponding to either the oxidation of decane or its oxidized dimers which allows for quick identification without overlapping of product ion peaks. Figure 5.3 displays the oxidative degradation of decane with the dominant contribution from $[M+O-H_2-H]^+$ at *m/z* 155. Several oxidized dimers were observed in the 300-400 *m/z* region of the spectra. Further interrogation at the higher mass range did not reveal any trimer species.

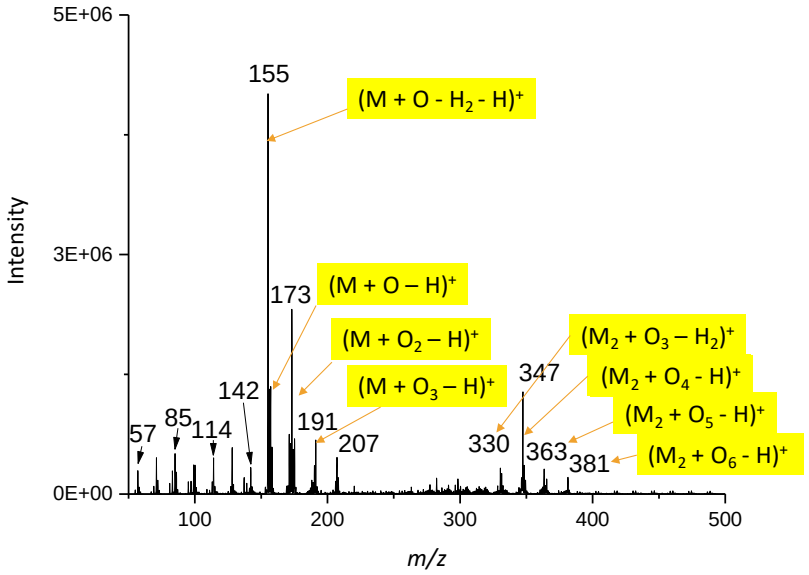

Figure 5.3 Representative MS of oxidation products, oxidized dimers and radical degradation of decane where *m/z* 142 represents the ionized alkane.

In the case of the forced degradation of nonane, several oxidized species were observed as seen in Figure 5.3. Nonane has a chemical formula of C_9H_{20} and is a colorless liquid used as a solvent, as a fuel additive, and a component in biodegradable detergents. The mono-oxidized products at *m/z* 141 and *m/z* 143, one di-oxidized product at *m/z* 157 and an oxidized dimer product at *m/z* 319 were identified. A significant peak appears at *m/z* 371 but could not be identified. The

most abundant peak in the spectra correlates to $[M+O-H_2-H]^+$ at *m/z* 141, in a similar manner to that observed in the oxidation of decane at *m/z* 155.

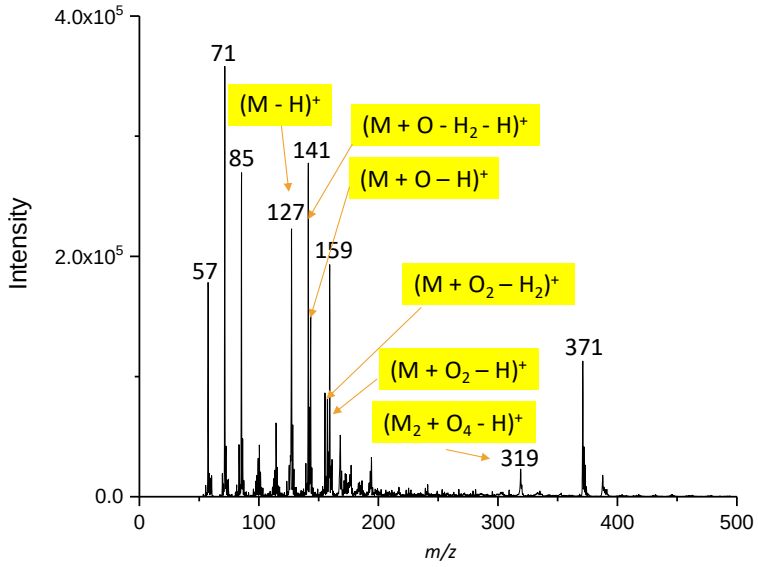

Figure 5.4 Representative MS of oxidation products, oxidized dimer and radical degradation of nonane where *m/z* 127 represents the ionized alkane

5.4.3 Branched alkane experiments

Many alkanes present in nature are known as branched alkanes and differ from the linear alkanes in that a few hydrogens are substituted with carbon chains, such as methyl groups. In the oxidation analysis of heptamethylnonane, the deprotonated alkane ion was observed at *m/z* 225, with the mono-oxidization product at *m/z* 241, as in Figure 5.5. Also known as isocetane, this highly branched alkane is a colorless liquid used as a reference standard in fuel measurements, and has a chemical formula of $C_{16}H_{34}$. No oxidized dimers or trimers were detected for this sample by this method. However, a tri-oxidized product was detected at *m/z* 271, and a highly oxidized product of $[M+O_9-H]^+$ was found at *m/z* 371.

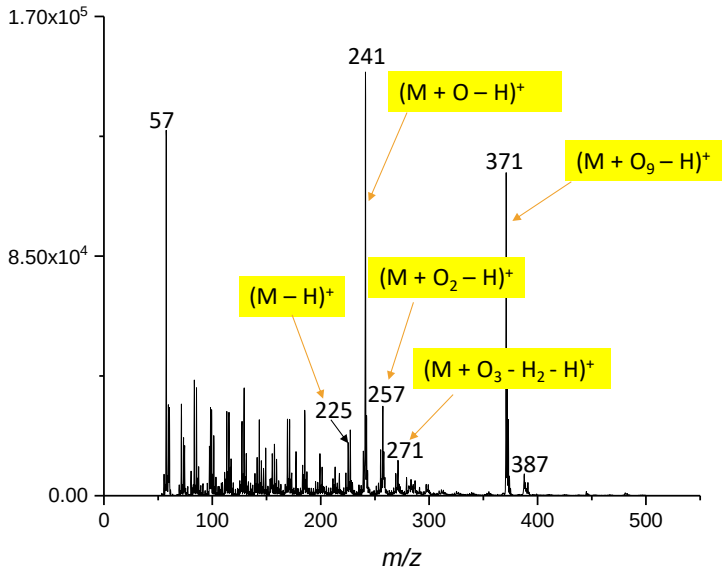

Figure 5.5 Representative MS of oxidation products, oxidized dimers and radical degradation of heptamethylnonane where *m/z* 225 represents the ionized alkane.

Interestingly, the peak at *m/z* 371 correlates to the unknown product peak found in the case of nonane oxidation, yet here the relative abundance is significantly greater than previously mentioned. The difference in the structure of the two compounds is the seven branched methyl groups attached the main alkane backbone chain.

Similarly, squalane was selected to investigate the effect of branching and can be seen in Figure 5.6. Squalane has a chemical formula of $C_{30}H_{62}$ and is primarily produced by hydrogenation of squalene, and not susceptible to autooxidation due to complete saturation. In addition to a base peak at *m/z* 435 of the mono-oxidation product of squalane, there is also evidence of degradation through the loss of pentyl groups. Di-oxidized and tri-oxidized oxidation products were reserved at *m/z* 451 and *m/z* 467, respectively. However, it seems the branching of the alkane structure has removed the appearance of oxidized dimers which were present in the degradation of linear alkanes.

This simple method demonstrates the capability of paper spray ionization mass spectrometry coupled with Fenton's reagent can generate various degradation and oxidation products of the representative alkanes as a model for short, long or branched structures containing as little as nine carbons to as many as thirty carbons making up the alkane.

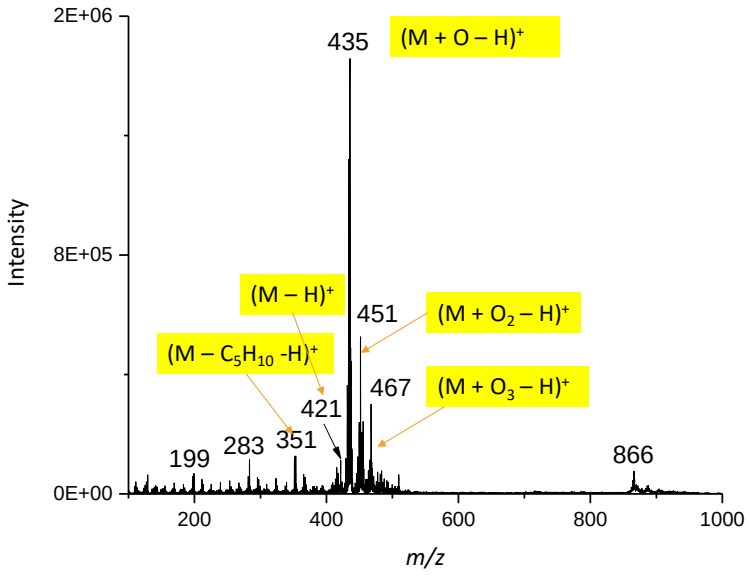

Figure 5.6 Representative MS of oxidation products of squalane where *m/z* 421 represents the ionized alkane.

5.5 Conclusion

This method is highly efficient as minimal sample is consumed to wet the paper triangle and signal stability is observed in less than .25 minutes and remains stable for over 5 minutes of spraying time. As this is a "soft" ionization technique, there is no evidence of fragmentation or ring opening. Analysis under negative mode polarity was also investigated, yet yielded no additional information. This work highlights the importance of a 2 min total analysis time of saturated hydrocarbons without the need for a chromatographic step that can be directly analyzed by paper spray ionization mass spectrometry.

5.6 References

1. Vikse, K. L.; Ahmadi, Z.; Manning, C. C.; Harrington, D. A.; McIndoe, J. S., Powerful insight into catalytic mechanisms through simultaneous monitoring of reactants, products, and intermediates. Angew. Chem. Int. Ed. 2011, 50 (36), 8304-6.

2. Crawford, E. A.; Esen, C.; Volmer, D. A., Real-time monitoring of containerless microreactions in acoustically levitated droples via ambient ionization mass spectrometry. Anal. Chem. 2017, 89 (22), 12511-9.

3. Bain, R. M.; Pullium, C. J.; Ayrton, S. T.; Bain, K.; Cooks, R. G., Accelerated hydrazine formation in charged microdroplets. Rapid. Commun. Mass. Spectrom. 2016, 30 (16), 1875-8.

4. Wu, C.; Qian, K.; Nefliu, M.; Cooks, R. G., Ambient analysis of saturated hydrocarbons using discharge-induced oxidation in desorption electrospray ionization. J. Am. Soc. Mass Spectrom. 2010, 21, 261-7.

5. Wu, C.; Ifa, D. R.; Manicke, N. E.; Cooks, R. G., Rapid, direct analysis of cholesterol by charge labeling in reactive desorption electrospray ionization.

6. Liang, Z.; Hsu, C. S., Molecular speciation of saturates by on-line liquid chromatography field ionization mass spectrometry. Energy fuels. 1998, 12, 637-643.

7. Gross, J. H.; Vekey, K.; Dallos, A., Field desorption mass spectrometry of large multiply branched saturated hydrocarbons. J. Mass Spectrom. 2001, 36, 522-528.

8. Crawford, K. E.; Campbell, J. L.; Fiddler, M. N.; Duan, P; Qian, K; Gorbaty, M. L; Kentamaa, H. I., Laser-indused acoustic desorption/fourier transform ion cyclotron resonance mass spectrometry for petroleum distallate analysis. Anal. Chem. 2005, 77, 7916-23.

9. Watts, R. J.; Haller, D. R.; Jones, A. P; Teel, A. L., A foundation for the risk-based treatment of gasoline-contaminated soils using modified Fenton's reactions. J. Hazard. Mater. 2000, B76, 73-89.

10. Atlas, R. Cerniglia, C. Bioremediation of petroleum pollutants, diversity and environmental aspects of hydrocarbon biodegradation. Bioscience, 1995, 45, 332-338.

11. Walling, C. Fenton's reagent revisited. Acc. Chem. Res., 1975, 8, 125-131.

12. Dorfman, L. Adams, G. Reactivity of the hydroxyl radical in aqueous solutions, Rep. No. NSRDS-NBS-46, National Bureau of Standards, Washington, DC, 1973

13. Haag, R., Yao, C. Rate constants for reaction of hydroxyl radicals with several drinking water contaminants. Environ. Sci. Technol., 26 (1992), pp. 1005-1013

14. Walling, C. Johnson, R. Fenton's reagent: V. Hydrocarbon and side-chain cleavage of aromatics. J. Am. Chem. Soc. 1975, 363-367.

15. Bowers, A., Eckenfelder Jr., W., Gaddipati, P., Monsen, R. Treatment of toxic or refractory wastewaters with hydrogen peroxide Water Sci. Technol., 21, 1989, 477-486

16. Moreda, W.; Perez-Camino, M. C.; Cert, A. Gas and liquid chromatography of hydrocarbons inedible vegetable oils. J Chrom A. 2001, 936,159-171.

17. Iyer, S. Millar, T. Clemens, S. Zachgo, M. Giblin, Taylor. Kunst, L. Sanchez, J. Gerda-Olmeo, E. Martinez-Force, E. Advances in plant lipid research, 1998, 87.

18. Lanzom, A. Albi, T. Cert, A, Gracian, J. J. Am Oil Chem Soc., 1994, 71, 285.

19. McGill, A. Moffat, C.F, Mackie, P. Cruickshank, P. J. Sci. Food Agric., 1993, 357.

CHAPTER 6. ELECTROCYCLIZATION AND DIMERIZATION OF ETHYNYL ANILINES IN MICRODROPLETS

6.1 Abstract

Reaction monitoring by electrospray ionization requires that ions observed in the gas-phase reflect the chemical composition of the solution phase. The electrocyclization of symmetrically substituted 4-ethynyl aniline derivatives containing electron-donating (*N*,*N*-dimethylamino or *N*,*N*-diethyl amino) groups has been investigated in some detail. Several products were observed in the charged electrospray microdroplet reaction that were not detected in the corresponding bulk solution reaction. The introduction of radical initiators in the solution phase reaction produces identical gas phase products confirmed by their CID fragmentation pattern. We attribute these observations to be a combined result of even-electron and radical processes. Future studies may reveal how this observation affects the interpretation of MS results produced by electrospray ionization.

6.2 Introduction

Recently, there has been a growing interest in the interrogation of chemical reactions in electrospray microdroplets due to the observed rate acceleration in confined volumes. Although the exact mechanisms are not well understood, several contributing factors have been hypothesized including increased molecular contacts[1-3], pH[4], reagent orientation on droplet surface[2,5], and partial solvation of reagents at the air-solution interface resulting in decreased activation barriers.[2,4-10] Previous studies have demonstrated reaction rate acceleration due to enhancement of surface reactivity in confined high-surface-area locations of chemical reagents in both microdroplet and bulk solution experiments.[11-22] Acceleration of reactions in electrospray droplets due to solvent evaporation and droplet lifetime has been examined in a separate experiment by varying the distance between the spray source and the inlet of the mass spectrometer.[3, 6-22]

Microdroplets produce a small volume reaction vessel that provides useful information on reaction intermediates, allows for organic synthesis and scale-up at ambient conditions, and accelerated rate kinetics in comparison to the bulk processes. In contrast, the reaction process does not occur in the solution phase without the addition of a catalyst, yet surprisingly occurs

spontaneously in microdroplets. There have been few studies previously demonstrating this effect of spontaneous occurrence in aqueous microdroplets while the bulk phase solution remains thermodynamically unfavorable.[23] Due to the partial solvation of reagents in microdroplets, it is expected to be a hybrid of the observed effects of the bare, gas-phase ion in contrast to that of the fully solvated solution-phase molecule.[24-25] This may provide evidence for the observation of alternate reaction mechanisms leading to unconventional reaction products.

In this chapter, three unexpected dimerization products of 4-ethynyl-*N*,*N*-dimethylaniline are observed to occur in microdroplets, but not in the bulk reaction. Products are characterized and the even-electron products undergo radical losses upon fragmentation by collision-induced dissociation, a direct violation of the 'even-electron rule'.[24-26] There has been report of a related compound forming dimer species in electrospray droplets observed to having radical fragments.[27-28] Additionally, the effect of the substituent symmetrically bound to the amino group of the aniline was investigated by the analysis of 4-ethynylaniline and 4-ethynyl-*N*,*N*-diethylaniline.

6.3 Experimental

6.3.1 Reagents

All chemicals for spray based reactions and the corresponding bulk-phase reactions were purchased from Sigma-Aldrich (MO, USA), including 4-ethynyl-*N*,*N*-dimethylaniline, 4-ethynylaniline, 4-ethynyl-N,N-diethylaniline, benzoyl peroxide, copper (II) perchlorate hexahydrate, tris(4-bromophenyl)aminium hexachloroantimonate, HPLC grade acetonitrile (CAN), dichlormethane (DCM) and methanol (MeOH). Deionized water was purchased by Thermo-Scientific Barnstead EasyPure II system.

6.3.2 Spray-based reactions

Nanoelectrospray ionization (nESI) was used to generate microdroplets analyzed in this work. A pre-washed, borosilicate nESI emitter was pulled to a tip size ca. 4 µm inner diameter and fitted with a platinum electrode. A +1.5 kV potential was applied for analysis in positive mode. All mass spectrometry measurements were made using an LTQ (Thermo-Fisher, San Jose, CA) ion trap mass spectrometer. Typical MS parameters included averaging of 6 microscans, 100 ms maximum injection time, 15 V capillary voltage, 150 ^{o}C capillary temperature, and 65 V tube lens

voltage. Tandem mass spectra were produced by collision-induced dissociation (CID) fragmentation. ^{1}H NMR, ^{13}C NMR and ^{1}H-^{1}H COSY spectra of **4** were recorded on a Bruker ARX 400 spectrometer at 293 K with deuterated chloroform as the solvent.

6.3.3 Bulk-phase reactions

Reagent **1** (10 mmol) was dissolved in ACN and reflux with or without adding free radical initators, respectively. Three kinds of radical initiators were tested respectively to investigate dimerization products, including benzoyl peroxide, copper (II) perchlorate, and tris(4-bromophenyl)aminium hexachloroantimonate. All bulk-phase reactions were monitored and detected using nESI-MS with the distance between the nanoelectrospray tip and the MS inlet kept minimal (< 1 cm) for off-line analysis under non-accelerating conditions.

6.3.4 Organic synthesis

Four compounds were synthesized in this study including deuterated variants of the starting material (**5-7**) and the covalent dimer (**2**). They were used to verify the electrocyclization occurred during the electrospray process, as well as to investigate the MS^2 fragmentation characteristics of the corresponding cyclization products. Synthetic routes of target molecules are shown below.

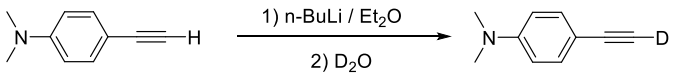

1 **5**

Scheme 6.1 Synthetic route to 4-(ethynyl-d)-N,N-dimethylaniline (**5**).

1H and 13C NMR spectra were recorded on a Bruker ARX 400 or Avance III 500 spectrometer with deuterated chloroform as the solvent.

Compound 5:

4-Ethynyl-*N*,*N*-dimethylaniline (**1**) (145 mg, 1 mmol) in ether (10 mL) was treated with ^{n}BuLi (1.6 M, mL, mmol) at 0 °C (Scheme 6.1). After stirring for 1 h at 0 °C, D_2O (1 mL) was added. The mixture was extracted with ether, and the extract was dried over anhydrous Na_2SO_4

and evaporated to dryness to give 4-(ethynyl-*d*)-*N*,*N*-dimethylaniline (**5**) (142.3 mg, 97.5 %). ESI-MS: *m/z* 147.1 [(M + H)$^+$]. ^{1}H NMR (400 MHz, $CDCl_3$, Figure 6.1) δ 7.41 (d, 2H), 6.64 (d, 2H), 2.98 (s, 6H). The product has no alkyne-H at ~δ 3.0, which means it has been substituted by deuterium.

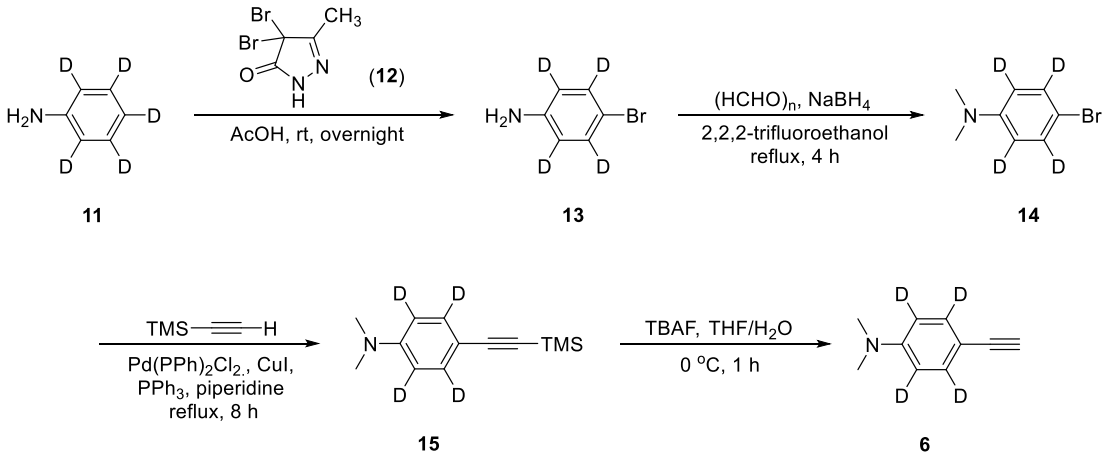

Scheme 6.2 Synthetic route of 4-ethynyl-*N*,*N*-dimethylaniline-2,3,5,6-d_4 (**6**).

Compound 13:

To a solution of aniline-d_5 (**11**) (500 mg, 5.1 mmol) in acetic acid (15 mL) was added 4,4-dibromo-3-methyl-2-pyrazolin-5-one (**12**) (1.42 g, 5.61 mmol) portion-wise over 30 minutes (Scheme 6.2). The reaction was stirred at room temperature overnight and the precipitate was removed via filtration rinsing with cold acetic acid. The acetic acid solution was then diluted with water and brought to pH > 7 via careful addition of solid K_2CO_3. The resulting solution was extracted with Et_2O/hexane = 1/1 (3 × 20 mL) and the organic layers were combined, washed with water, dried over $MgSO_4$, filtered and concentrated under reduced pressure. The resulting residue was purified via silica gel column chromatography Hex/EA = 100/0 to 7/3) to afford 4-bromo-2,3,5,6-tetradeuteroaniline-d_4 (**13**) (580 mg, 64%) as a brown solid. ESI-MS: *m/z* 176.1 [(M + H)$^+$].

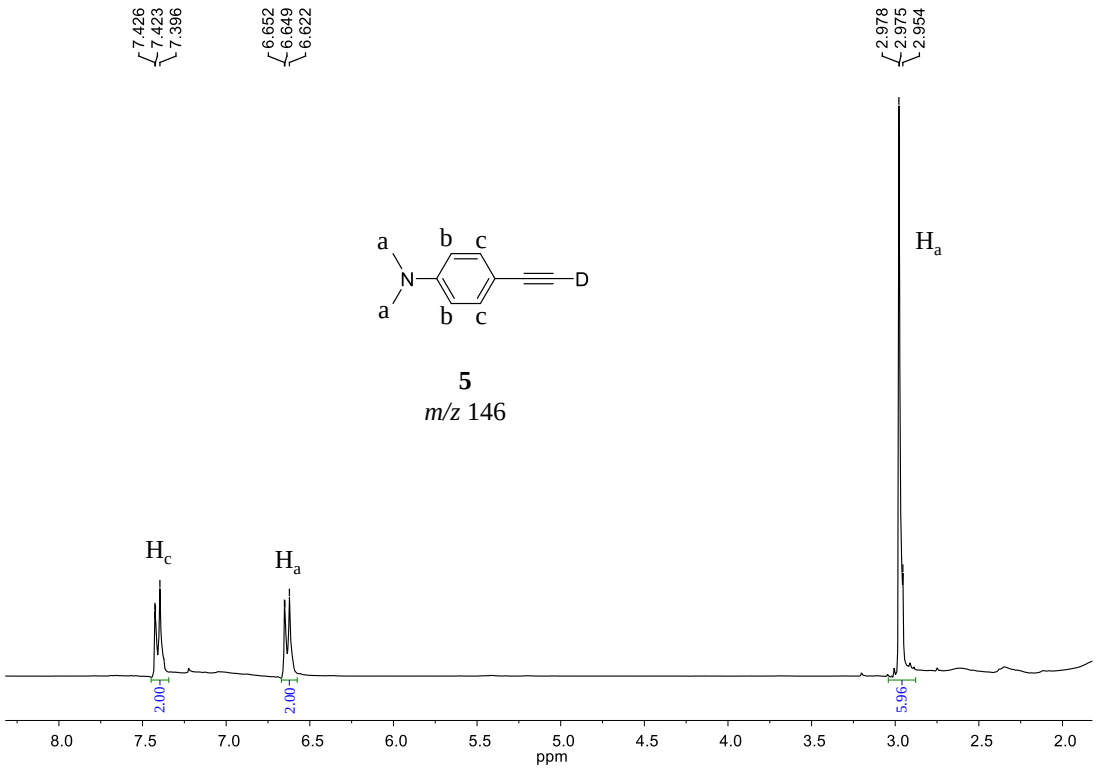

Figure 6.1 400 MHz 1H NMR spectrum of compound (**5**) in CDCl3.

Compound 14:

To a solution of 4-bromo-2,3,5,6-tetradeuteroaniline-d_4 (**13**) (200 mg, 1.39 mmol) in 2,2,2-trifluoroethanol (5 mL) was added paraformaldehyde (168 mg, 5.56 mmol) and $NaBH_4$ (105 mg, 2.78 mmol). The resulting suspension was heated at reflux for 2 h, and cooled to room temperature, then another portion of paraformaldehyde (168 mg, 5.56 mmol) and $NaBH_4$ (105 mg, 2.78 mmol) were added. It was stirred at reflux until the starting material was fully consumed. The solids were filtered off and washed with DCM. It was concentrated to give a residue, which was purified by silica gel column chromatography (Hex/EA = 100/0 to 80/1) to give 4-bromo-*N*,*N*-dimethylaniline-2,3,5,6-d_4 (**14**) (185 mg, 61%) as a brown solid. ESI-MS: *m/z* 204.1 [$(M + H)^+$].

Compound 15:

To a solution of 4-bromo-*N*,*N*-dimethylaniline-2,3,5,6-d_4 (**14**) (92 mg, 0.453 mmol) in piperidine (2.0 mL) was added trimethylsilylacetylene (98 mg, 0.997 mmol, 2.2 eq), CuI (8.6 mg, 0.0453 mmol, 0.1 eq), PPh_3 (23.7 mg, 0.0906 mmol, 0.2 eq) and bis-(triphenylphosphine) palladium(II) chloride (15.9 mg, 0.0227 mmol, 0.05 eq). The resulting mixture was degassed and

charged with Argon (×3), and heated at reflux for 8 h. The reaction mixture was concentrated in vacuo and saturated $NaHCO_3$ was added. The product was extracted with hexane. The combined hexane extracts were washed with water and brine, dried over $MgSO_4$, and concentrated to give a residue, which was purified by silica gel column chromatography to give *N*,*N*-dimethyl-4-((trimethylsilyl)ethynyl)aniline-2,3,5,6-d_4 (**15**) (48 mg, 48%) as a yellow solid. ^{1}H NMR (400 MHz, $CDCl_3$) δ 2.99 – 2.93 (m, 6H), 0.27 – 0.17 (m, 9H). ^{13}C NMR (100 MHz, $CDCl_3$) δ 150.2, 133.1, 132.9, 132.6, 111.6, 111.4, 111.1, 109.8, 106.7, 91.3, 40.3, 0.4.

Compound 6:

To a solution of *N*,*N*-dimethyl-4-((trimethylsilyl)ethynyl)aniline-2,3,5,6-d_4 (**15**) (36 mg, 0.162 mmol) in THF (2 mL) and H_2O (0.3 mL) was added TBAF (1.0 M, 0.18 mL, 0.18 mmol) at 0 ℃ and the reaction was stirred for 1 h at 0 ℃. The reaction mixture was concentrated and H_2O (20 mL) was added. The mixture was extracted with hexane and the combined extracts were dried over Na_2SO_4 and concentrated to give a residue, which was purified by silica gel column chromatography to give 4-ethynyl-*N*,*N*-dimethylaniline-2,3,5,6-d_4 (**6**) (18 mg, 74%) as a yellow-orange solid. ^{1}H NMR (300 MHz, $CDCl_3$) δ 2.98 (s, 1H), 2.97 (s, 6H). ^{13}C NMR (100 MHz, $CDCl_3$) δ 150.4, 133.2, 133.0, 132.7, 111.7, 111.4, 111.2, 109.4, 108.7, 85.0, 74.9, 40.3.

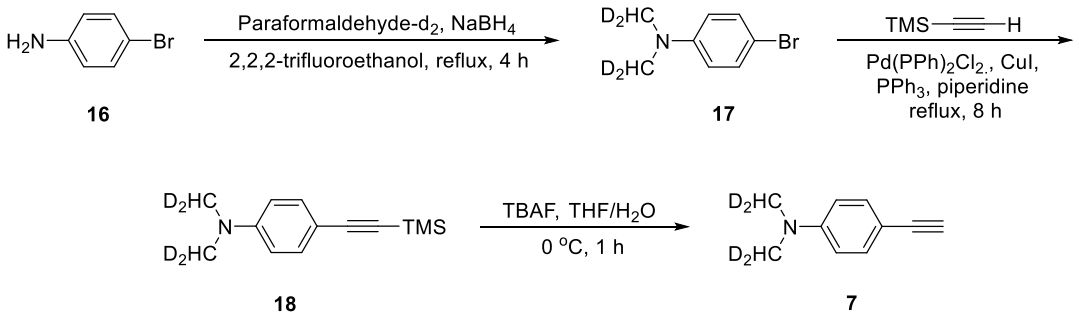

Scheme 6.3 Synthetic route of 4-ethynyl-N,N-bis(methyl-d_2)aniline (**7**).

Compound 17:

To a solution of 4-bromoaniline (344 mg, 2 mmol) in 2,2,2-trifluoroethanol (7 mL) was added paraformaldehyde-d_2 (240 mg, 8 mmol) and $NaBH_4$ (151.3 mg, 4 mmol). The resulting suspension was heated at reflux for 2 h, and cooled to room temperature, then another portion of paraformaldehyde-d_2 (240 mg, 8 mmol) and $NaBH_4$ (151.3 mg, 4 mmol) were added (Scheme 6.3).

It was stirred at reflux until the starting material was fully consumed. The solids were filtered off and washed with TFE. It was concentrated to give a residue, which was purified by silica gel column chromatography (Hex/EA = 100/0 to 80/1) to give 4-bromo-*N*,*N*-bis(methyl-d_2)aniline (**17**) (380 mg, 93.1 %) as a brown solid. ^{1}H NMR (400 MHz, $CDCl_3$) δ 7.31 (d, *J* = 9.2 Hz, 2H), 6.59 (d, *J* = 9.2 Hz, 2H), 2.89 (s, 1H), 2.88 (s, 1H). ^{13}C NMR (100 MHz, $CDCl_3$) δ 149.6, 131.8, 114.1, 108.5, 40.4, 40.2, 40.0, 39.8, 39.6.

Compound 18:

To a solution of 4-bromo-*N*,*N*-bis(methyl-d_2)aniline (**17**) (98 mg, 0.48 mmol) in piperidine (2.5 mL) was added trimethylsilylacetylene (104 mg, 1.06 mmol, 2.2 eq), CuI (9.1 mg, 0.048 mmol, 0.1 eq), PPh_3 (25 mg, 0.096 mmol, 0.2 eq) and bis-(triphenylphosphine) palladium(II) chloride (16.8 mg, 0.024 mmol, 0.05 eq). The resulting mixture was degassed and charged with Argon (×3), and heated at reflux for 8 h. The reaction mixture was concentrated in vacuo and saturated $NaHCO_3$ was added. The product was extracted with hexane. The combined hexane extracts were washed with water and brine, dried over $MgSO_4$, and concentrated to give a residue, which was purified by silica gel column chromatography to give *N*,*N*-bis(methyl-d_2)-4-((trimethylsilyl)ethynyl)aniline (**18**) (78.2 mg, 73.6%) as a yellow solid. ^{1}H NMR (400 MHz, $CDCl_3$) δ 7.34 (d, *J* = 8.8 Hz, 2H), 6.59 (d, *J* = 8.8 Hz, 2H), 2.92 (d, *J* = 1.3 Hz, 2H), 0.30 – 0.15 (m, 9H). ^{13}C NMR (100 MHz, $CDCl_3$) δ 150.4, 133.3, 111.7, 110.0, 106.7, 91.3, 39.9, 39.7, 39.5, 39.3, 0.4.

Compound 7:

To a solution of *N*,*N*-bis(methyl-d_2)-4-((trimethylsilyl)ethynyl)aniline (**18**) (30 mg, 0.136 mol) in THF (2 mL) and H_2O (0.3 mL) was added TBAF (1.0 M, 0.15 mL, 0.15 mmol) at 0 °C and the reaction was stirred for 1 h at 0 °C. The reaction mixture was concentrated, and H_2O (20 mL) was added. The mixture was extracted with hexane and the combined extracts were dried over Na_2SO_4 and concentrated to give a residue, which was purified by silica gel column chromatography to give 4-ethynyl-*N*,*N*-bis(methyl-d_2)aniline (**7**) (16.0 mg, 79.2%) as a yellow-orange solid. ^{1}H NMR (400 MHz, $CDCl_3$) δ 7.38 (d, *J* = 8.7 Hz, 2H), 6.62 (d, *J* = 8.7 Hz, 2H), 2.98 (s, 1H), 2.94 (d, *J* = 1.5 Hz, 2H). ^{13}C NMR (100 MHz, $CDCl_3$) δ 150.6, 133.4, 111.8, 108.9, 85.0, 74.9, 40.1, 39.9, 39.7, 39.5, 39.2.

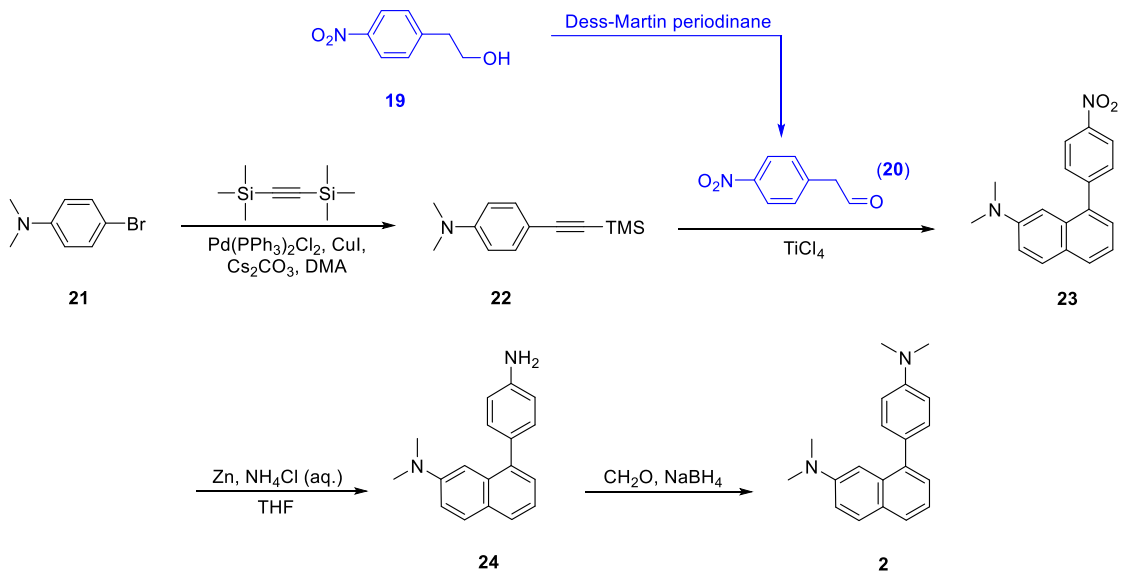

Scheme 6.4 Synthetic route of 8-(4-(dimethylamino)phenyl)-N,N-dimethylnaphthalen-2-amine (**2**).

Compound 20:

To a solution of 2-(4-nitrophenyl)ethanol (**19**) (8.5 g, 50 mmol) in DCM (100 mL) was added Dess-Martin periodinane (DMP) (21 g, 50 mmol) with stirring at 0 °C. And then, the reaction was stirred at room temperature overnight. The solids were filtered off and washed with DCM. It was concentrated to give a residue, which was purified by silica gel column chromatography (PE /EA = 1/1) to give 2-(4-nitrophenyl)acetaldehyde (**20**) (5.2 g, 60%) as a light yellow solid. The product was kept in the refrigerator. ESI-MS: *m/z* 166.1 $[(M + H)^+]$.

Compound 22:

To a solution of 4-bromo-*N*,*N*-dimethylaniline (**21**) (2 g) in DMA (20 mL) was degassed and charged with Argon (×3). $Pd(PPh_3)_2Cl_2$ (350 mg), CuI (100 mg) and Cs_2CO_3 (328 mg) were added and heated at 120 °C. The solution was added 1,2-bis(trimethylsilyl)ethyne (3.4 g) dorpwise and then heated at 120 °C for 1 h. After being cooled to room temperature, the reaction mixture was extracted with EA (70 mL), washed by 10% NaCl (70 mL ×2), dried over anhydrous Na_2SO_4 and evaporated to dryness to give crude product. Silica gel column chromatography was used to purify the crude product to give *N*,*N*-dimethyl-4-((trimethylsilyl)ethynyl)aniline (**22**) (90 mg, 4%) as a light yellow solid. ESI-MS: *m/z* 218.1 $[(M + H)^+]$.

Compound 23:

To a solution of *N*,*N*-dimethyl-4-((trimethylsilyl)ethynyl)aniline (**22**) (220 mg) in DCM (15 mL) was added **20** (340 mg). The solution was added $TiCl_4$-DCM solution (570 mg $TiCl_4$ desolved in 5 mL DCM) dorpwise at room temperature, and then was stirred at room temperature for 2 h. TLC showed the reaction was completed, and the saturated Na_2CO_3 (60 mL) was added. The reaction mixture was extracted with EA (70 mL ×3), dried over anhydrous Na_2SO_4 and evaporated to dryness to give crude product **23** (420 mg). ESI-MS: *m/z* 293.1 [$(M + H)^+$]. The crude product was used for next step directly.

Compound 24:

To a solution of crude *N*,*N*-dimethyl-8-(4-nitrophenyl)naphthalen-2-amine (**23**) (420 mg) in THF (20 mL) and saturated NH_4Cl aq. (20 mL) was added Zn powder (560 mg), and the reaction mixture was stirred at room temperature. TLC was used to monitor the reaction process. After complete reaction, the solution was adjusted to pH ~8 using saturated Na_2CO_3, extracted with EA (70 mL ×2), dried over anhydrous Na_2SO_4 and evaporated to dryness to give crude product. Silica gel column chromatography (PE → PE/DCM=1/1 → DCM/MeOH=100/1) was used to purify the crude product to give 8-(4-aminophenyl)-*N*,*N*-dimethylnaphthalen-2-amine (**24**) (150 mg) as a light yellow solid. ESI-MS: *m/z* 263.1 [$(M + H)^+$].

Compound 2:

To a solution of 8-(4-aminophenyl)-*N*,*N*-dimethylnaphthalen-2-amine (**24**) (100 mg) in THF (20 mL) and formaldehyde aq. (5 mL) was added concentrated H_2SO_4 (1 mL). The reaction solution was added $NaBH_4$ portionwise (100 mg ×3), and then it was stirred at room temperature. After complete reaction (TLC), the solution was adjusted to pH ~8 using saturated Na_2CO_3, extracted with EA (100 mL ×2), dried over anhydrous Na_2SO_4 and evaporated to dryness to give crude product. Silica gel column chromatography (PE → PE/DCM=1/1 → DCM/MeOH=100/1) was used to purify the crude product to give 8-(4-(dimethylamino)phenyl)-*N*,*N*-dimethylnaphthalen-2-amine (**2**) (10 mg, 9%) as a light yellow solid. ^1H NMR (400 MHz, $CDCl_3$, Figure 6.2) δ 7.75 – 6.85 (Ar-H, 10H), 3.03 (s, 6H), 2.94 (s, 6H).

The MS and MS^2 spectra of the synthesized covalent bond dimer (**2**) was showed in Figure 6.3a and 6.3b. The fragmentation rule of the synthesized covalent bond dimers is as same as the covalent bond dimers generated by spray experiments (Figure 6.3c).

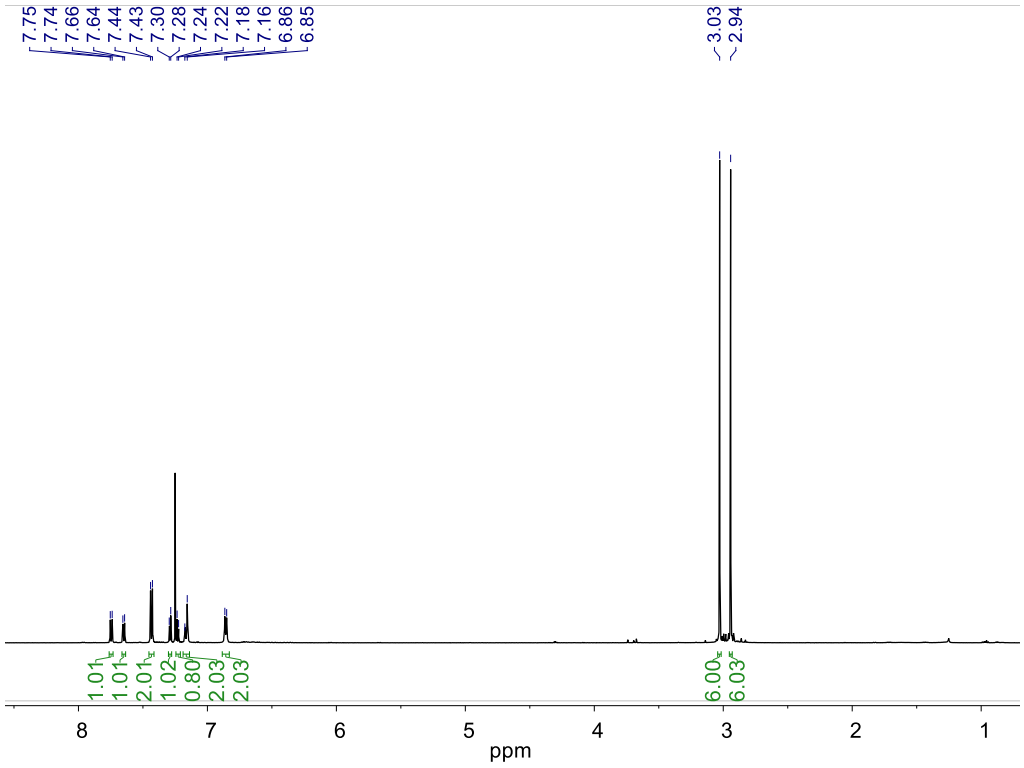

Figure 6.2 400 MHz 1H NMR spectrum of compound **2** in CDCl3.

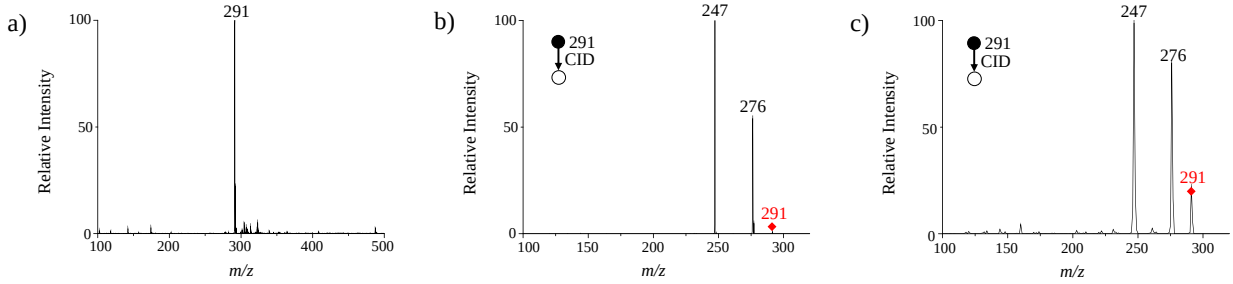

Figure 6.3 MS and MS^2 spectra: a-b) synthesized covalent bond dimer; c) covalent bond dimer generated in spray experiments.

The ^{13}C NMR spectrum of compound **4** is given in Figure 6.4. ^{13}C NMR (100 MHz, $CDCl_3$) δ 158.5, 152.4, 149.4, 138.8, 137.3, 132.8, 132.1, 127.1, 123.5, 121.2, 118.5, 112.2, 81.7, 80.7, 44.8. 40.0.

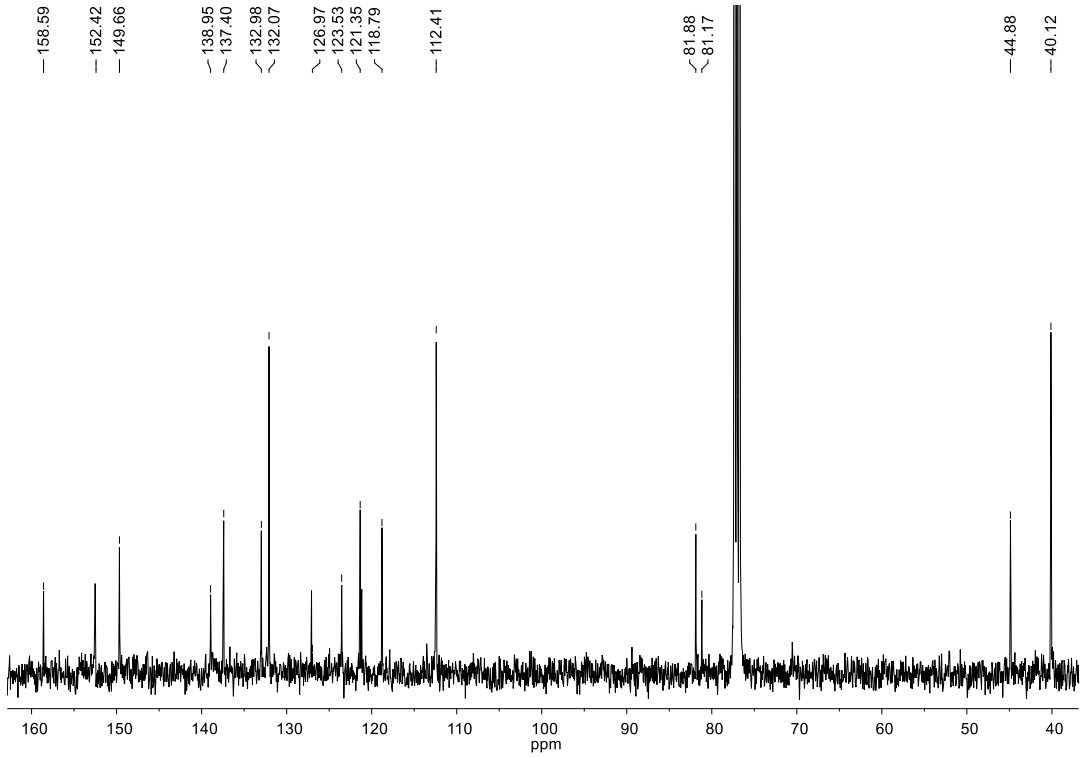

Figure 6.4 400 MHz ^{13}C NMR spectrum of compound 4 in $CDCl_3$.

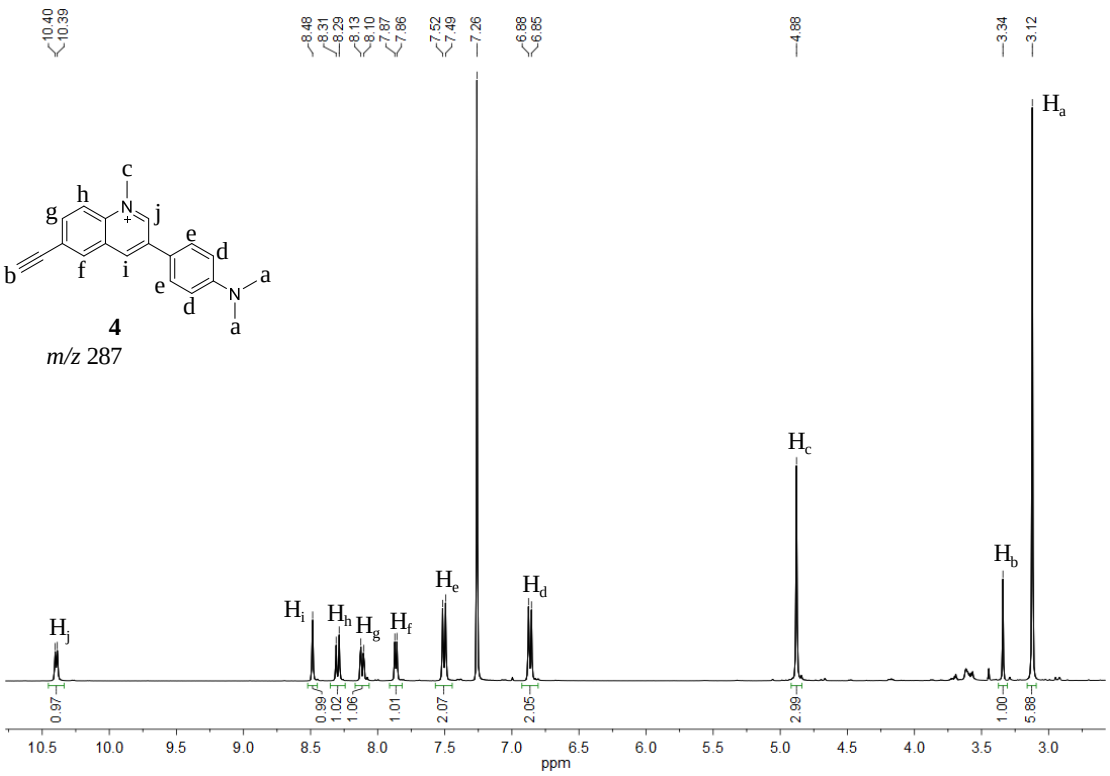

Figure 6.5 400 MHz ^{1}H NMR spectrum of compound 4 in $CDCl_3$.

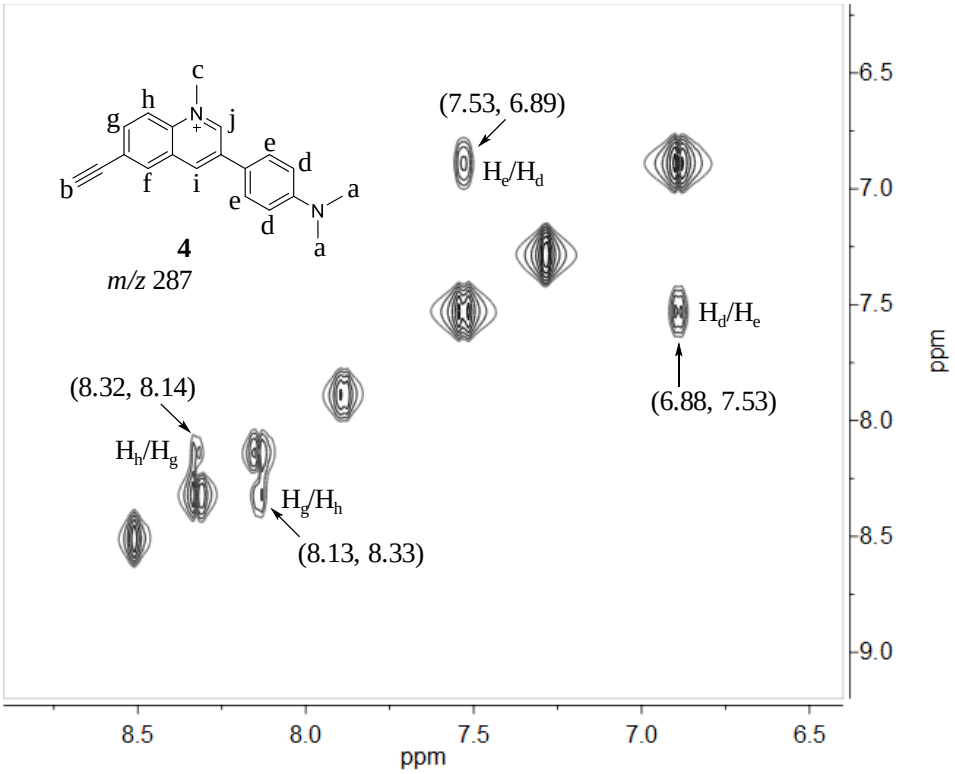

Figure 6.6 400 MHz ^{1}H-^{1}H COSY spectrum of compound 4 in $CDCl_3$.

6.3.5 Theoretical chemistry

All density functional theory (DFT) calculations were performed using the Gaussian 09[15] program package employing the hybrid B3LYP[16,17] exchange correlation functional. For all reaction pathways, the 6-311+G(d) basis sets[18] were used for C, H, N atoms. The reaction calculations involve geometry optimization of reactant and products. Vibrational frequency calculations were performed to ensure the reactant and product have zero frequency. The reported energies (ΔH_{0K} in eV) are corrected with zero-point vibrations. The results of simulations have been summarized in Figure 6.7.

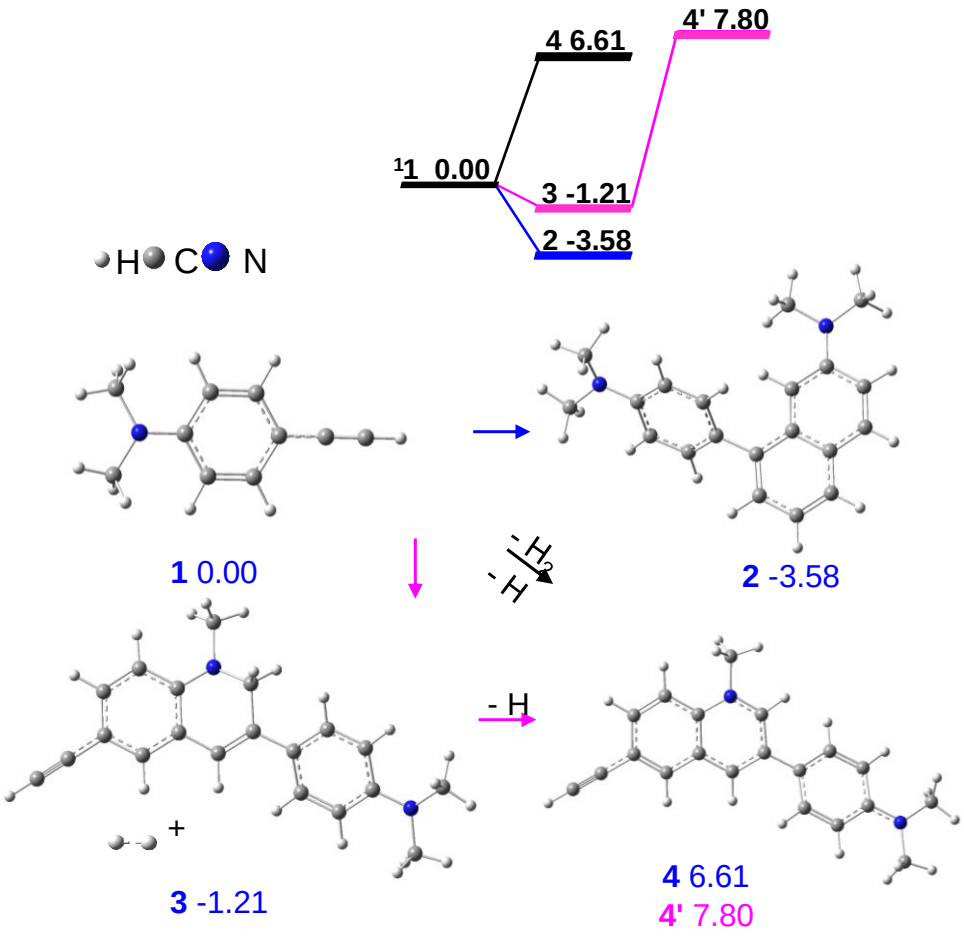

Figure 6.7 Chemical process simulated by computation (eV).

6.4 Results and Discussion

6.4.1 4-Ethynyl-N,N-dimethylaniline dimerization

Microdroplets generated by the electrospray process resulted in the expected protonated monomer **1**, but also results in the formation of three dimer species (Scheme 6.5, Figure 6.8). Other isomers are possible for the structure of these compounds. The relative intensity of these dimer species is increased with increased distance between the spray source and the MS inlet. It is hypothesized that these reactions occur in the droplets and not in bulk solution. To test this hypothesis, reagent **1** was reacted under reflux conditions and analyzed by NMR. Spray experiments with different spray distances were performed by coupling with a stainless steel transfer tube to study whether the covalent dimer product is formed in the spray process.

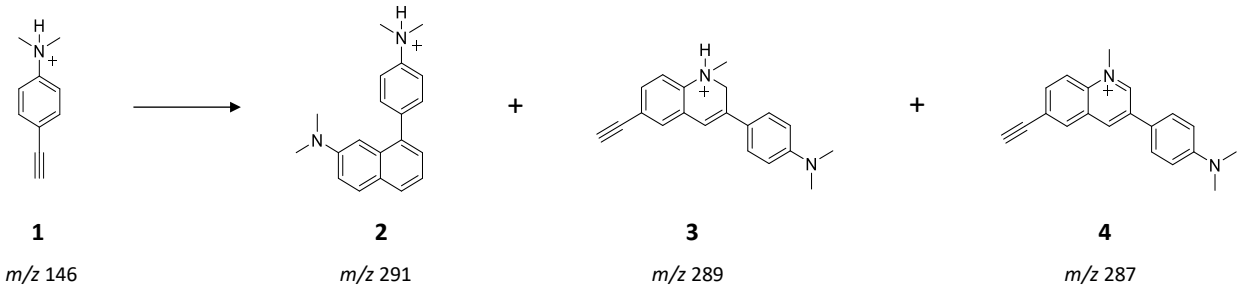

Scheme 6.5 4-ethynyl-*N*,*N*-dimethylaniline (**1**, *m/z* 146) forms three dimer species when electrosprayed, a covalent bond dimer (**2**, *m/z* 291) and two dehydrogenation products, **3** (*m/z* 289), and **4** (*m/z* 287).

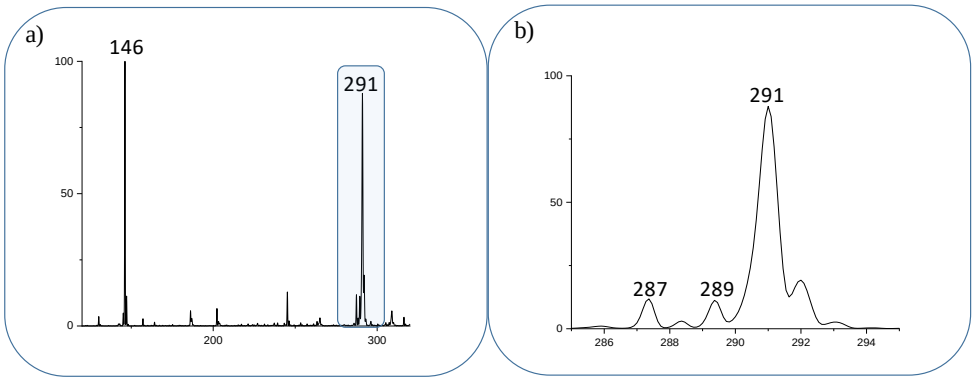

Figure 6.8 a) MS analysis of 4-Ethynyl-*N*,*N*-dimethylaniline (**1**, observed at *m/z* 146 as $[M+H]^+$) forms three dimer species **2** ($[2M+H]^+$ observed as at *m/z* 291), **3** ($[2M-H]^+$ observed at *m/z* 289) and **4** ($[2M-3H]^+$ observed at *m/z* 287), b) highlighted region of interest expanded to show the three products observed in electrospray analysis.

Nanoelectropray droplets results in the observation of the electrocyclization of the covalent dimer (**2**) synthesized by carbon-carbon bond formation. Surprisingly, after further investigation two dehydrogenated dimer products (**3** and **4**) were synthesized in the electrospray process. This sugests that the formation of covalent dimer product (**2**) and dimer products (**3** and **4)** undergo different reaction pathways. Due to the lone pair of electrons on the nitrogen of aromatic amines, dimer products can be generated by head-to-tail (htt), tail-to-tail (ttt), or head-to-head (hth) linkages. Dimethylanilines have been shown to dimerize in several electrochemical and electrospray experiments to form both tail-to-tail (ttt) coupling and head-to-tail (htt) coupling products.[21-23] However, it seems unlikely in this case to form the substituted diphenyl diacetylene or ttt product which requires initiation by means of thermal, photochemical, or irradiation sources. A head to tail structure has also been considered, yet based upon fragmentation patterns seem to

be less likely. A previous study demonstrated the ability of a nitrogen in an amino form bound to an aromatic system transforms into a quartenary ammonium form when analyzed by ESI.[24] The dimethylamino and alkyl groups of the aromatic ring are strong electron-donating groups, allowing for possible attack from the protonated monomer initiated in the spray method to form these dimers.

Tandem mass analysis of the covalent dimer (**2**) was utilized for the confirmation of the proposed dimer observed in the spray method. The major fragments are the result of the loss of a methyl radical (•CH_3) at *m/z* 276 (Figure 6.9) and the loss of a dimethylamino radical (•$N(CH_3)_2$) at *m/z* 247 (Figure 6.10). Spray-based experiments were also carried out using synthetized deuterated variants of the starting materials (**5-7**) to verify the fragmentation of these covalent dimers (Figure 6.11). The radical losses that are observed here are contradictory to the "even-electron rule" where a closed-shell species does not normally fragment to form an open-shell species. This rule is violated when a particularly stable radical cation species is formed, as is the case here where a resonance stabilized radical cation species is formed by the loss of a methyl or dimethylamino radical species[24-26].

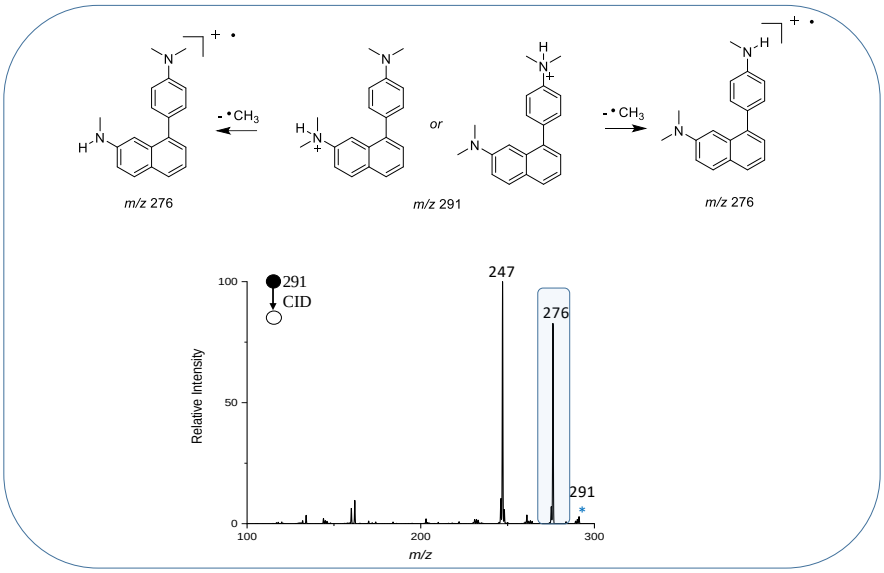

Figure 6.9 CID spectrum of covalent bond dimer **2** results in a major peak observed at *m/z* 276 due to loss of a methyl radical.

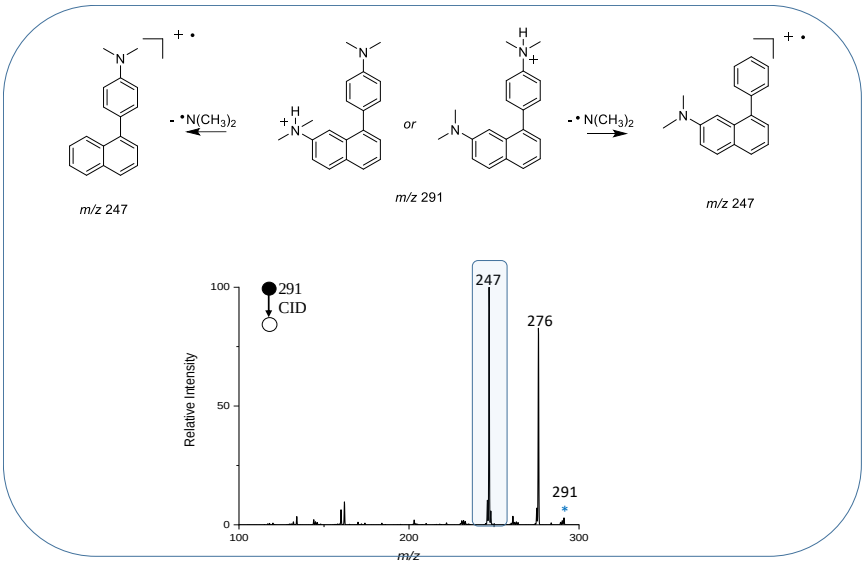

Figure 6.10 CID spectrum of covalent bond dimer **2** results in a major peak observed at *m/z* 247 due to loss of a dimethylamino radical.

The structure of the covalent dimer was first suggested as compound **2** based on high resolution mass spectrometry (HRMS) detection. To validate the structure of the covalent dimer, we synthesized **2** and characterized it with NMR. This confirmed our previous deduction on its structure as the fragmentation of the bulk synthesized compound matches that of the compound observed in spray. The structure of the covalent dimer has also been confirmed by collection and purification of an offline electrospray experiment (Bulk Organic Synthesis section, Figure 6.3).

In addition to the formation of the major product **2**, a secondary (**3**) and tertiary (**4**) reduced dimer products are observed at lower intensity when compared to product **2**. Though dimer species **3** and **4** are observed in the gas phase, the chemistry can be interrogated through solution phase chemistry through the addition of a radical initiator. Various radical initiators, including benzoyl peroxide (**8**), copper (II) perchlorate hexahydrate (**9**) and tris(4-bromophenyl)aminium hexachloroantimonate (**10**), have been used in this study to produce radicals by various mechanisms (Figure 6.12).

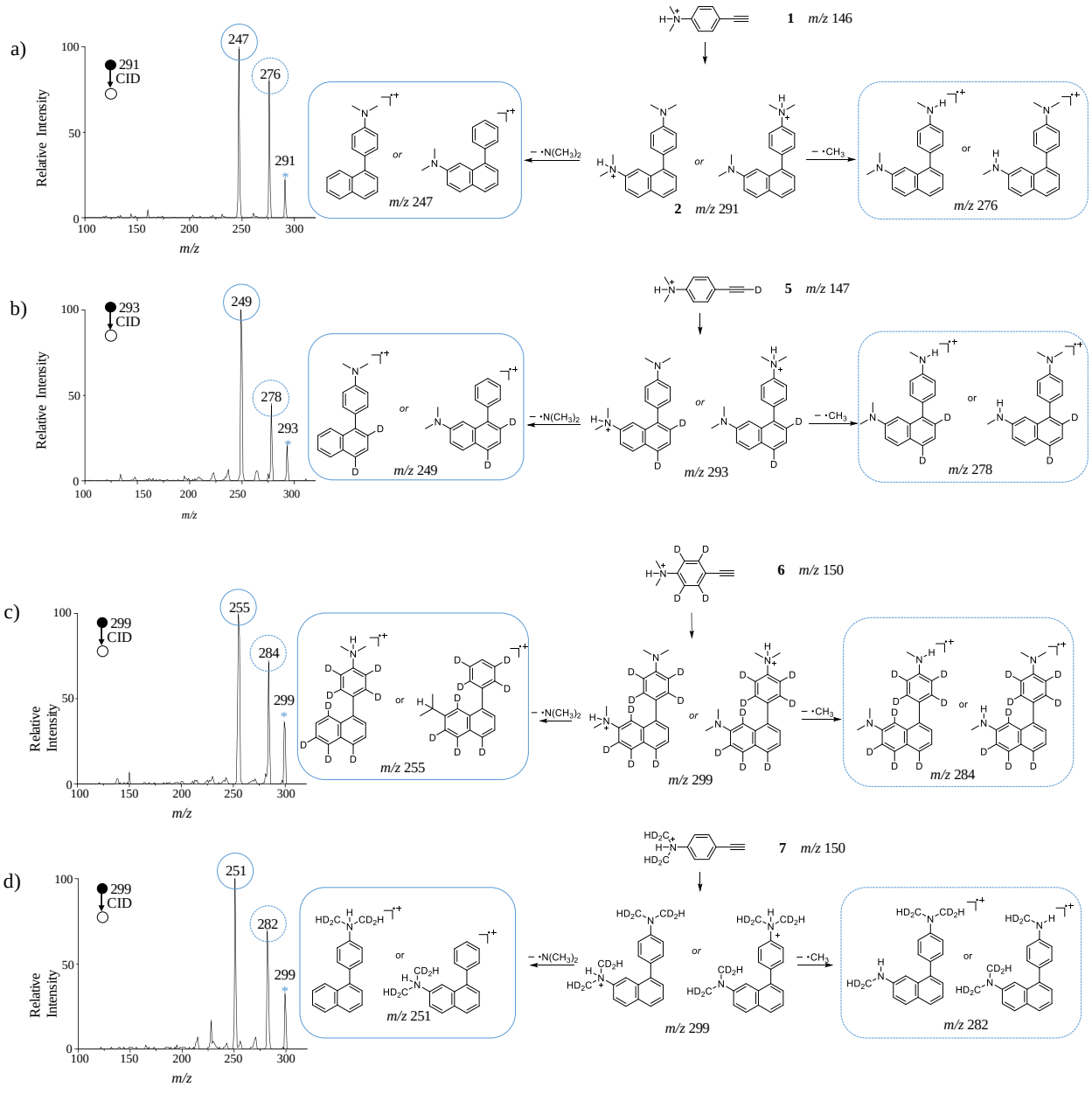

Figure 6.11 CID spectra of covalent bond dimers result in major peaks at the loss of a methyl radical and a dimethylamino radical: a) dimer *m/z* 291 formed from **1**; b) dimer *m/z* 293 formed from **5**; c) dimer *m/z* 299 formed from **6**; b) dimer *m/z* 299 formed from **7**. The corresponding fragments observed in the MS^2 were shown in right hand side.

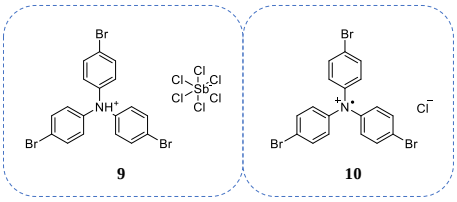

Figure 6.12 Radical initiators **9** and **10** utilized in bulk synthesis.

In previous studies, the oxidative dimerization of *N*,*N*-dimethylaniline was observed in acetonitrile solution via cyclic voltammetry and a reactive dimethylaniline radical intermediate species was observed.[27,29] This reaction is also observed in electrospray microdroplets and the radical intermediate species has been observed via desorption electrospray ionization on a platinum electrode by Zare and co-workers.[26] This reaction is also observed in bulk by a radical initiator species, such as copper (II).

$$M + Cu^{2+} \rightarrow M^{+\bullet} + Cu^{+} \qquad \text{Eq. 1}$$

This method has been used to dimerize *N*,*N*-dimethylaniline in a bulk-phase reaction.[52] Copper species with a counter ion that is not a strong nucleophile result in the dimerization of *N*,*N*-dimethylaniline; when a strong nucleophile is present, such as Cl^-, a chlorine addition product is observed. Benzoyl peroxide is a free radical initiator that is commonly used for initiation of polymerization.[53] Benzoyl peroxide has also been used in small molecule chemistry for the oxidation of pyroles.[54] In addition, tris(4-bromophenyl)aminium hexachloroantimonate is a stable radical species that is commonly used to initiate C-H bond transformations through radical chemistry.[55] In our case, these radical initiation species synthesized in the bulk solution produces the same compounds observed in the gas phase. This solution phase chemistry allows for their synthesis and purification for NMR structural determination.

The reaction of **1** with **8**, a very good oxidizing agent, results in the formation of **3** or with **9**, a common radical initiator, resulting in the formation of **4**. Dehydrated dimer products **3** and **4** are both formed in the presence of **10**, a stable radical species commonly used to initiate carbon-hydrogen bond transformations. This difference may be due to the different activity of free radicals themselves. These dimer species were confirmed as the observed spray-based product by comparison of CID fragmentation. The structure of **4** was further confirmed by NMR analysis. The use of bulk phase chemistry to inform spray- based reactions has not been previously done.

This analysis not only identifies the spray product but also gives insight into the mechanism of the reaction, (described later in Figures 6.17 and 6.18).

Copper (I) forms a very stable complex with acetonitrile which allows copper (II) salts to be very good oxidizing agent in acetonitrile.[56] The perchlorate salt is used because in the presence of a strong nucleophile, such as Cl^- or Br^-, nucleophilic attack to the aromatic ring occurs. Figure 6.13a shows the bulk reaction of **1** with copper (II) perchlorate hexahydrate after initial mixing.

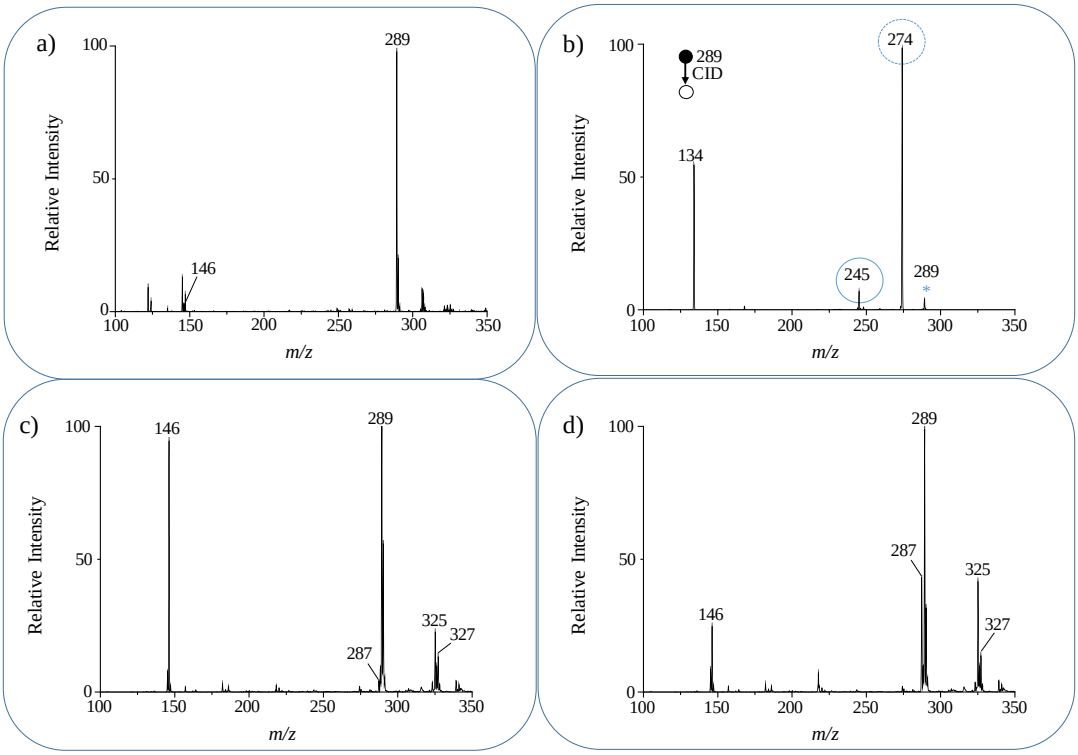

Figure 6.13 Bulk reaction progress of **1** with copper (II) perchlorate hexahydrate radical intiator: a) MS spectrum of after initial mixing; b) MS^2 spectrum of *m/z* 289 shows the loss of a methyl radical and a dimethylamino radical, which mirrors the covalent dimer CID spectrum; Bulk reaction progress of **1** with tris(4-bromophenyl)aminium hexachloroantimonate c) MS spectrum after initial mixing; d) MS spectrum after 1 hr of reaction time.

Figure 6.13b shows the MS^2 of *m/z* 289, and the loss of a methyl radical and a dimethylamino radical, which mirrors the covalent dimer CID spectrum after initial mixing as Attempts to purify the compound with *m/z* 289 from the copper (I) salt have not been successful. Because of the stable complex with acetonitrile, it is difficult to get an NMR where the *m/z* 289 signal is not swamped by the acetonitrile signal. This reaction does not form *m/z* 287 and the sole

dimer product is *m/z* 289. There are peaks at *m/z* 325 and *m/z* 327 that potentially correspond to a dimer where the aromatic ring has undergone a nucleophilic substitution with a chlorine, but this product has not been investigated.

The radical initiators discussed have produced either *m/z* 287 or *m/z* 289, while reactions with the stable radical species tris(4-bromophenyl)aminium hexachloroantimonate (**10**) has resulted in the formation of both *m/z* 287 and *m/z* 289. Immediately after mixing, shown in Figure 6.13c, the major peak is *m/z* 289. After 1 h. of mixing, shown in Figure 6.13d, a much greater fraction of *m/z* 287 is formed. In addition, the possible chlorinated dimer species is formed, but this species has not been characterized. Preliminary separation experiments have been done and show positive results that *m/z* 289 can be isolated and its structure confirmed via NMR.

Tandem mass analysis of **3** formed in the spray based method reveals fragmentation due to radical losses (Figure 6.14) and neutral losses (Figure 6.15). The radical losses observed for this structure are a result of a loss of a methyl radical ($\bullet CH_3$) at *m/z* 274 and the loss of a dimethylamino radical ($\bullet N(CH_3)_2$) at *m/z* 245, following the same fragmentation pattern as observed for the covalent dimer, **2**.

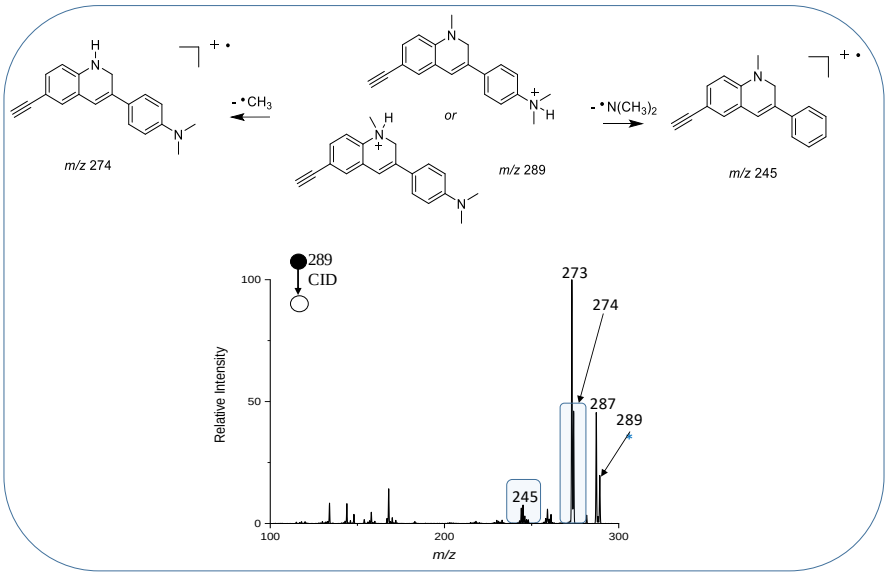

Figure 6.14 CID spectrum of dimer **3** results in a major peak observed at *m/z* 274 due to loss of a methyl radical and *m/z* 245 corresponds to a loss of a dimethylamino radical.

MS/MS data of the major fragments of **3** reflects fragmentation due to neutral losses of (H_2) at *m/z* 287 forming the compound **4,** and a loss of methane (CH_4) observed at *m/z* 273, as

highlighted in Figure 6.15. CID validates structure of m/z 289 formed by the electrospray process and by bulk organic synthesis.

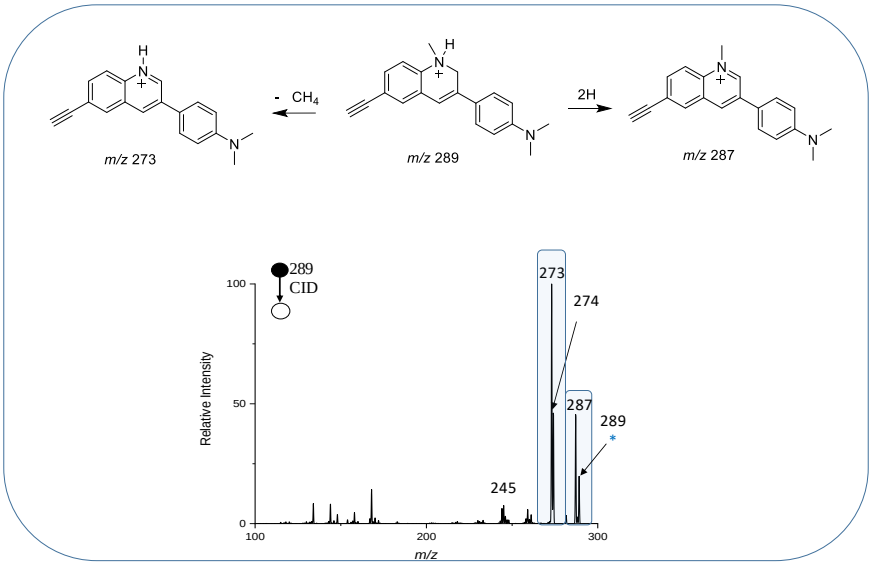

Figure 6.15 CID spectrum of dimer **3** results in a major peak observed at *m/z* 287 due to loss of dihydrogen and *m/z* 273 corresponds to a loss of a methane.

As mentioned previously, the addition of benzoyl peroxide results in the formation of *m/z* 287, which is observed in spray experiments in smaller abundance. Figure 6.16 shows the progression of the bulk reaction over time. Spectrum in Figure 6.16a shows the reaction after the initial mixing in which one of the most abundant peaks is starting material at *m/z* 146. After 24 hours, shown in Figure 6.16b, the base peak corresponds to the product at *m/z* 287. The MS/MS data for *m/z* 287 is shown in Figure 6.16c and 6.16d. CID spectrum of compound **4** produced during the spray process is shown in Figure 6.17, and experiences both radical and neutral loss fragments. The major fragments are the result of the loss of a methyl radical ($\bullet CH_3$) at *m/z* 272, with the dominant ion intensity due to loss of methane (CH_4) at *m/z* 271.

The complementary information gained by comparison of the MS/MS data provides confirmation that the *m/z* 287 product produced in the spray method was the same structure as that produced by synthesis with benzoyl peroxide. The product **4** (*m/z* 287) was purified by a liquid-liquid extraction followed by preparative TLC. One of the byproducts of the benzoyl peroxide reaction is benzoic acid, which is believed to have hindered the separation when not first removed. Since benzoic acid is not soluble in water, a chloroform-water liquid-liquid extraction was done to

remove this species. This allowed for the *m/z* 287 product to be purified by an alumina preparative TLC plate with DCM:MeOH = 9 : 1 (v/v) mobile phase. The ^{13}C NMR spectrum of **4** (*m/z* 287) is given in Figure 6.4 of the Organic Synthesis section of this chapter. The ^{1}H NMR and ^{1}H-^{1}H COSY spectra of the pure compound are shown in the same section as Figure 6.5 and 6.6.

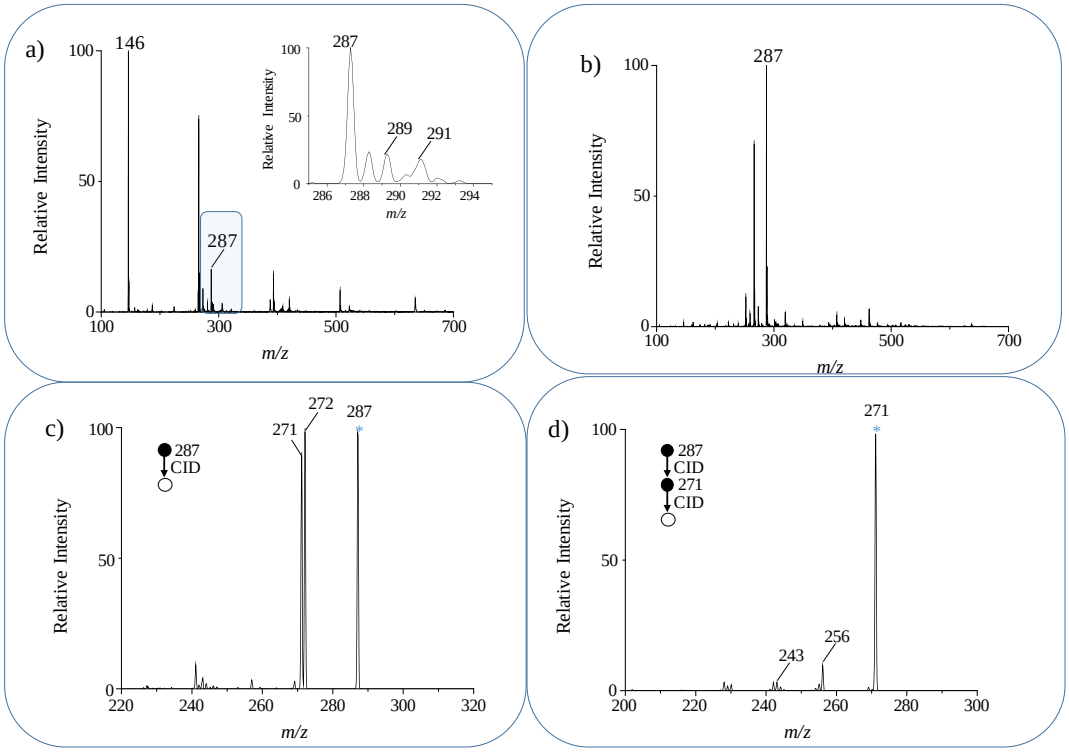

Figure 6.16 Bulk reaction progress of **1** with benzoyl peroxide radical initiator: a) MS spectrum after initial mixing; b) MS spectrum after 24 h of reaction time; c) MS^2 spectrum of *m/z* 287 where *m/z* 271 corresponds to a methyl radical loss and *m/z* 272 corresponds to a loss of methane; d) MS^3 spectrum for *m/z* 287 and *m/z* 271.

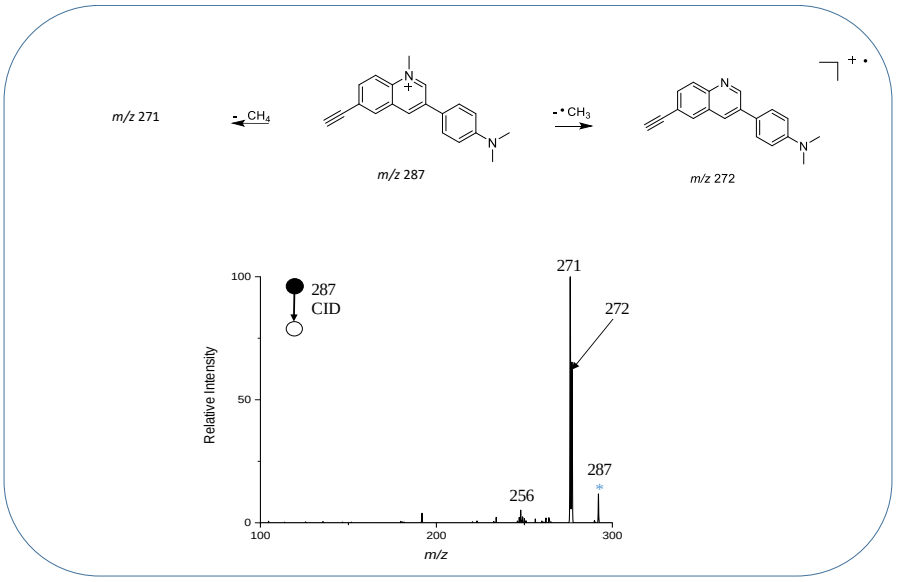

Figure 6.17 CID spectrum of dimer **4** results in a major peak observed at *m/z* 272 due to loss of a methyl radical and *m/z* 271 corresponds to a loss of a methane.

In this study, three products were produced from **1** by spray-based cyclization, including one covalent bond dimer **2** (*m/z* 291) and the two other dimer species **3** (*m/z* 289) and **4** (*m/z* 287). The reaction mechanism has not been supported by the demonstration of intermediates

Dimers **3** and **4** were likely formed through a free radical pathway, because they are able to be found in the bulk-phase reactions mediated by free radical initiators. As stated above, copper (II) perchlorate hexahydrate (**8**) radical initiation forms compound **3**, whereas tris(4-bromophenyl)aminium hexachloroantimonate (**9**) radical initiation forms both **3** and **4**. This difference may be due to the different activity of free radicals. Due to the relatively weak binding capacity of the outer electrons, one electron lost from transition metal copper was obtained by the starting material (**1**) to form a Cu-mediated free radical.

Meanwhile, the Copper (I) salt forms a tetrahedral complex with acetonitrile. As a result, the activity of Cu-mediated free radical is relatively high, and it forms only one product. Compound **9** is also a common free radical initiator, which is able to form a free radical cation (**10**) at room temperature. The activity of **10** is not as high as the Cu-mediated free radical, therefore **10** mediates generation of various products.

The reasoning behind the formation of these two different species in a radical environment, as well as the reaction pathways, is not well understood at this time. It is possible that there are

two competing reaction pathways for the monomer radical to follow. Another possibility is that a radical of *m/z* 289 goes on to fully aromatize to *m/z* 287. One possible experiment is once *m/z* 289 is isolated to subject this pure compound to radical conditions and to see if it reacts to form *m/z* 287. However, we prefer to think that the two pathways are relatively independent, rather than **4** is obtained by **3** oxidative dehydrogenations. One reason is that the oxidation of **8** is stronger than that of **9**. Therefore, if **4** is generated from **3** by oxidative dehydrogenation, one would expect that the **8**-mediated reaction would generate more **4** than the reaction mediated by **9**, which is not the case from our experimental data. Just as the benzoyl peroxide, the one with strongest oxidation capacity among three radical initiators used in this study, only results in the formation of **4**. Another reason is that the simulation result of theoretical chemistry shows $\Delta H > 0$ of the reaction of **4** generated from **3.**

In this study, three products were produced from **1** by spray-based cyclization, including one covalent bond dimer **2** (*m/z* 291) and the two other dimer species **3** (*m/z* 289) and **4** (*m/z* 287). The reaction mechanism has not been supported by the demonstration of intermediates**.** Free radical dimer **3** and **4** were likely formed through a free radical pathway, because they are able to be found in the bulk-phase reactions mediated by free radical initiators. As stated above, copper (II) perchlorate hexahydrate (**8**) radical initiation forms compound **3**, whereas tris(4-bromophenyl)aminium hexachloroantimonate (**9**) radical initiation forms both **3** and **4**. This difference may be due to the different activity of free radicals. Due to the relatively weak binding capacity of outer electron, one electron lost from transition metal copper was obtained by the starting material (**1**) to form a Cu-mediated free radical. Meanwhile, the Copper (I) salt forms a tetrahedral complex with acetonitrile. As a result, the activity of Cu-mediated free radical is relatively high, and it forms only one product. Compound **9** is also a common free radical initiator, which is able to form a free radical cation (**10**) at room temperature. The activity of **10** is not as high as the Cu-mediated free radical, therefore **10** mediates generation of various products.

6.4.2 4-Ethynylaniline dimerization

Encouraged by these findings, we investigated the role that the alkylamine substituents of the aromatic acetylenes might play in the types of dimers formed by this spray method. It is known that the anodic oxidation of aniline and its derivatives proceeds through a series of reactions resulting in various products.

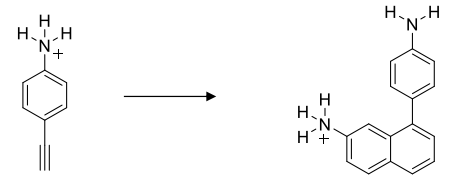

25
m/z 118

26
m/z 235

Scheme 6.6 4-ethynylaniline (**25**, *m/z* 118) forms one dimer when electrosprayed, a covalently bound dimer species **26** ($[2M+H]^+$ observed as at *m/z* 235).

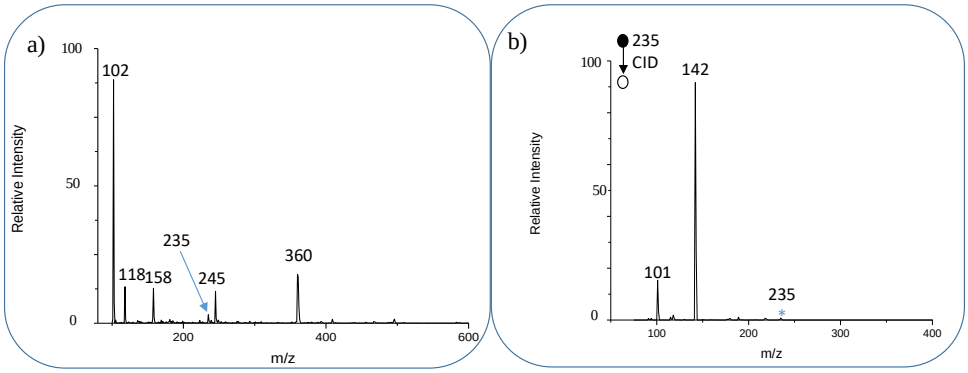

Figure 6.18 a) MS analysis of 4-ethynylaniline (**25**, observed at *m/z* 118 as $[M+H]^+$) forms one dimer species **26** ($[2M+H]^+$ observed as at *m/z* 235), b) MS^2 spectra of covalent bond dimer at *m/z* 235 shows a fragment loss of aniline forming *m/z* 142.

Mass spectra of 4-ethynylaniline (**25**) displays a $[M+H]^+$ peak observed at m/z 118 and an eletrocyclized dimer peak (**26**) representing $[2M+H]^+$ at m/z 235, seen in Figure 6.20a. The data suggests that the ionization efficiency of the solvent peak at *m/z* 102 is larger than the ions of interest, greatly suppressing signal intensity generated from the reagent and product from ions. Tandem mass spectra of the dimer **26** displays a strong signal intensity at *m/z* 142 was observed as the major fragment due to loss of aniline (C_6H_7N). Minor fragment peaks were also observed at *m/z* 118 due to loss of the monomer and at *m/z* 101 due to loss of $C_8H_{10}N_2$, as seen in Figure 6.20b. These results suggest there is a contribution from the electron-donating alkyl groups bound to the amine as the conversion from methyl to hydrogen has reduced the number of dimerized species observed in the electrospray process. Therefore, by lengthening the alkyl chain which in turn increases the electron contribution to the aromatic ring, there is the possibly to further observe increased dimerization.

6.4.3 4-Ethynyl-N,N-diethylaniline dimerization

MS analysis of the diethyl derivative (**27**) yields one dimer species in a similar fashion as the dimethyl derivative, as seen in Figure 6.19. The lengthening of the alkyl chain of the amino group from methyl to ethyl produces significantly more species in the mass spectrum, as shown in 6.19a and enlarged in 6.19b. The dimer species formed by this compound appears 1 mass unit above the expected dimer product thought to form in a similar manner observed in the dimethyl analysis. However, in the previous case the covalently bound dimer **2** was the predominate peak in the spectra, and the other two dimer species were found at mass units 2 or 4 mass units lower. Interestingly, the dominate dimer peak in this case corresponds to a $[2M+2H]^+$ structure appearing at *m/z* 348. However, there was no detection of the covalently bound analog which is expected to appear at *m/z* 347.

A slow scan analysis was implemented to determine if there were any other dimer species could be detected once instrumental resolution capabilities were enhanced, and is displayed in Figure 6.20. After careful inspection, three dimer products were observed in the spectra representing $[2M]^+$ at *m/z* 346, $[2M+H]^+$ at *m/z* 347, and $[2M+2H]^+$ previously mentioned at *m/z* 348 (Scheme 6.7). Additionally, a doubly charged dimer species was detected at *m/z* 174, yet the mass for this peak is shifted 0.5 mass units higher than the monomer peak and confirming its structure.

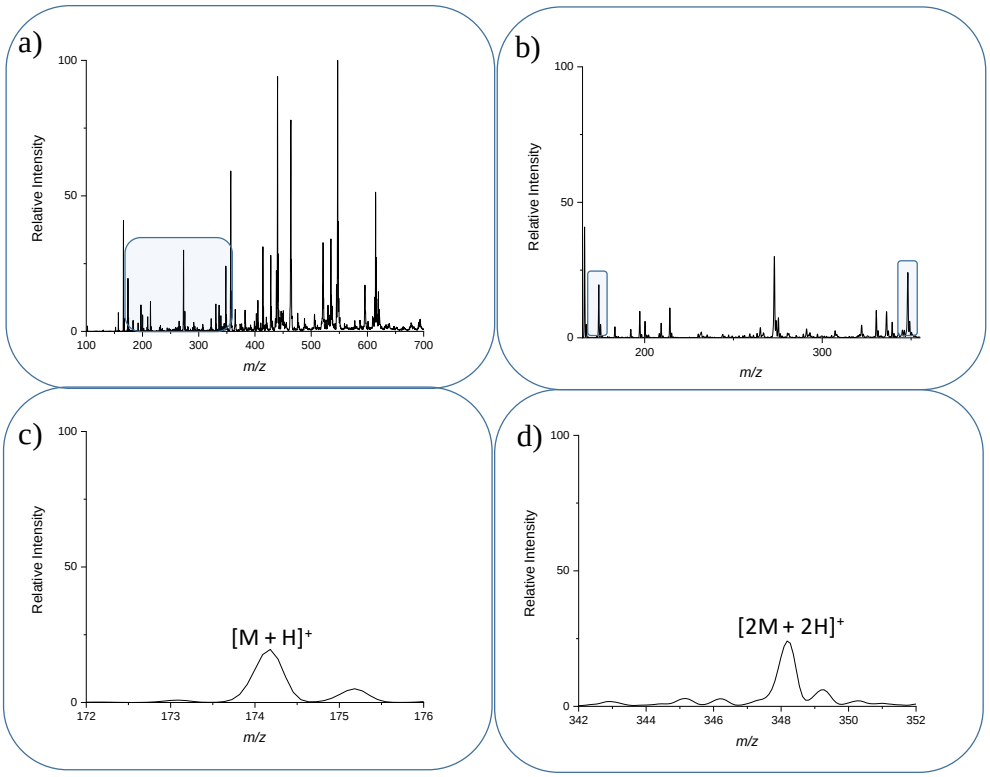

Figure 6.19 nESI-MS analysis of 4-Ethynyl-*N*,*N*-diethylaniline (**27**) a) MS spectrum with the region of interest highlighted; b) highlighted region is expanded to show the monomer and dimer product observed in the spray; c) expanded region of monomer observed at *m/z* 174 as $[M+H]^+$; expanded region of unexpected dimer $[2M+H]^+$ observed as at *m/z* 348.

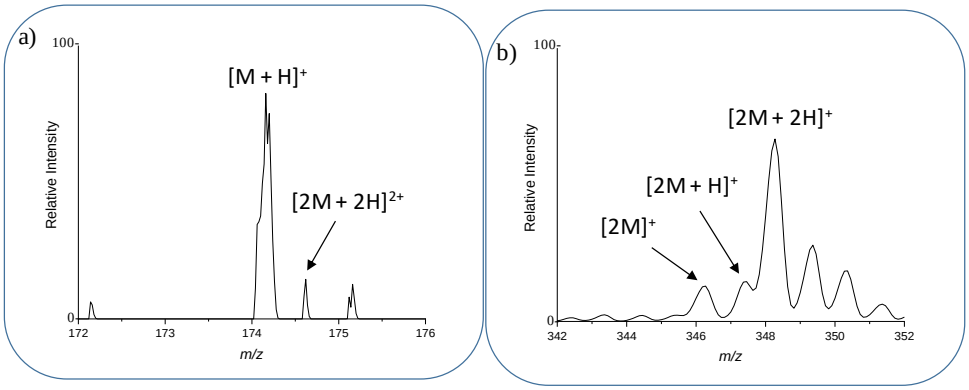

Figure 6.20 Enhanced scan nESI-MS analysis of 4-Ethynyl-*N*,*N*-diethylaniline.

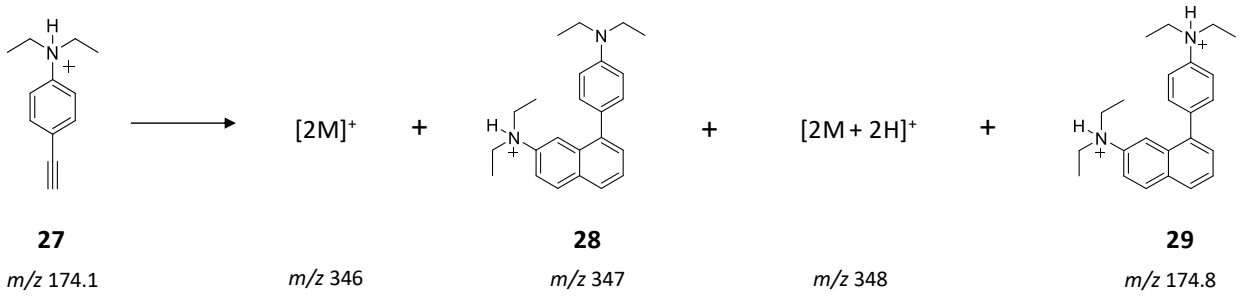

Scheme 6.7 4-Ethynyl-*N*,*N*-diethylaniline (**27**, *m/z* 174.1) forms four dimer species when electrosprayed, a dimer with delocalized charge (*m/z* 346), a covalently bound dimer (**28**, *m/z* 347) a doubly bound dimer (m/z 348), and a doubly charged dimer species (**29**, *m/z* 174.8).

MS/MS spectra of the three dimer products displays the same overall fragmentation pattern (Figure 6.21) where major fragments are due to the loss of a methyl radical (•CH_3), an ethyl radical (•CH_2CH_3), a methyl and ethyl radical (•C_3H_8) and the loss of a diethylamino radical (•$N(CH_2CH_3)_2$). Interestingly, the fragment peaks due to loss of an ethyl radical (•CH_2CH_3) at *m/z* 319 for the $[2M+2H]^+$ dimer (Figure 6.20a) and *m/z* 318 for the $[2M+H]^+$ dimer (Figure 6.20b) produce the greatest signal intensity during fragmentation. The fragment peak due to loss of a methyl radical (•CH_3) at *m/z* 331 is the base peak in the CID spectra of **28**.

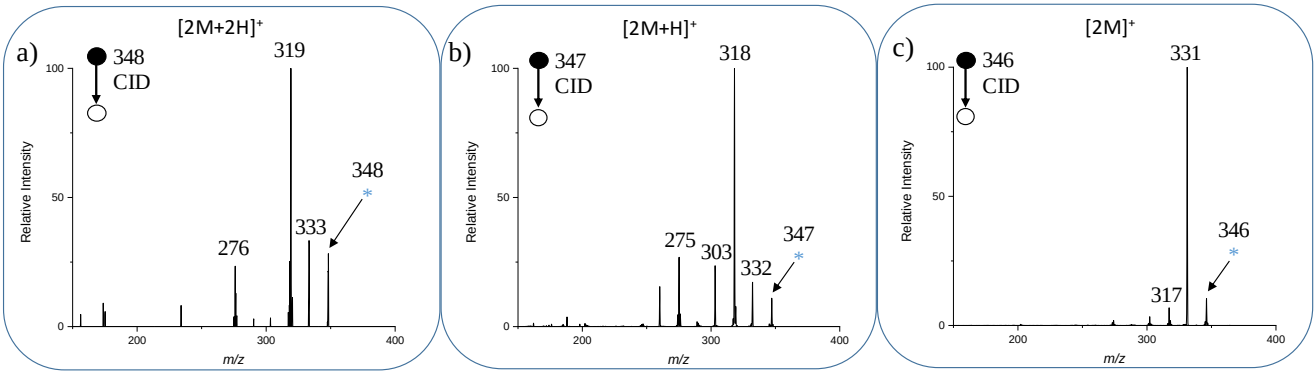

Figure 6.21 CID spectrum of three observed dimers observed at: a) *m/z* 348; b) *m/z* 347; and c) *m/z* 346; with peaks representing fragmentation due to losses of a methyl radical, ethyl radical, methyl and ethyl radicals or a dimethylamino radical, and a diethylamino radical.

Structural elucidation for the covalently bound dimer at *m/z* 347 was achieved by tandem mass analysis and is highlighted in Figures 6.22-6.25. Radical losses for compound **28** obtained

during the enhanced scan method shown in Figure 6.22 correlates with data collected during the normal scan. It appears the dimer peak is not visible in the traditional, full scan analysis but can be isolated in a narrow window and fragmented reproducibly.

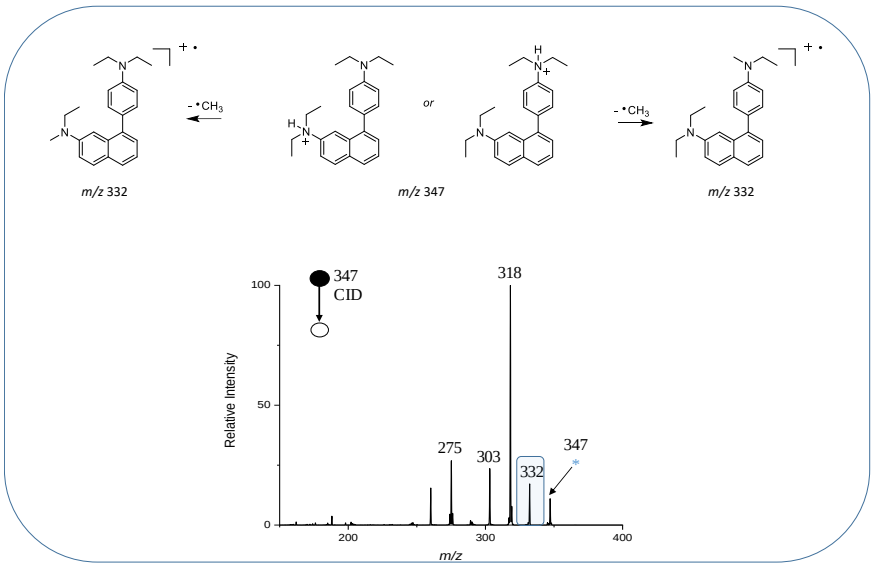

Figure 6.22 CID spectrum of dimer **28** results in a minor peak observed at *m/z* 332 due to loss of a methyl radical.

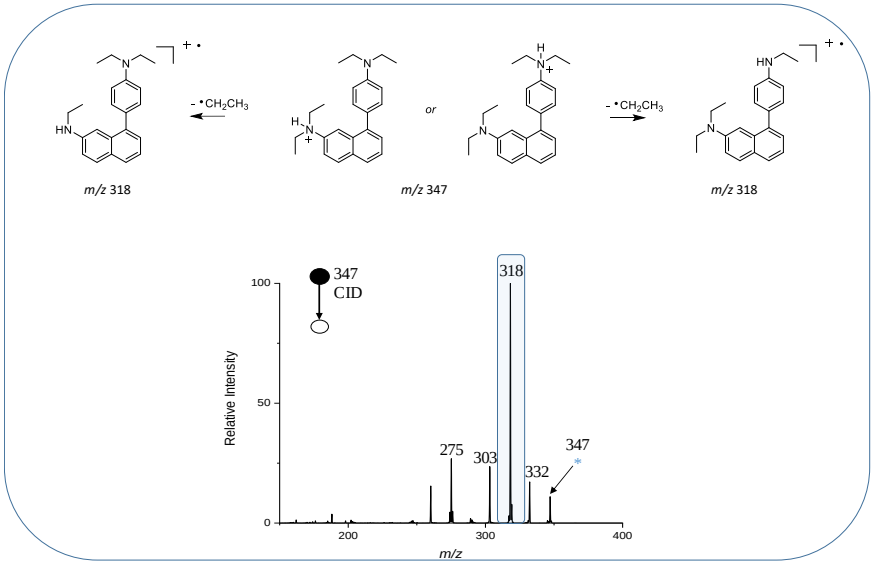

Figure 6.23 CID spectrum of dimer **28** results in a major peak observed at *m/z* 318 due to loss of an ethyl radical.

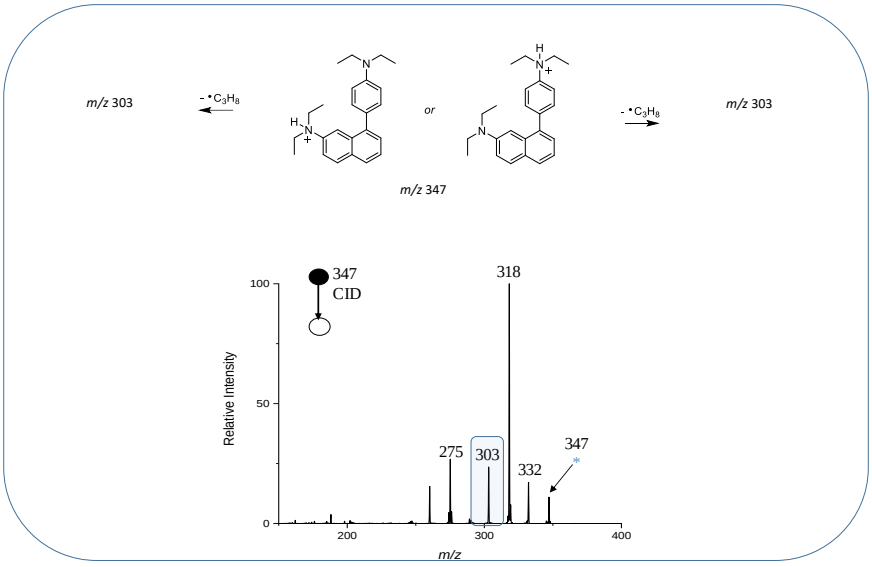

Figure 6.24 CID spectrum of dimer **28** results in a minor peak observed at *m/z* 303 due to loss of a methyl and ethyl radical.

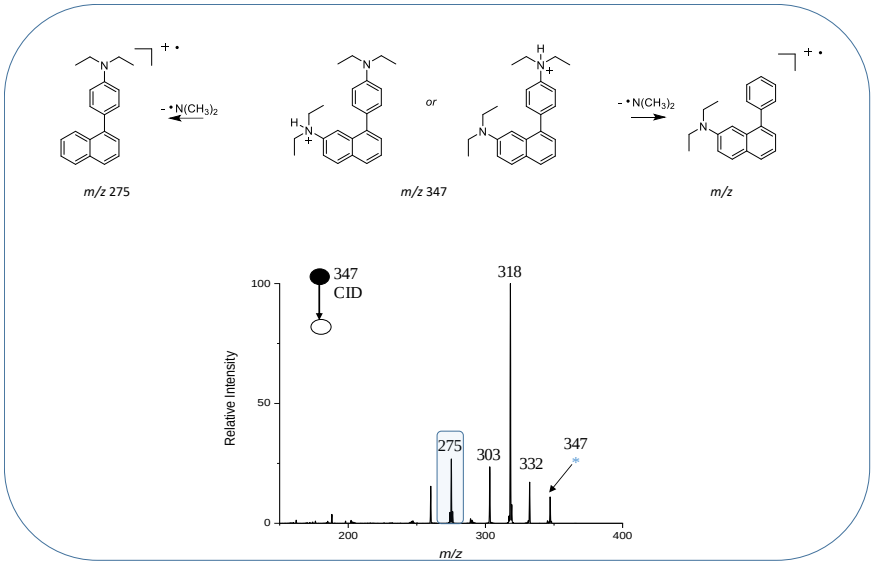

Figure 6.25 CID spectrum of dimer **28** results in a major peak observed at *m/z* 275 due to loss of a dimethylamino radical.

6.5 Conclusions

We presented evidence here showing that compounds are generated by electrospray. In the case of 4-ethynyl-*N*,*N*-dimethylaniline (**1**) dissolved in acetonitrile, three dimer products (**2**-**4**) were observed in microdroplet reactions. The covalent bond dimer product (**2**) does not occur in a corresponding bulk-phase reaction. This product has been further characterized by various methods as an electrocyclized dimer product, a reaction type that has not previously been reported in electrospray droplets. A secondary product (**3**) is formed in which a pyridinium salt is formed via radical reaction. This gas-phase reaction has been interrogated via solution phase chemistry with radical initiators and characterized by NMR. A third dimer product (**4**) is formed, but has not yet been characterized. It is believed to be a methyl pyridine species that is dehydrogenated to aromatize to the pyridinium species.

In the case of 4-ethynylaniline (**25**) dissolved in acetonitrile, one dimer product (**26**) was observed in the microdroplet reactions with no further dimer species detected. However, the analysis of 4-ethynyl-*N*,*N*-diethylaniline (**27**) in acetonitrile produced two dimer products representing a [2M+2H]+ species and a [2M]+ product observed at *m/z* 348 and *m/z* 346, respectively. Upon further inspection, a covalently bound dimer product (**28**) was detected and deemed analogous to the dimer product (**2**) previously characterized for the dimethyl derivative.

Additionally, a doubly charged dimer species (**29**) was detected and characterized by its fragmentation pattern upon collision-induced dissociation.

6.6 References

1. R. G. Cooks, Z. Ouyang, Z. Takats, J. M. Wiseman, Science 2006, 311, 1566–1570.
2. G. A. Harris, A. S. Galhena, F. M. Fernandez, Anal. Chem. 2011, 83, 4508–4538.
3. L. S. Santos, G. B. Rosso, R. A. Pilli, M. N. Eberlin, J. Org. Chem. 2007, 72, 5809–5812.
4. M. N. Eberlin, Eur. J. Mass Spectrom. 2007, 13, 19–28.
5. C. Vicent, M. Viciano, E. MasMarza, M. Sanau, E. Peris, Organometallics 2006, 25, 3713–3720.
6. F. C. C. Moura, M. H. Araujo, I. Dalmazio, T. M. A. Alves,L. S.Santos,M. N.Eberlin,R.Augusti,R. M.Lago,Rapid Commun. Mass Spectrom. 2006, 20, 1859–1863.
7. J. H. Liu, C. D. Marquez, S. T. Weintraub, P. C. Smith, Pharm. Res. 1998, 15, 343–346.
8. Y. Yang, K. Janota, K. Tabei, N. Huang, M. M. Siegel, Y. I. Lin, B. A. Rasmussen, D. M. Shlaes, J. Biol. Chem. 2000, 275, 26674–26682.
9. L. S. Santos, C. H. Pavam, W. P. Almeida, F. Coelho, M. N. Eberlin, Angew. Chem. Int. Ed. 2004, 43, 4330–4333.
10. Angew. Chem. 2004, 116, 4430–4433.
11. G. W. Amarante, H. M. S. Milagre, B. G. Vaz, B. R. V. Ferreira, M. N. Eberlin, F. Coelho, J. Org. Chem. 2009, 74, 3031–3037.
12. V. Carrasco-Sanchez, M. J. Simirgiotis, L. S. Santos, Molecules 2009, 14, 3989–4021
13. B. V. Silva, F. A. Violante, A. C. Pinto, L. S. Santos, Rapid Commun. Mass Spectrom. 2011, 25, 423–428
14. O. O. Sogbein, D. A. Simmons, L. Konermann, J. Am. Soc. Mass Spectrom. 2000, 11, 312–319
15. K. L. Vikse, Z. Ahmadi, C. C. Manning, D. A. Harrington, J. S. McIndoe, Angew. Chem. Int. Ed. 2011, 50, 8304–8306
16. Angew. Chem. 2011, 123, 8454– 8456
17. C. A. Marquez, F. Fabbretti, J. O. Metzger, Angew. Chem. Int. Ed. 2007, 46, 6915–6917

18. Angew. Chem. 2007, 119, 7040–7042

19. C. Iacobucci, S. Reale, J.-F. Gal, F. De Angelis, Angew. Chem. Int. Ed. 2015, 54, 3065–3068

20. Angew. Chem. 2015, 127, 3108–3111

21. Jiří Schulz, Lucie Jašíková, Anton Škríba, and Jana Roithová, J. Am. Chem. Soc. 2014, 136, 11513–11523.

22. Li, Y.; Mehari, T. F.; Wei.; Z.; Liu, Y.; Cooks, R. G., J. Mass. Spec. 2020, 4585.

23. Fenn, J. B.; Mann, M.; Meng, C. K.; Wong, S. F.; Whitehouse, C. M., Electrospray ionization–principles and practice. Mass Spectrom. Rev. 1990, 9 (1), 37-70.

24. Levsen, K.; Schiebel, H.-M.; Terlouw, J. K.; Jobst, K. J.; Elend, M.; Preiß, A.; Thiele, H.; Ingendoh, A., Even-electron ions: a systematic study of the neutral species lost in the dissociation of quasi-molecular ions. J. Mass Spectrom. 2007, 42 (8), 1024-1044.

25. Thurman, E. M.; Ferrer, I.; Pozo, O. J.; Sancho, J. V.; Hernandez, F., The even-electron rule in electrospray mass spectra of pesticides. Rapid Commun. Mass Spectrom. 2007, 21 (23), 3855-3868.

26. Williams, J. P.; Nibbering, N. M. M.; Green, B. N.; Patel, V. J.; Scrivens, J. H., Collision-induced fragmentation pathways including odd-electron ion formation from desorption electrospray ionisation generated protonated and deprotonated drugs derived from tandem accurate mass spectrometry. J. Mass Spectrom. 2006, 41 (10), 1277-1286.

27. Cao, F.; Kim, J.; Bard, A. J., Detection of the Short-Lived Cation Radical Intermediate in the Electrochemical Oxidation of N,N-Dimethylaniline by Scanning Electrochemical Microscopy. J. Am. Chem. Soc. 2014, 136 (52), 18163-18169.

28. Yang, H.; Wipf, D. O.; Bard, A. J., Application of rapid scan cyclic voltammetry to a study of the oxidation and dimerization of N,N-dimethylaniline in acetonitrile. J. Electroanal. Chem. 1992, 331 (1), 913-924.

29. Brown, T. A.; Chen, H.; Zare, R. N., Detection of the Short-Lived Radical Cation Intermediate in the Electrooxidation of N,N-Dimethylaniline by Mass Spectrometry. Angew. Chem. 2015, 127 (38), 11335-11337.

30. Kirchgessner, M.; Sreenath, K.; Gopidas, K. R., Understanding Reactivity Patterns of the Dialkylaniline Radical Cation. The Journal of Organic Chemistry 2006, 71 (26), 9849-9852.

31. Konermann, L.; Ahadi, E.; Rodriguez, A. D.; Vahidi, S., Unraveling the Mechanism of Electrospray Ionization. Analytical Chemistry 2013, 85 (1), 2-9.

32. https://en.wikipedia.org/wiki/Electrospray_ionization#Ionization_mechanism

33. Yamashita, M.; Fenn, J. B. J. Phys. Chem. 1984,88, 4451.

34. Fenn, J. B.; Mann, M.; Meng, C. K.; Wong, S. K.; Whitehouse, C. M. Science 1989, 246, 64.

35. Fenn, J. B.; Mann, M.; Meng, C. K.; Wong, S. K. Mass Spectrom. Rev. 1990, 9, 37.

36. Smith, R. D.; Loo, J. A.; Edmonds, C. G.; Barinaga, C. J.; Udseth, H. R. Anal. Chem. 1990, 62, 882.

37. Huang, E. C.; Wachs,T.; Conboy, J. J.; Henion, J. D. Anal. Chem. 1990, 62, 713A.

38. Mann, M. Org. Mass Spectrom. 1990, 25, 575.

39. M. Girod, E. Moyano, D. I. Campbell, R. G. Cooks, Chem. Sci. 2011, 2, 501–510.

40. Y. Li, X. Yan, R. G. Cooks, Angew. Chem. Int. Ed. 2016, 55, 3433–3437

41. Angew. Chem. 2016, 128, 3494–3498.

42. R. M. Bain, C. J. Pulliam, R. G. Cooks, Chem. Sci. 2015, 6, 397– 401.

43. S. Banerjee, R. N. Zare, Angew. Chem. Int. Ed. 2015, 54, 14795– 14799;

44. Angew. Chem. 2015, 127, 15008–15012.

45. T. M ller, A. Badu-Tawiah, R. G. Cooks, Angew. Chem. Int. Ed. 2012, 51, 11832–11835;

46. Angew. Chem. 2012, 124, 12002–12005.

47. J. K. Lee, S. Kim, H. G. Nam, R. N. Zare, Proc. Natl. Acad. Sci. USA 2015, 112, 3898–3903

48. J. K. Lee, S. Banerjee, H. G. Nam, R. N. Zare, Q. Rev. Biophys. 2015, 48, 437–444.

49. Q Rev Biophys. 2015,48(4): 437-444

50. Wei Z, Wleklinski M, Ferreira C, Cooks RG. Angew Chem Int Ed Engl. 2017 Aug 1;56(32):9386-9390.

51. Levsen, K.; Schiebel, H.-M.; Terlouw, J. K.; Jobst, K. J.; Elend, M.; Preiß, A.; Thiele, H.; Ingendoh, A., Even-electron ions: a systematic study of the neutral species lost in the dissociation of quasi-molecular ions. J. Mass Spectrom. 2007, 42 (8), 1024-1044.

52. Thurman, E. M.; Ferrer, I.; Pozo, O. J.; Sancho, J. V.; Hernandez, F., The even-electron rule in electrospray mass spectra of pesticides. Rapid Commun. Mass Spectrom. 2007, 21 (23), 3855-3868.

53. Williams, J. P.; Nibbering, N. M. M.; Green, B. N.; Patel, V. J.; Scrivens, J. H., Collision-induced fragmentation pathways including odd-electron ion formation from desorption electrospray ionisation generated protonated and deprotonated drugs derived from tandem accurate mass spectrometry. J. Mass Spectrom. 2006, 41 (10), 1277-1286.

54. Cao, F.; Kim, J.; Bard, A. J., Detection of the Short-Lived Cation Radical Intermediate in the Electrochemical Oxidation of N,N-Dimethylaniline by Scanning Electrochemical Microscopy. J. Am. Chem. Soc. 2014, 136 (52), 18163-18169.

55. Yang, H.; Wipf, D. O.; Bard, A. J., Application of rapid scan cyclic voltammetry to a study of the oxidation and dimerization of N,N-dimethylaniline in acetonitrile. J. Electroanal. Chem. 1992, 331 (1), 913-924.

56. Brown, T. A.; Chen, H.; Zare, R. N., Detection of the Short-Lived Radical Cation Intermediate in the Electrooxidation of N,N-Dimethylaniline by Mass Spectrometry. Angew. Chem. 2015, 127 (38), 11335-11337.

57. Kirchgessner, M.; Sreenath, K.; Gopidas, K. R., Understanding Reactivity Patterns of the Dialkylaniline Radical Cation. The Journal of Organic Chemistry 2006, 71 (26), 9849-9852.

58. Su, W.-F., Radical Chain Polymerization. In Principles of Polymer Design and Synthesis, Su, W.-F., Ed. Springer Berlin Heidelberg: Berlin, Heidelberg, 2013; pp 137-183

59. Howard, J. K.; Rihak, K. J.; Bissember, A. C.; Smith, J. A., The Oxidation of Pyrrole. Chemistry – An Asian Journal 2016, 11 (2), 155-167.

60. Jia, X., Radical Cation Salts: From Single-Electron Oxidation to C–H Activation-. Synthesis 2016, 48 (01), 18-30.

VITA

Education

Doctorate of Philosophy (PhD)-Chemistry
Purdue University, 2020
West Lafayette, IN, United States
Advisor: Dr. R. Graham Cooks
Dissertation: "Mechanistic Probing of Compounds of Biological and Pharmaceutical Interests by Ambient Ionization Mass Spectrometry."

Master of Science (MS)-Chemistry
North Carolina A&T State University, 2016
Greensboro, NC, United States
Advisor: Dr. Sayo O. Fakayode
Thesis: "Influence of Heavy Metal (Arsenic, Cadmium, Chromium, Mercury, and Lead) Ions on Human Triple Negative Breast Cancer Cell Viability."

Bachelor of Science (BS)- Chemistry; Biology
North Carolina A&T State University, 2014.
Greensboro, NC, United States
Advisor: Dr. Sayo O. Fakayode
Research Topic: "Trace and Macro Elements Concentrations in Selected Fresh Fruits, Vegetables, Herbs, and Processed Foods in North Carolina, USA."

Selected Awards and Recognition

Special Diversity and Inclusion in Chemistry Award (Purdue, 2019)
Iota Sigma Pi Women's Graduate Chemistry Honors Society (Purdue, 2017)
College of Science and Technology Graduate Thesis Award Finalist (NCAT,2017)
Zero Year Summer Research Fellowship (Purdue, 2016)
College of Arts and Sciences Outstanding Graduate Award for Academic Citation (NCAT, 2016)

Research Initiative for Scientific Enhancement (RISE) Graduate Scholar Research Training Program Fellowship (NCAT, 2015)

Annual Biomedical Research Conference for Minority Students Travel Award (ABRCMS, 2015)

National Organization of Black Chemists and Chemical Engineers Advancing Science Travel Grant ((NOBCChE, 2014)

Department of Chemistry Undergraduate Inorganic Award (NCAT, 2014)

Peer-reviewed Publications

Li, Y*., **Mehari, T. F***., Wei, Z., Liu, Y., Cooks, R. G. (2020) Reaction Acceleration at air-solution interfaces: anisotropic rate constants for Katritzky Transamination. *Journal of Mass Spectrometry*, https://doi.org/10.1002/jms.4585

Schrader, R. L., Fedick, P. W., **Mehari, T. F**., Cooks, R. G. (2019) Accelerated chemical synthesis: Three ways of performing the Katritzky transamination reaction. *Journal of Chemical Education*, 96, 360-5.

Fedick, P. W., Bain, R. M., Bain, K., **Mehari, T. F**., Cooks, R. G. (2018) Accelerated tert-butyloxycarbonyl deprotection of amines in microdroplets produced by a pneumatic spray. *International Journal of Mass Spectrometry*, 430, 98-103.

Mehari, T. F., Jones Jr., D., Rorie, C.J. and Fakayode, S.O. (2017) Influence of Heavy Metal (Arsenic, Cadmium, Chromium, Mercury, and Lead) Ions on Human Triple Negative Breast Cancer Cell Viability. *Journal of Chemical Health Risks*, 7.

Alzahrani, H., Kumakli, H., Ampiah, E., **Mehari, T. F**., Babyak, C. M., Fakayode, S. O. (2017) Determination of Macro, Essential Trace Elements, Toxic Heavy Metal Concentrations, Crude Oil Extracts and Ash Compositions from Saudi Arabian Fruits and Vegetables having medicinal values. *Arabian Journal of Chemistry*, 10, 7, 906-13.

Kumakli, H., Duncan, A. V., McDaniel, K., **Mehari, T. F**., Stephenson, J., Maple, L., Crawford, Z., Macemore, C. L., Babyak, C. M., Fakayode, S. O. (2017) Environmental Biomonitoring of Essential and Toxic Elements and Toxic Elements in Human Scalp Hair using Accelerated Microwave-Assisted Sample Digestion and Inductively Couple Plasma Optical Emission Spectroscopy, *Chemosphere*, 174, 708-15.

Mehari, T. F., Greene, L., Duncan, A.L. and Fakayode, S.O. (2015) Trace and Macro Elements Concentrations in Selected Fresh Fruits, Vegetables, Herbs, and Processed Foods in North Carolina, USA. *Journal of Environmental Protection*, 6, 573-583.

Roberts, T. J., **Mehari, T. F**., Hamby, T.; Sykora, R., Assefa, Z. (2015). Bis (1,3-diamino propane) bis(2-(4- nitrophenyl acetate) zinc (II)). *Acta Crystallographica Section E*, 6, 71.

Research Experience

Doctoral Research, 08/2016 – 08/2020
Purdue University
Department of Chemistry
560 Oval Drive
West Lafayette, IN 47906, United States
Principal Investigator: Dr. R. Graham Cooks

- Developed analytical methods for mass spectrometry allowing for reaction monitoring and acceleration of heterogeneous samples, and pharmaceutical molecules of interest at ambient conditions.
- Experience in glioma and oral cancer tissue diagnosis by DESI-MS through identification and quantitation of lipids and small metabolites in mouse and human samples.
- Method development of drugs, metabolites and lipids from urine, plasma, blood and saliva by liquid-liquid and solid-phase extraction and mass spectrometric analysis.
- Collaborated with peers to develop reaction acceleration methods for multi-step, organic synthesis in undergraduate teaching laboratories.
- Maintained, evaluated, analyzed and synthesized scientific data with meticulous record keeping.
- Interpreted key findings, reviewed scientific literature, evaluated limitations, determined general approach and communicated with peers and supervisor through written reports and oral presentations on a weekly basis.
- Skills in experimental design, raw data analysis, scientific review and writing, human and small animal sample collection and analysis, organic synthesis, analytical method development

and instrumentation, NMR, Gas Chromatography-Mass Spectrometry, Liquid Chromatography-Mass Spectrometry, and miniature Mass Spectrometry.

Graduate Research, 01/2015 – 05/2016
North Carolina A & T State University
Department of Chemistry – Department of Cancer Biology
1601 E. Market Street
Greensboro, NC 27411, United States
Principal Investigator: Dr. Sayo O. Fakayode

- Experience in cancer biology research with focus on investigation of influence of environmental chemicals of concern and heavy metal ions on brain tumor and human triple negative breast cancer cell viability.
- Collaborated with peers to determine the trace elements concentrations of environmental samples and human scalp hair.
- Collaborated with peers on the analysis of antimicrobial activity isolated from selected Saudi Arabian fruits and vegetables.
- Trained four undergraduate researchers to independently design and execute solutions to complex chemistry issues in accordance to cGMP and non-standard laboratory practices.
- Skills in inorganic analysis, cell culturing, agarose gel electrophoresis, flow cytometry, Fluorescence Spectrophotometry and Inductively Coupled Plasma-Optical Emission Spectroscopy.

Undergraduate Research, 01/2013 – 12/2014
North Carolina A & T State University
Department of Chemistry
1601 E. Market Street
Greensboro, NC 27411, United States
Principal Investigator: Dr. Sayo O. Fakayode

- Investigated and determined the concentration of essential and heavy metals in natural and processed food products.

- Developed an electrochemical bio-sensor for the determination and quantitation of biologically active molecules.
- Lead team of peers in development of methodology, synthesis, and characterization of novel metal organic framework leading to publication of data.
- Skills in biosensor development, natural product analysis, inorganic synthesis, cyclic voltammetry, Fourier Transform Infrared UV-Vis Spectroscopy, X-ray crystallography, Mars microwave assisted digestion, and Flame Atomic Absorption Spectroscopy.

Teaching and Leadership

Center for analytical instrumentation development planning committee
2019-2020

- Assisted in the planning and execution of CAID meeting by disseminating information, organizing experiments, invitation and coordination of all students, academic and industrial visitors to Purdue University

National Organization for the Professional Advancement of Black Chemist and Chemical Engineers (NOBCChE) – Treasurer
2018-2020

- Oversee organization accounts, budgeting and approval of monetary transactions
- Participate in underrepresented minority recruitment and retention in the Purdue Chemistry Dept.

Chemistry Diversity Initiative (CDI) Conference/ University Recruitment Co-Chair
2017-2020

- Leading recruitment efforts of underrepresented minorities through visits at HBCUs/HSIs and conferences
- Continued mentorship of incoming and current minority graduate students to improve retention

Department of Chemistry Teaching Assistant (General Chemistry/ Instrumental Analysis I & II)
2016-2019

- Managed a total of fourteen undergraduate teaching labs and recitations
- Maintained safe and engaging laboratory environment for 275 undergraduate students

College of Science STEM Boot-camp Summer Instructor (General Biology/ Chemistry)
2017-2019

- Prepared incoming undergraduate STEM students for upcoming biology/chemistry coursework
- Designed and implemented all lesson plans, course material, grading rubric and administration of grades

Department of Chemistry Graduate Tutor (Chemistry)
2015-2016

- Assisted undergraduate students in various levels of coursework

Center for Academic Excellence Undergraduate Tutor (Mathematics/Chemistry)
2013-2015

- Acted as a liaison between faculty and students to reinforce course material

Oral and Poster Presentations

Li, Y*., **Mehari, T. F***., Wei, Z., Liu, Y., Cooks, R. G. "Reaction Acceleration at Air-Solution Interfaces." 2020. American Society for Mass Spectrometry Reboot, June 1-12, 2020.

Mehari, T. F.; Fedick, P. W.; Bain, R. M.; Bain, K.; Cooks, R. G. "Accelerated tert-Butoxycarbonyl Deprotection of Amines in Microdroplets: A Laboratory Exercise." 2018. The National Organization for the Professional Advancement of Black Chemists and Chemical Engineers, Orlando, Florida, September 17-21, 2018. ANA Poster #024.

Tomeau B.; Godfrey S.; **Mehari T. F**.; Fakayode S. O.; Rorie, C. "Investigating the cellular and molecular response of breast cancer cells to heavy metal ion mercury II." 2017. Annual Biomedical Research Conference for Minority Students, Phoenix, Arizona, November 1-7, 2017, Poster Number E074.

Mehari, T. F.; Fakayode, S. O.; Jones Jr., D.; Rorie, C. J. "Influence of Heavy Metal (Arsenic, Cadmium, Chromium, Mercury, and Lead) Ions on Human Triple Negative Breast Cancer Cell Viability". 2015. Annual Biomedical Research Conference for Minority Students, Seattle, Washington, November 11-14, 2015.

Maple, L.; Kumakli, H.; Stephenson, J.; McDaniel, K.; **Mehari, T. F**.; Duncan, A. V.; Macemore, C.; Babyak, C. M.; Fakayode, S. O. "Use of Microwave Assisted Sample Digestion and Inductively Coupled Plasma Atomic Emission Spectroscopy for the Determination of Levels of Arsenic (As), Cadmium (Cd), Lead (Pb), Chromium (Cr), Selenium (Se), and Nickel (Ni) in Human Scalp Hair". 2015. Annual Biomedical Research Conference for Minority Students, Seattle, Washington, November 11-14, 2015.

Crawford, Z.; Kumakli, H.; Stephenson. J.; McDaniel, K.; **Mehari, T. F**.; Duncan, A. V.; Macemore, C.; Babyak, C. M.; Fakayode, S. O. "Determination of Trace and Macro Element (Ca, Cu, K, Mg, Na, Zn, and Fe) Concentrations in Human Scalp Hair using Inductively Plasma Atomic Emission Spectroscopy". 2015. Annual Biomedical Research Conference for Minority Students, Seattle, Washington, November 11-14, 2015.

Mehari, T. F.; Fakayode, S. O.; Jones Jr., D., Rorie, C.J. "Investigation of Influence of Polycyclic Aromatic Hydrocarbons on Human Triple Negative Breast Cancer Cell Viability." 2015. The National Organization for the Professional Advancement of Black Chemists and Chemical Engineers, Orlando, Florida, September 22-25, 2015. ENVIRO Poster # 004

Greene, L. V.; **Mehari, T. F**.; Adeniyi, W. K.; Fakayode, S. O. "Analysis of Trace/Macro Elements Concentrations of Dead Sea Water by Flame Atomic Absorption Spectroscopy". 2015. The National Organization for the Professional Advancement of Black Chemists and Chemical Engineers, Orlando, Florida, September 22-25, 2015.

Mehari, T. F.; Fakayode, S. O.; Greene, L.; McDaniel, K.; King, J. "Trace Elements Concentrations in Fresh Fruits and Processed Foods." 2014. The National Organization for the

Professional Advancement of Black Chemists and Chemical Engineers, New Orleans, Louisiana, September 23-26, 2014. SPEC M Poster # 004

Greene, L. V.; Mehari, T. F.; Fakayode, S. O.; McDaniel, K.; King, J. "Comparative Analysis of Trace Elements Concentrations in Vegetables, Herbs, Powdered, and Processed Foods." 2014. The National Organization for the Professional Advancement of Black Chemists and Chemical Engineers, New Orleans, Louisiana, September 23-26, 2014. SPEC M Poster # 006

Mehari, T. F.; Fakayode, S. O.; Greene, L.; McDaniel, K.; King, J. "Trace Elements Concentrations in Fresh Fruits and Processed Foods." 2014. The North Carolina Agricultural and Technical State University Undergraduate Research Symposium, Greensboro, NC, October 16, 2014.

Mehari, T. F.; Adeniyi, W.; "Determining the Presence of Biologically Important Molecules by Chemically modified Electrodes through the use of Electrochemistry." 2014. The North Carolina Agricultural and Technical State University Chemistry Department, Greensboro, NC, April 10, 2014.

Memberships

American Chemical Society ● American Society for Mass Spectrometry ● Iota Sigma Pi Women's Chemistry Honors Society ● National Organization for the Professional Advancement of Black Chemist and Chemical Engineers (NOBCChE)

Scientific Outreach

- Center for Analytical Instrumentation and Development (CAID) Coordinator
- College of Science and Diversity Minority Student Panelist
- Wayne County Science Fair
- Active Learning Professional Workshop for 6-12 Science Educators
- Advancing Mathematics and Science Skills Program
- Sophomore Immersion Program in Research and Academics

- Future College Students Saturday Academy
- American Chemical Society National Chemistry Week